In-Situ BrO Measurements in the Upper Troposphere / Lower Stratosphere: Validation of the ENVISAT Satellite Measurements and Photochemical Model Studies

Dissertation
presented by
Serhiy Hrechanyy

University of Wuppertal
Faculty C – Mathematics and Natural Sciences
Januar 2007
WUB-DIS 2007-01

Diese Dissertation kann wie folgt zitiert werden:

urn:nbn:de:hbz:468-20070768
[http://nbn-resolving.de/urn/resolver.pl?urn=urn%3Anbn%3Ade%3Ahbz%3A468-20070768]

Zusammenfassung

Anorganische Bromspezies sind die zweitwichtigste Halogenfamilie in der Chemie der stratosphärischen Ozonzerstörung. Das Mischungsverhältnis der Bromspezies liegt etwa zwei Größenordnungen unter dem der Chlorspezies, aber Brom weist ein deutlich höheres Ozonzerstörungspotential (Faktor von ca. 45) auf als Chlor.

In dieser Arbeit werden atmosphärische Messungen von Brommonoxid, BrO, im Höhenbereich 15-30 km präsentiert und diskutiert. Die Messungen wurden durchgeführt mit dem Ballon-getragenen TRIPLE- und dem Flugzeug-getragenen HALOX-Instrument des Forschungszentrums Jülich, basierend auf der Chemischen-Konversions-Resonanz-Fluoreszenz-Methode, der einzigen etablierten In-Situ-Messtechnik für BrO. Es wurden 57 HALOX-Flüge aus fünf Messkampagnen von arktischen bis tropischen Breiten und drei TRIPLE-Messflüge im Rahmen der SCIAMACHY(SCanning Imaging Absorption spectroMeter for Atmospheric CHartographY)-Validierung durchgeführt. Die Ballonmessungen ergeben vertikale Profile von BrO im Höhenbereich 15-30 km bei mittleren nördlichen und arktischen Breiten. Aus den Flugzeugmessungen wurde ein gemitteltes vertikales BrO-Profil in den Tropen und meridionale BrO-Verteilungen für den Höhenbereich 15-20 km abgeleitet.

Im Rahmen der SCIAMACHY-Validierung wurden die TRIPLE-Profile anhand des Jülicher CLaMS(Chemisch Lagrangesches Modell der Stratosphäre)-Modells photochemisch korrigiert um den Tagesgang der BrO-Mischungsverhältnisse zu berücksichtigen und die Profile auf die photochemischen Bedingungen der zu vergleichenden SCIAMACHY-Messungen zu konvertieren. Der Vergleich ergibt systematisch höhere Mischungsverhältnisse der Satellitenmessung am Rande der experimentellen Fehlergrenzen beider Messungen. Entsprechende Verbesserungen in den SCIAMACHY Retrieval-

Verfahren sind zur Zeit im Gang.

Um die im CLaMS-Modell implementierte Brom-Chemie zu überprüfen wurde das BrO-Profil der TRIPLE-Messung vom 9. Juni 2003 unter arktischen Frühlings-/Sommerbedingungen verglichen mit simulierten Profilen. Die Simulationen wurden hierzu mit unabhängigen Ballon- und Satellitenmessungen und einem Brom-Gesamtmischungsverhältnis von 18.4 pptv initialisiert. Hier wurde eine sehr gute Übereinstimmung der TRIPLE-Messung und des Simulationsergebnisses festgestellt, was auf eine gute Repräsentation der stratosphärischen Brom-Chemie im Modell hindeutet oder umgekehrt formuliert: Die TRIPLE-Messung ist mit der gegenwärtig akzeptierten Brom-Chemie kompatibel.

Messungen von BrO in der tropischen Tropopausenregion (TTL) eignen sich zur Untersuchung des Beitrages von sehr kurzlebigen Bromspezies (VSLS) zum anorganischen Brom, Br_y. Da die tropischen HALOX-Profile aus den TROCCINOX- und SCOUT-O3-Messkampagnen im Höhenbereich 15-20 km an der unteren Grenze vergleichbarer DOAS-Messungen liegen wurde eine CLaMS-Modellstudie zur Freisetzung von Br_y aus den Quellgasen durchgeführt. Hierzu wurde ein Trajektorienensemble, das im Zeitraum 6 bis zu mehr als 90 Tagen von der unteren Troposphäre in die TTL transportiert wurde, mit in der Grenzschicht beobachteten Mischungsverhältnissen aller wichtigen Brom-Quellgase initialisiert und die Freisetzung von Br_y durch chemische und photochemische Reaktionen wurde simuliert. Bromoform, $CHBr_3$, war die Hauptquelle für Br_y in der TTL. Die abgeleitete troposphärische Lebensdauer von Bromoform ist etwa 33 Tage. Das modellierte maximale BrO-Mischungsverhältnis an der Tropopause ist 2.5 pptv. Dies ist konsistent mit den HALOX-Messungen, die dort keine signifikanten Mengen (<1-2 pptv) von BrO nachweisen. Messungen von mehr als 4 pptv (wie aus SCIAMACHY-Messungen abgeleitet) können somit nur durch andere nicht modellierte Prozesse, wie sehr schnellen Aufstieg von Luftmassen aus starken Bromoform-Quellgebieten oder Injektion von anorganischen Bromverbindungen auf verdampfenden Partikeln, erklärt werden.

Abstract

Inorganic bromine species form the second most important halogen family affecting stratospheric ozone (*WMO*, 2003). Although the stratospheric bromine mixing ratio is about two orders of magnitude lower than the chlorine one, bromine has much higher ozone depleting potential (factor of about 45) compared to chlorine.

This study reports and discusses atmospheric bromine monoxide, BrO, measurements in the altitude range 15-30 km performed by the balloon-borne instrument TRIPLE and aircraft instrument HALOX employing the chemical conversion resonance fluorescence technique, which is the only proven in-situ technique for the measurements of BrO. 57 HALOX flights have been performed in the frame of five field campaigns ranging from the Arctic to tropics. Three TRIPLE flights were carried out at high and mid latitudes in the frame of the SCIAMACHY (SCanning Imaging Absorption spectroMeter for Atmospheric CHartographY) validation. Calibration, consistency checks, data analysis, and error assessment for the in-situ measurements are described. The balloon measurements have yielded vertical profiles of BrO between 15 and 30 km altitude at northern mid- and at arctic latitudes. From the aircraft measurements a meridional BrO distribution from tropical to the arctic latitudes between 15 and 20 km altitude was obtained.

For the SCIAMACHY validation the TRIPLE BrO profiles have been photochemically corrected by means of the Jülich CLaMS (Chemical Lagrangian Model of the Stratosphere) model in order to reflect the diurnal variation of BrO and adjust the profiles to the photochemical conditions of the corresponding SCIAMACHY measurements. Hereby appropriate SCIAMACHY profiles have been found to be systematically higher than the TRIPLE profiles but mostly within the bounds of the accuracies of both techniques. Improvements in the satelite retrieval procedures are ongoing.

In order to check the reliability of the bromine chemistry in the CLaMS model the BrO profile measured by TRIPLE on June 9, 2003 in Arctic spring/summer conditions was compared to a simulated BrO profile. For the simulation the model was initialized with appropriate satellite and balloon measurements and with a total stratospheric bromine of 18.4 pptv. Very good agreement between the TRIPLE measurements and model results was found indicating that the model captures stratospheric bromine chemistry quite well or put the other way the TRIPLE measurement is compatible with currently accepted bromine chemistry.

Measurements of BrO in the tropical tropopause layer (TTL) are well suited to investigate the contribution of very short-lived bromine species (VSLS) to the inorganic bromine, Br_y. Since tropical HALOX BrO measurements from TROCCINOX and SCOUT-O3 in the 15-20 km altitude regime are at the low side of comparable DOAS measurements a CLaMS study of the evolution of Br_y from the source gases has been carried out. For this purpose an ensemble of trajectories rising from the lower troposphere to the TTL within 6 to more than 90 days were initialized with observed mixing ratios in the boundary layer of all important organic bromine source gases and the free-up of Br_y by chemical and photochemical reactions was simulated. Bromoform, $CHBr_3$, was found to be the main source of inorganic bromine at the tropopause. The derived tropospheric lifetime of bromoform is 33 days. The modelled BrO mixing ratio at the tropopause (less than 2.5 pptv) is consistent with HALOX measurements which do not detect significant amounts of BrO there (<1-2 pptv). Therefore measurements of more than 4 pptv (as retrieved from SCIAMACHY) can only be explained trough processes not included in the model, i.e. very fast ascent of air masses from strong bromoform source regions or by injection of inorganic bromine on evaporating particles.

CONTENTS

LIST OF FIGURES

LIST OF TABLES

"A scientific approach to the examination of phenomena
is a defence against the pure emotion of fear."
(Tom Stoppard. Rosencrantz and Guildenstern Are Dead)

CHAPTER 1

Introduction

Long-term measurements have clearly shown that human activities are changing the composition of the Earth's atmosphere. These changes have caused the alteration of some natural atmospheric processes (e.g., greenhouse effect) along with the creation of several environmental problems (e.g., photochemical smog, stratospheric ozone depletion, acid precipitation, etc.) that did not exist prior to human industrialization.

Unlike the issue of acid rain, which has long been associated with human activities and documented by environmental observations, scientific concern about human-induced destruction of the stratospheric ozone layer dates only to about 1970. Ozone is a chain molecule consisting of three oxygen atoms (O_3) that absorbs certain wavelengths of biologically damaging ultraviolet light, which otherwise would cause undesirable consequences on the ecological system (losses in phytoplankton, etc.) and human health (an increase of skin cancer risk, cataracts, and a weakening of the immune system). Therefore the ozone layer plays an essential role in the Earth's ecological balance. The evolution of land life is believed to be tied closely to the formation of the protective ozone layer (*Solomon*, 1989). Chlorine and bromine containing compounds are able to catalyze ozone depletion and have been shown to threaten the ozone layer (*McElroy et al.*, 1986).

1.1 History and general relevance of bromine in the atmosphere

This work focuses on the role of Br species and their effect on ozone in the upper troposphere and lower stratosphere ($\sim$10-30 km altitude). Br chemistry also plays an important role in the boundary layer. This, however, will not be discussed here.

Ozone depletion observed in the stratosphere over the past three decades occurred because of the increase of some trace gas concentrations in the atmosphere. Bromine and chlorine species play a prominent role here. The increase in the atmospheric bromine amount was caused by anthropogenic production and use of brominated gases (such as Halons or methyl bromide) during the second half of the 20th century. Although natural sources of bromine exist as well, about half of the Br in the stratosphere originated from anthropogenic activities by the late 1990s (*WMO*, 2003).

The suggestion that bromine compounds released at the Earth's surface could destroy ozone in the stratosphere was first made in 1975 by *Wofsy et al.* (1975) and *Watson* (1975). In particular, stratospheric catalytic cycles involving bromine were discussed in these publications. But the effect on ozone was thought to be small. During the following decade bromine largely remained ignored except the publication from *Yung et al.* (1980), where he introduced the coupled BrO-ClO catalytic cycle to stratospheric halogen chemistry. However, *Yung et al.* (1980) concluded that bromine compounds were responsible for only slightly more then 2% of the total ozone depletion. A renewed interest in bromine chemistry was initiated in the middle of the 1980s after massive seasonal losses of ozone over Antarctica were reported. It has been shown that bromine plays a significant role in ozone depletion and thus in the formation of the ozone hole in polar stratospheric regions (*McElroy et al.*, 1986). McElroy estimated the effect of bromine in the polar stratosphere as high as 20-25% of the total ozone destruction.

A very important property of bromine is that compared to chlorine it is present in the stratosphere mostly in the active form of BrO (40-75%), capable to destroy ozone directly (*Lary*, 1996). Consequently, bromine has a high ozone depleting potential (by a factor of 45 higher than chlorine) (*WMO*, 1990, 1992).

1.2 Bromine sources, partitioning and chemistry

As mentioned above bromine enters the atmosphere by a variety of natural processes and anthropogenic activities. The main bromine source gases that can reach the stratosphere (i.e. could not be removed from the troposphere by rainout, reaction with OH or photolysis) are halons and methyl bromide (CH_3Br). The latter is the most abundant of these source gases. Its natural source is mainly due to oceanic biological processes and biomass burning. The main industrial use of bromine compounds is in fire extinguishers (halons) as well as a tool for the treatment of soils and wood (methyl bromide). It is also used in quarantine treatments and in insect and rodent control. An other minor source of bromine compounds is of volcanic activity (*Bobrowski et al.*, 2003). Information about bromine source gases is summarized in Table 1.1.

When these substances are transported to higher altitudes in the troposphere and the stratosphere, they are converted into inorganic forms of bromine ($Br_y = Br + BrO + HOBr + BrONO_2 + HBr + BrCl$) by photolysis or reactions with OH and $O(^1D)$. Model simulations suggest that almost all stratospheric inorganic bromine is in the form of BrO, $BrONO_2$, and $HOBr$ (Fig. 1.1) (and $BrCl$ if chlorine is activated) and that BrO can represent 30-70% of the total Br_y during sunlit hours (*Lary*, 1996; *Sinnhuber et al.*, 2002). *Avallone et al.* (1995) mentioned 40% as the fraction of BrO in Br_y.

At mid-latitudes $HOBr$ and $BrONO_2$ are supposed to be the main reservoir bromine compounds (*Lary*, 1996). This state is due to abundant HO_2 and NO_2 there. They react with BrO yielding those reservoirs. But in the polar winter the amounts of HO_2 and NO_2 are significantly smaller. That is why, if chlorine is activated, $BrCl$ is supposed to be the main reservoir there (*McKinney*, 1998). The reaction between ClO and BrO is the source of $BrCl$ in the polar winter.

Since bromine monoxide is the key compound in the stratospheric bromine chemistry, it is essential to indicate its sources and sinks separately.

The main sources of BrO are the reactions:

$$Br + O_3 \rightarrow BrO + O_2 \tag{1.1}$$

$$BrONO_2 + hv \rightarrow BrO + NO_2 \tag{1.2}$$

Table 1.1: The main bromine source gases

Source Gas	**Formula**	**Local Lifetime (days)**	**Atmospheric Source (N=natural; A=anthropogenic)**	**Reported Tropospheric Mixing Ratio (ppt)**
Bromochloromethane (Halon-1011)	CH_2BrCl	150	entirely N	0.38-0.59
Dibromomethane	CH_2Br_2	120	entirely N	0.8-3.4
Dibromochloromethane (Halon-1012)	$CHBr_2Cl$	78	N (open ocean) (partly A)	0.1-0.5
Bromodichloromethane (Halon-1021)	$CHBrCl_2$	69	N (open ocean) (partly A)	0.12-0.6
Bromochlorodifluoromethane (Halon-1211)	$CBrClF_2$	12-15 years	A (fire extinguisher)	4
Bromotrifluoromethane (Halon-1301)	$CBrF_3$	110 years	A (fire suppression agent)	2.6-3.3
Tribromomethane (bromoform)	$CHBr_3$	26	N (partly A)	0.6-3.0
Bromomethane (methyl bromide)	CH_3Br	256	N (ocean algae and kelp) (partly anthropogenic (agriculture and industry))	8.1-8.5

In the lower stratosphere the destruction of BrO occurs mainly by photolysis and reactions with NO, NO_2, and HO_2:

$$BrO + hv \rightarrow Br + O \tag{1.3}$$

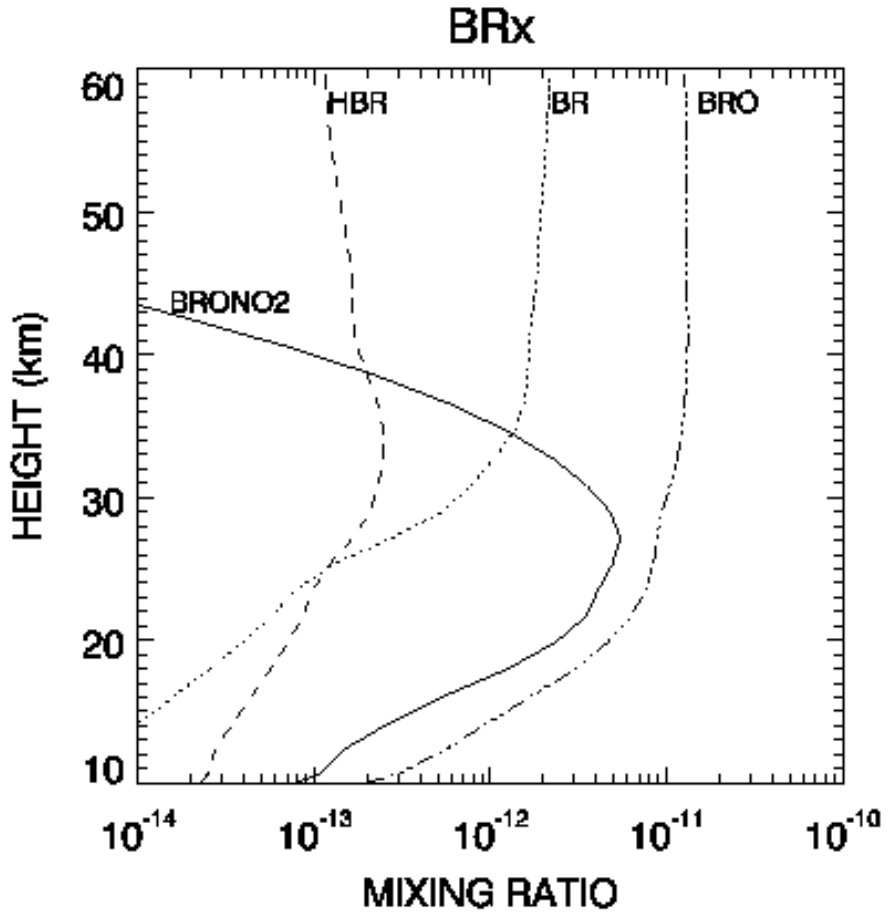

Figure 1.1: Approximate vertical distribution of the Br_y family in atmosphere from Mainz-2D model (*Gidel et al.*, 1983; *Grooß*, 1996) (daytime mid-latitude conditions). $HOBr$ is not included in this model.

$$BrO + NO \rightarrow Br + NO_2 \tag{1.4}$$

$$BrO + NO_2 \rightarrow BrONO_2 \tag{1.5}$$

$$BrO + HO_2 \rightarrow HOBr + O_2 \tag{1.6}$$

In the lower stratosphere the reaction of BrO with ClO contributes a few percent to the loss rate of BrO. The scheme of atmospheric bromine chemistry is shown in Fig.1.2. All measurements suggest that the BrO mixing ratio increases with altitude in the stratosphere at all latitudes reaching its maximum of $8 - 15$ pptv around $25 - 30$ km.

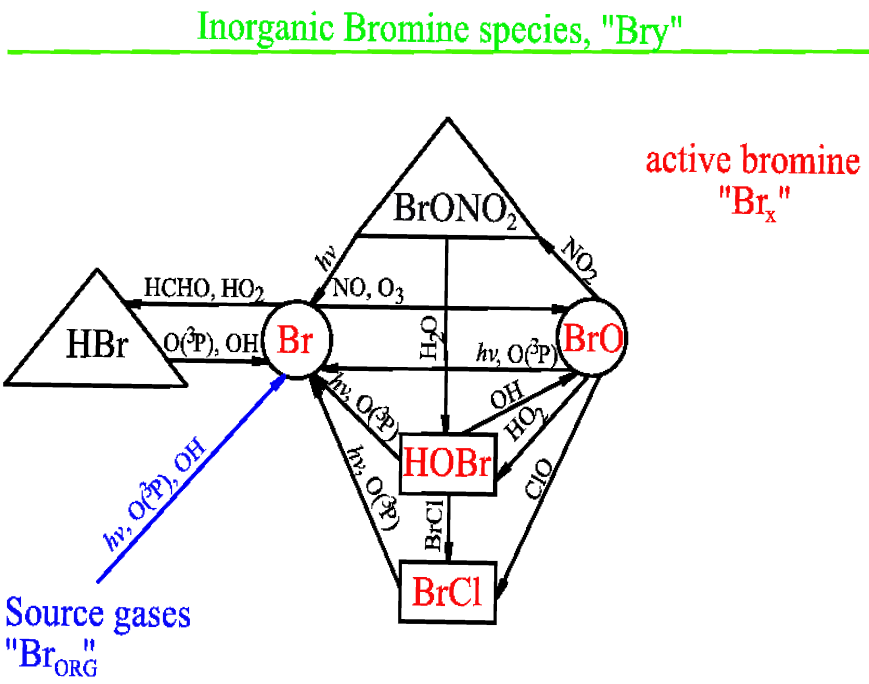

Figure 1.2: Scheme of atmospheric bromine chemistry (adopted from *Lary* (1996))

1.3 Motivation of this work

The Montreal Protocol on Substances that Deplete the Ozone Layer was signed in 1987, aiming the phase-out of many ozone-depleting substances (including bromine). Because of insufficient effectiveness of the original protocol, it has been strengthened by a number of amendments and adjustments (London, 1990; Copenhagen, 1992; Vienna, 1995; Montreal, 1997; Beijing, 2000). The effect of the protocol and its amendments has to be monitored to see if the stratospheric bromine load is leveling off, decreasing or will even increase in future.

The further development of the stratosphere is rather uncertain. The stratosphere is expected to cool in the future, because of greenhouse gases reducing the heat flow from the Earth surface. The dynamics of the stratosphere may change and its consequences are not clear. This will lead, for example, to more effective chlorine activation and additional ozone loss. Thus, it is very important to reduce emissions of all ozone depleting substances including bromine as much as possible and to monitor the temporal trend of bromine in the stratosphere, most effectively by means of well validated satellite measurements.

Despite the importance of bromine compounds mentioned in the previous Section, there are only few measurements of them in the stratosphere (apart from BrO).

Several CH_3Br measurements have been made in different parts of the world (*Berg et al.*, 1984; *Rasmussen and Khalil*, 1984; *Penkett et al.*, 1985; *Cicerone et al.*, 1988; *Fabian et al.*, 1994; *Kaye et al.*, 1994). Only a few measurements of stratospheric HBr and an upper limit of $HOBr$ are available (*Johnson et al.*, 1995; *Nolt et al.*, 1997). The measurements suggest that in the range 22-34 km the average mixing ratio of HBr is 2.0±0.8 ppt, and that the average mixing ratio of $HOBr$ is less than 2.8 ppt. Br, $BrONO_2$, and $BrCl$ have never been measured.

As already mentioned, BrO represents 30-70% of the total inorganic bromine during sunlit hours (*Lary*, 1996; *Sinnhuber et al.*, 2002). As a consequence, most of the experimental information about stratospheric bromine comes from BrO. The ground-based measurements report significant seasonal and latitudinal variations of BrO column amounts. The column density is larger in the winter and at high latitudes than in the mid-latitude summer (*Arpag et al.*, 1994; *Fish et al.*, 1997; *Richter et al.*, 1999; *Kreher et al.*, 1997; *Otten et al.*, 1998; *Sinnhuber et al.*, 2002). Global observations by GOME and SCIAMACHY demonstrate similar latitudinal and seasonal variations (*Wagner and Platt*, 1998; *Richter et al.*, 1998, 2002; *Wagner*, 1999; *Sinnhuber et al.*, 2005). According to these measurements, the variation of the stratospheric column of BrO anticorrelates with that of NO_2 measured by the same instruments. That is why it has been suggested that the amount of BrO is considerably controlled by nitrous oxide through their reaction with each other having $BrONO_2$ as a product (*Fish et al.*, 1997; *Richter et al.*, 1999). The influence of chlorine is still not unambiguously characterized. Some groups report an increase of BrO columns inside the vortex (*Aliwell et al.*, 1997; *Otten et al.*, 1998), others do not (*Grendel et al.*, 1996; *Richter et al.*, 1999). The situation is the same for in-situ measurements: some of them reveal increased BrO mixing ratios in the vortex (*Brune et al.*, 1989b; *Toohey et al.*, 1990), other do not (*Avallone et al.*, 1995).

Another aspect is that measurements of vertical BrO distribution are mainly available in the stratosphere only, because BrO mixing ratios in the tropopause and below it are usually close to the detection limits of the instruments. That is why there are only assumptions about the amount of tropospheric bromine. In particular, it has been proposed that significant amounts of inorganic bromine could be present in the troposphere and transported into the stratosphere (*Ko et al.*, 1997). The vertical BrO column from GOME satellite measurements (*Chance*, 1998) during May 1997 is much larger than that of the AER (Atmospheric and Environmental Research) model of Jet

Propulsion Laboratory in the USA (*Salawitch et al.*, 2005). As a possible reason, an unaccounted global background level of 1 to 2 ppt of BrO in the free troposphere was proposed by *Platt and Hönninger* (2003). This statement was supported by observations of *Richter et al.* (1998); *Van Roozendal M. et. al* (2002); *McElroy et al.* (1999); *Pundt et al.* (2002); *Fitzensberger et al.* (2000); *Sinnhuber et al.* (2005) in the free troposphere. There BrO concentrations of the order of 1 - 3 pptv have been observed. This amount of BrO in the troposphere was attributed to processes on sea ice releasing bromine into the atmosphere (*Kaleschke et al.*, 2004). Therefore, such processes could lead to higher total bromine amounts in the stratosphere (*Dvortsov et al.*, 1999; *Schauffler et al.*, 1999; *Sturges et al.*, 2000; *Pfeilsticker et al.*, 1994). The suggested tropospheric background was, however, not supported by ground-based measurements of diffuse and direct sunlight over Lauder, New Zealand (45°S), which revealed a mean value for tropospheric BrO of 0.2 ppt reaching a maximum of 0.9 ppt (*Schofield et al.*, 2004).

The Very Short-Lived organic bromine Substances VSLS (i.e. bromoform, $CHBr_3$) contribution to the entire bromine budget is of crucial importance, but only poorly understood. The easiest way to assess the influence of short-lived organic bromine species is to measure BrO profiles in the tropics, since air masses quickly ascend from the lower atmosphere to the upper tropospheric and lower stratospheric layers in this region. Unfortunately, measurements performed by different instruments demonstrate significant discrepancies exactly in this region. That is why additional measurements close to the tropopause are essential to clear up the above-mentioned vagueness.

The Chemical Lagrangian Model of the Stratosphere (CLaMS) is an appropriate tool for simulations of tropospheric and stratospheric chemistry. Initializing the CLaMS using organic bromine source gases measurements at the Earth's surface, it is possible to assess the contribution of organic bromine species to the stratospheric bromine and to calculate an amount of BrO in the tropopause region. Such simulation was performed within this work.

Since 2002 the SCIAMACHY instrument on-board the ENVISAT satellite provides daily measurements of BrO. Considering the importance of BrO, SCIAMACHY measurements require appropriate validation, i.e. the estimation of the satellite data quality by means of its comparison with independent measurements obtained by other well-established instruments which are co-located in time and space as closely as possible. Currently, three different groups retrieve vertical BrO profiles from the SCIAMACHY satellite data. Unfortunately retrievals differ from each other significantly. These differences reach sometimes 100%. Since the TRIPLE balloon instrument, used in this work, performs its measurements using a completely different detec-

tion technique than SCIAMACHY employs, its measurement results are very important for the validation of this satellite instrument.

There is certainly a counter-question: does TRIPLE itself provide reliable measurements? To proof this numerous laboratory calibrations and internal consistency checks were needed and performed within this work.

The present thesis is organized as follows. Chapter 2 introduces the chemistry of bromine compounds in the upper troposphere and lower stratosphere. Chapter 3 presents the chemical conversion resonance fluorescence technique for the measurement of ClO and BrO as well as its calibration. Since a main aspect of the measurements was satellite validation, the ultra-violet absorption technique employed by SCIAMACHY satellite instrument is also briefly discussed. Chapter 4 describes the flights performed by the TRIPLE balloon and HALOX instruments considered in this work. Chapter 5 gives an overview of the CLaMS chemical model employed in this thesis. It also presents results of a measurement-model comparison for the flight on 9 June 2003. Chapter 6 presents the results of TRIPLE and HALOX BrO measurements as well as their comparison with the SCIAMACHY BrO profiles. The CLaMS simulations of the tropical tropospheric bromine chemistry are presented in Chapter 7, which is followed by Chapter 8 containing conclusions and an outlook.

CHAPTER 2

The Role of bromine in ozone depletion

This chapter introduces the chemistry of bromine compounds in the upper troposphere and lower stratosphere as well as their role in ozone depletion. A short review of the atmospheric structure is given in Appendix A.

2.1 Vertical and global distribution of ozone

Most of the Earth's ozone is found in the stratosphere, in the region which is commonly called "ozone layer" (Fig.A.1), and its daily creation and destruction is a natural process. But even there, near the peak of its concentration, it reaches a value of about 10 ppm (part per million), only 10 ozone molecules per 1 million of others.

The depth of the ozone layer is measured in Dobson units. If all ozone above a certain point would be compressed to 1 atmosphere pressure and its temperature would be $0°C$, then 1 mm of this layer thickness would correspond to 100 Dobson units (DU). Typical values vary between 200 and 500 DU over the globe.

Ozone is absorbing UV radiation of wavelengths shorter than 300 nm.

From November 1978 the Total Ozone Mapping Spectrometer (TOMS) on-board the American satellite Nimbus-7 provided global measurements of total column ozone on a daily basis (Fig.2.1). From the figure one can see that ozone varies strongly with latitude over globe, with the largest values occurring at middle and high latitudes. This is a result of the global circulation that moves tropical air rich in ozone toward the poles in fall and winter.

The so-called ozone hole was discovered taking the average vertical Oc-

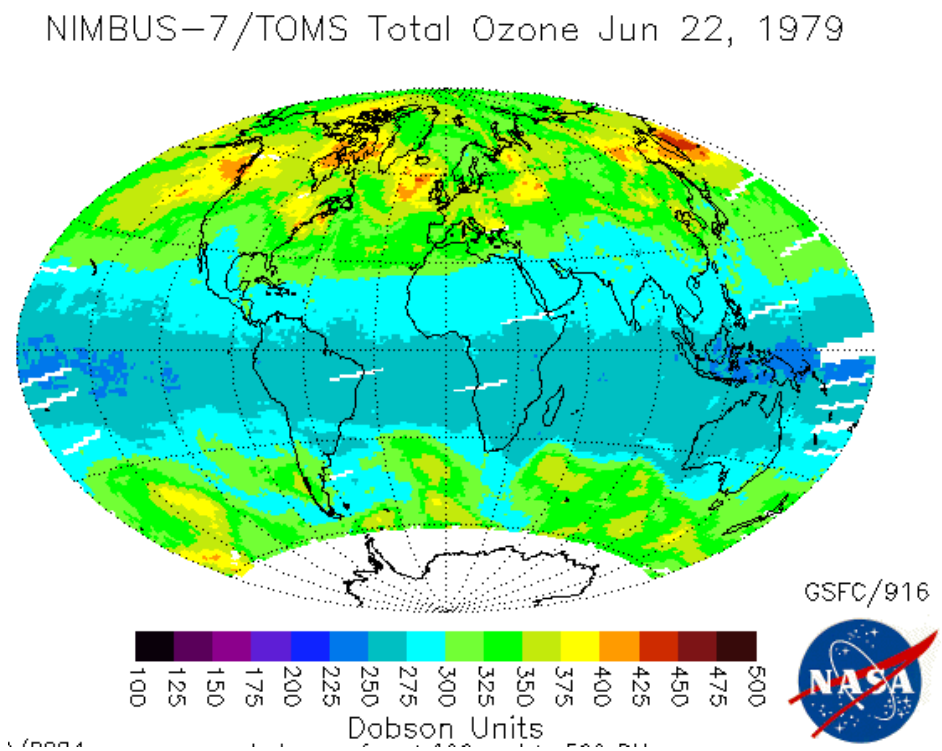

Figure 2.1: Global ozone (*TOMS team*, 2006)

tober Antarctic ozone profiles into consideration, it can be seen that before the 1980s the ozone layer was clearly present as shown using average ozone values from balloon observations made between 1962 and 1971 (blue line left in Fig.2.2). In more recent years, as shown for 2^{nd} October 2001, ozone is destroyed completely between 14 and 20 km in the Antarctic in spring (red line left in Fig.2.2). Average October values in the ozone layer now are reduced by 90% from pre-1980 values (green line in Fig.2.2). The Arctic ozone layer is still present in spring as shown by the average March profile obtained over Finland between 1988 and 1997 (blue line right in Fig.2.2). However, March Arctic ozone values in some years are often below normal average values as shown here for 30^{th} March 1996 (red line right in Fig.2.2).

The above-mentioned phenomenon is commonly known as ozone "hole". The ozone "hole" is not a real hole. It is actually a reduction in concentrations of ozone in the stratosphere. The ozone hole is defined geographically as the area wherein the total ozone amount is less than 220 Dobson Units (*Bureau of Meteorology, Ozone Science Unit*, 1991).

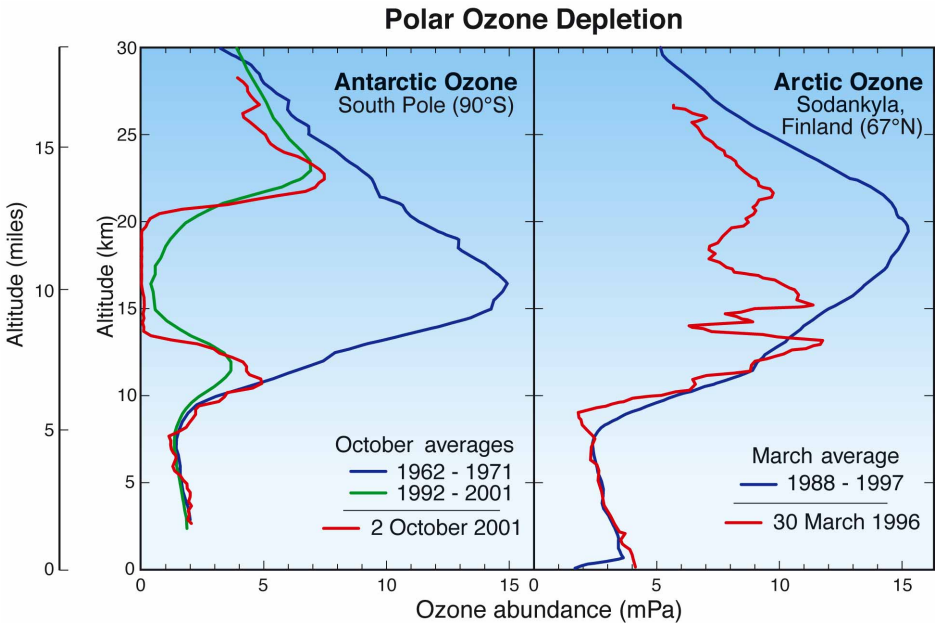

Figure 2.2: Arctic and Antarctic ozone vertical distribution (*Fahey*, 2003)

2.2 Ozone destructive catalytic cycles involving bromine

Catalytic cycles involving bromine are responsible for a significant fraction of the ozone loss. They are schematically represented in Fig.2.3 and will now be considered in turn.

2.2.1 BrO/ClO

In winter polar regions, when chlorine is activated (its reactive fraction is higher then usually), the coupling of BrO and ClO chemistry via the BrO/ClO catalytic cycle is very important. There are two routes for it. In the first one (Route I) $BrCl$ is formed:

$$BrO + ClO \rightarrow BrCl + O_2 \tag{2.1}$$

$$BrCl + h\nu \rightarrow Br + Cl \tag{2.2}$$

$$Br + O_3 \rightarrow BrO + O_2 \tag{2.3}$$

$$\underline{Cl + O_3 \rightarrow ClO + O_2} \tag{2.4}$$

$$Net : 2O_3 \rightarrow 3O_2 \tag{2.5}$$

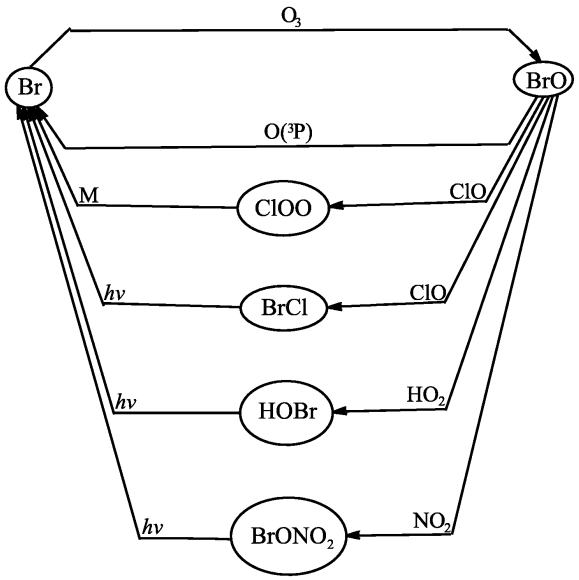

Figure 2.3: The bromine gas phase catalytic ozone destruction cycles (adopted from *Lary* (1996))

In 1996 D. J. Lary introduced the concept of the chain effectiveness (*Lary*, 1996). It is the chain length (number of times the catalytic cycle can repeat) multiplied by the rate of the cycle's rate-limiting step. For instance, in the lower stratosphere the rate-limiting step for Route I is the photolysis of $BrCl$. However, higher up in the stratosphere the rate-limiting step is the formation of $BrCl$. The chain effectiveness of this cycle as well as other catalytic cycles mentioned below is listed in Table 2.1.

Table 2.1: Chain effectiveness of some ozone destruction catalytic cycles

Cycle	**Chain effectiveness** ($molecules \cdot cm^{-3} \cdot s^{-1}$)
BrO/ClO	10^6 (Route I) - 10^8 (Route II)
BrO/HO_2	10^6
$BrO/O(^1D)$	10^3 (at 12 km) - 10^9 (at 38 km)
Cl/ClO	10^2 (at 12 km) - 10^{10} (at 38 km)
BrO/NO_2	10^7
ClO/NO_2	10^5 (at tropopause) - 10^2 (at 38 km)

The alternative cycle (Route II) forms $ClOO$:

$$BrO + ClO \rightarrow Br + ClOO \tag{2.6}$$

$$ClOO + M \rightarrow Cl + O_2 \tag{2.7}$$

$$Br + O_3 \rightarrow BrO + O_2 \tag{2.8}$$

$$\underline{Cl + O_3 \rightarrow ClO + O_2} \tag{2.9}$$

$$Net : 2O_3 \rightarrow 3O_2 \tag{2.10}$$

The rate-limiting step for this cycle is the $ClOO$ formation.

The reaction between BrO and ClO can follow one more route (*Vaida and Simon*, 1995):

$$BrO + ClO \rightarrow OClO + Br \tag{2.11}$$

$$OClO + hv \rightarrow ClO + O \tag{2.12}$$

$$O + O_2 \rightarrow O_3 \tag{2.13}$$

At 195 K using JPL 2002 kinetics (*Sander et al.*, 2003), the modeling suggests that 59% of the reaction between BrO and ClO follow this route. However, this route does not destroy ozone, because (2.12) regenerates odd oxygen.

2.2.2 BrO/HO_2

The BrO/HO_2 catalytic cycle involves the formation of $HOBr$:

$$HO_2 + BrO \rightarrow HOBr + O_2 \tag{2.14}$$

$$HOBr + hv \rightarrow OH + Br \tag{2.15}$$

$$Br + O_3 \rightarrow BrO + O_2 \tag{2.16}$$

$$\underline{OH + O_3 \rightarrow HO_2 + O_2} \tag{2.17}$$

$$Net : 2O_3 \rightarrow 3O_2 \tag{2.18}$$

Below about 15 km the rate-limiting step for this cycle is the photolysis of $HOBr$. Higher up - the formation of $HOBr$. At 20 km this cycle is twice as effective as the NO/NO_2 catalytic cycle.

The analogous ClO/HO_2 catalytic cycle has a much shorter chain length (less than 50) above 15 km, where the rate-limiting step is the photolysis of $HOCl$. Between 15 and 20 km the BrO/HO_2 cycle is between 1 and 2 orders of magnitude more effective than the ClO/HO_2 cycle in terms of destroying ozone. This fact underlines the importance of atmospheric bromine for catalytic ozone destruction.

2.2.3 $BrO/O(^1D)$

The importance of the Br/BrO catalytic cycle increases with altitude, because of the abundance of atomic oxygen

$$Br + O_3 \rightarrow BrO + O_2 \tag{2.19}$$

$$\underline{BrO + O \rightarrow Br + O_2} \tag{2.20}$$

$$Net : O_3 + O \rightarrow 2O_2 \tag{2.21}$$

The reaction of BrO with atomic oxygen is the rate limiting step. The analogous Cl/ClO cycle has a shorter chain length - from 10 in the lower stratosphere to 10^3 higher up.

Comparing the chain effectiveness of different catalytic cycles *Lary* (1996) came to the conclusion that at 38 km the NO/NO_2 cycle is the most effective ozone loss cycle but higher up the Cl/ClO becomes more effective (*Stolarski and Cicerone*, 1974; *Molina and Rowland*, 1974).

2.2.4 BrO/NO_2

Burkholder et al. (1995) has pointed out that a very effective BrO/NO_2 catalytic cycle can exist:

$$BrO + NO_2 + M \rightarrow BrONO_2 \tag{2.22}$$

$$BrONO_2 + hv \rightarrow Br + NO_3 \tag{2.23}$$

$$NO_3 + hv \rightarrow NO + O_2 \tag{2.24}$$

$$NO + O_3 \rightarrow NO_2 + O_2 \tag{2.25}$$

$$\underline{Br + O_3 \rightarrow BrO + O_2} \tag{2.26}$$

$$Net : 2O_3 \rightarrow 3O_2 \tag{2.27}$$

Depending on the conditions, the rate-limiting step of the cycle is the photolysis of $BrONO_2$ or of NO_3. *Toumi et al.* (1993) showed that the ClO/NO_2 cycle is only important for high levels of ClO and NO_2. For typical levels of $BrONO_2$ and $ClONO_2$ the BrO/NO_2 cycle is more effective at removing ozone than the analogous ClO/NO_2 cycle.

So in the low stratosphere the most effective ozone loss cycles involving bromine are the BrO/HO_2 and BrO/ClO cycles. These cycles are effective in terms of ozone destruction even when no polar stratospheric clouds are present, however, the BrO/ClO cycle is much faster, when ClO is activated.

2.3 Bromine as a very effective catalyst

To illustrate the effectiveness of bromine in ozone destruction let us consider in detail the reaction of ozone destruction by atomic oxygen:

$$O_3 + O \rightarrow O_2 + O_2(k_1) \tag{2.28}$$

This reaction is quite slow: the rate constant is $k_1 = 8. \times 10^{12} exp(\frac{-2060}{T})$ (*Atkinson et al.*, 2001). For typical stratospheric temperatures around 220 K, we obtain $k_1 = 6.9 \times 10^{-16} cm^3 \cdot s^{-1}$. The rate of this reaction is $v = \frac{-d[O_3]}{dt} = k_1 \cdot [O_3] \cdot [O]$. Approximate ozone concentration at the altitude of 25 km is $4. \times 10^{12} cm^{-3}$ (*Brasseur et al.*, 1999), concentration of atomic oxygen is $3. \times 10^6 cm^{-3}$. Therefore the rate of the reaction (2.28) is $v = 4.4 \times 10^3 cm^{-3} \cdot s^{-1}$ (≈0.45 ppb/day). In the presence of a catalyst there will be following reactions simultaneously with (2.28):

$$O_3 + X \rightarrow XO + O_2(k_2) \tag{2.29}$$

$$\underline{O + XO \rightarrow X + O_2}(k_3) \tag{2.30}$$

$$Net : O_3 + O \rightarrow 2O_2 \tag{2.31}$$

The total reaction rate of these reactions can be significantly faster than that of the reaction (2.28). Important is that the catalyst is reformed after each cycle. The chain can be repeated indefinitely until all O_3 is destroyed or until the catalyst is removed by some competing process. The total rate of the reaction of ozone destruction in a system consisting of O_3, O, X, and XO can be calculated from the system of kinetic equations:

$$v_i = k_1 \cdot [O_3] \cdot [O] + k_2 \cdot [O_3] \cdot [X] \tag{2.32}$$

$$\frac{d[X]}{dt} = k_3 \cdot [O] \cdot [XO] - k_2 \cdot [O_3] \cdot [X] = 0, \tag{2.33}$$

where the index "i" means that the reaction runs in presence of catalyst, k_2 and k_3 - the reaction rates of reactions (2.29) and (2.30) correspondingly. Assuming that total catalyst concentration in a system $[X + XO] = [X] + [XO]$, we obtain $v_i = k_1 \cdot [O_3] \cdot [O] + \frac{k_2 \cdot k_3 \cdot [O] \cdot [O_3] \cdot [X+XO]}{k_2 \cdot [O_3] + k_3 \cdot [O]}$. The ratio of $\frac{v_k}{v} = A_i$ could be interpreted as the rate of the reaction acceleration. It depends on the ratios between the reaction rates k_1, k_2, and k_3, and on the concentrations $[O_3]$, $[O]$, and the catalyst $[X + XO]$.

There are a lot of catalytic ozone destruction cycles. Let, as example, consider three of them: nitrogen, chlorine, and bromine cycles. In the nitrogen cycle $X = NO$, $XO = NO_2$; for chlorine: $X = Cl$, $XO = ClO$; and for bromine: $X = Br$ and $XO = BrO$. If we assume the temperature to be 220 K then the corresponding reaction rates will be equal:

- for the nitrogen cycle:
  $k_2 = 3.7 \times 10^{-15} cm^3 \cdot s^{-1}$ (*Atkinson et al.*, 2001);
  $k_3 = 1.4 \times 10^{-11} cm^3 \cdot s^{-1}$ (*Estupinan et al.*, 2001);
- for the chlorine cycle:
  $k_2 = 8.8 \times 10^{-12} cm^3 \cdot s^{-1}$ (*Atkinson et al.*, 2001);
  $k_3 = 2.1 \times 10^{-11} cm^3 \cdot s^{-1}$ (*Goldfarb et al.*, 2001);
- for the bromine cycle:
  $k_2 = 4.5 \times 10^{-13} cm^3 \cdot s^{-1}$ (*Atkinson et al.*, 2001);
  $k_3 = 5.4 \times 10^{-11} cm^3 \cdot s^{-1}$ (*DeMore et al.*, 1997);

The dependence of the rate of the acceleration on the ratio of catalyst $[X + XO]$ to ozone ($A_i = \frac{v_k}{v}$) is shown in Fig. 2.4. It obviously shows that BrO

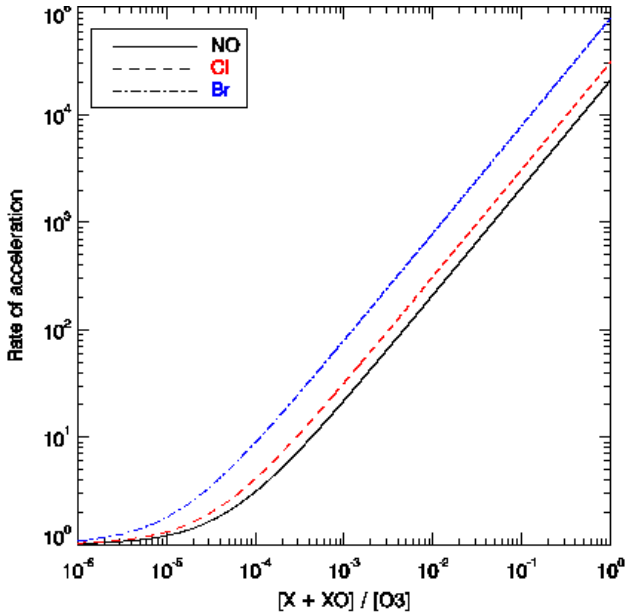

Figure 2.4: The dependence of the rate of ozone destruction acceleration on the ratio of catalyst and ozone concentrations

is a very effective catalyst. One has, however, to keep in mind that all these calculations are relevant at altitudes higher than 20 km, where atomic oxygen concentration is high. On the other hand Br_y is luckily less abundant than Cl_y and NO_y.

CHAPTER 3

The TRIPLE balloon and HALOX aircraft instruments

This chapter presents the chemical conversion resonance fluorescence (CCRF) technique for the measurement of ClO and BrO as well as its calibration. Since a main aspect of the measurements was satellite validation the ultraviolet absorption technique employed by the SCIAMACHY satellite instrument is also briefly discussed.

To complete the understanding of ozone depletion in the atmosphere, it is essential to measure the abundance of halogen species, especially the halogen oxides ClO and BrO. This task, however, is very challenging. Stratospheric mixing ratios of halogen radicals range from less than 1 ppt up to 2000 pptv (in polar vortex) for ClO and up to 20 pptv for BrO. Hence, appropriate measurement techniques have to be very sensitive in order to detect such low mixing ratios.

Secondly, since both chlorine and bromine monoxide are very reactive, not every technique can be applied for their detection. For example, whole air sampling is not an appropriate method as the halogen radicals decompose or react at the inner surface of the collecting container. Besides, chlorine and bromine monoxides are rather short-lived even in the gas phase (the stratospheric lifetime about is 10-15 s), so they could never be transported in a laboratory for subsequent detection there.

3.1 The measurement of BrO in the atmosphere

There are not many observational techniques for BrO. For its detection, both in-situ (observation at the location of the instrument) and remote sensing (observation of the interaction of electromagnetic waves with the species in the atmosphere along the line of sight of the instrument) techniques can be used. The only in-situ technique is the chemical convertion resonance fluorescence (CCRF). This will be presented in detail below in this Chapter.

BrO abundances have also been estimated indirectly by spectroscopic measurements of $OClO$ (*Solomon et al.*, 1989). It is possible, because $OClO$ is only produced in the reaction of BrO and ClO and is therefore an evidence of the presence of both species.

The only other well described method is the differential optical absorption spectrometry (DOAS).

UV-visible absorption spectrometry

Since the early 1970s ground-based measurements of the UV and visible light scattered from the zenith sky have been used by several research groups (*Brewer et al.*, 1973; *Pommereau and Goutail*, 1988) to determine the absorption and thereby the atmospheric column densities of various trace gases (e.g., O_3, NO_2). These measurements identify specific absorption features by use of the DOAS method (*Platt et al.*, 1979). DOAS enabled the detection of some gases for the first time ($HONO$, OH, NO_3, BrO, $OClO$).

DOAS uses the narrow molecular absorption bands to identify trace gases and their absorption strength to retrieve tropospheric and stratospheric trace gas concentrations. The major advantage of DOAS is the ability to measure absolute trace gas concentrations without disturbing their chemical behavior. DOAS is therefore especially useful to measure highly reactive species, such as the free radicals OH, NO_3, or BrO. The measurements can be performed continuously and with a high time resolution of typically a few minutes.

DOAS can be subdivided into 2 principal categories: passive and active ones. Active DOAS systems use an artificial lamp as a light source. Passive DOAS, in contrast, uses an extraterrestrial light source (the Sun, the Moon or stars). Passive DOAS measurements, in their turn, can be subdivided into two further categories: the first one uses direct solar, lunar or stellar light, and the second one - scattered sun light. The direct sun light measurements have the advantage of a high amount of analyzed photons and an easy geometry, but are limited along the line-of-sight from the detector to the Sun. Ground-

based applications are additionally limited to cloud-free conditions.

The general principle of DOAS is the following: light, with an intensity $I_0(\lambda)$, emitted by a suitable source passes through the atmosphere and is collected by a telescope. During its way through the atmosphere the light undergoes absorption processes by different trace gases and scattering by air molecules and aerosol particles. The intensity $I(\lambda, L)$ at the end of the light path is given by expression (3.1) with Lambert-Beer's law. The absorption of a trace species j is characterized by its absorption cross section $\sigma_j^{ABS}(\lambda, p, T)$, which depends on the wavelength λ, the pressure p and the temperature T, and by its number density $\rho_j(l)$ at the position l along the light path. The Rayleigh extinction (because of scattering by molecules of air) and Mie extinction (by aerosols) is described here by $\varepsilon_R(\lambda, l)$ and $\varepsilon_M(\lambda, l)$. $N(\lambda)$ is the photon noise depending on $I(\lambda, L)$.

$$I(\lambda, L) = I_0(\lambda)\times$$
$$\times\, exp\left\{\int_L \sum_j \left[-\sigma_j^{ABS}(\lambda, p, T) \times \rho_j(l)\right] - \varepsilon_R(\lambda, l)dl - \varepsilon_M(\lambda, l)dl\right\} + N(\lambda) \tag{3.1}$$

L indicates the entire light path through the atmosphere and j - all species met along the light path. Relation (3.1) is taken from *Stutz and Platt* (1996).

The typical quantity derived from such measurements is a differential slant column density (Fig.3.1). Figure 3.2 shows schematically the paths of sunlight reaching the satellite through the atmosphere, reflected by the earth's surface and scattered in the atmosphere. As the light follows these paths, some of the photons are absorbed by the trace gases in the atmosphere. The spectrum of the light measured by the satellite thus provides information on the trace gases along the entire light path. In other words, the measured quantity for a given gas, such as BrO, is the amount of this gas along the entire path. This is usually called the slant column density.

Since 1993 the so called BREDOM (Bremian DOAS Network for Atmospheric Measurements) exists. It consists of four ground-based DOAS instruments placed in: Bremen (Germany), Ny-Ålesund (Norway), Nairobi (Kenya), and Mérida (Venezuela). The BREDOM network is mainly designed for satellite validation. All instruments are measuring continously. Using the zenith-viewing direction, the stratospheric column amount of BrO is retrieved routinely.

The same type of measurements is performed from time to time using DOAS instruments developed at the University of Heidelberg. Several field campaigns were performed at Arrival heights (Antarctica), on the coast of the

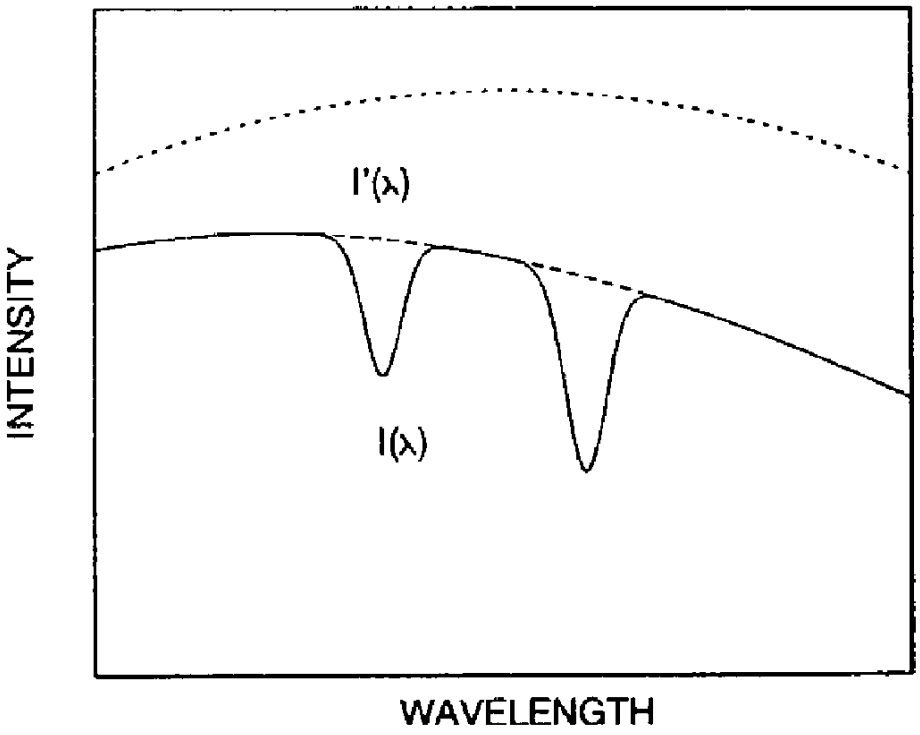

Figure 3.1: Principle of DOAS: Dotted curve, initial intensity distribution of the light source $I_0(\lambda)$; solid curve, measured intensity at the end of the light path $I(\lambda, L)$; dashed curve, calculated new baseline $I_0'(\lambda)$. The differential slant column density is proportional to $ln(\frac{I_0'(\lambda)}{I(\lambda,L)})$ (*Brauers et al.*, 1995)

Hudson Bay (Canada). In the frame of the BREDOM network additional instruments have been set-up temporarily in different stations such as the Zugspitze (Germany), Summit (Greenland) or Sylt (Germany) (*Carroll et al.*, 1989; *Solomon et al.*, 1989; *Fish et al.*, 1997; *Richter et al.*, 1999; *Otten et al.*, 1998; *Friess et al.*, 1999; *Sinnhuber et al.*, 2002).

The DOAS technique for BrO detection has successfully been used on satellite platforms. Since 1996 the GOME (Global Ozone Monitoring Experiment) instrument on-board ERS-2 satellite has routinely monitored global atmospheric BrO vertical columns (*Wagner and Platt*, 1998; *Richter et al.*, 2002; *Hegels et al.*, 1998; *Burrows et al.*, 1999). Another source that provides a global view on stratospheric BrO is the Scanning Imaging Absorption Spectrometer for Atmospheric Cartography (SCIAMACHY) on-board the ENVISAT satellite. It provides BrO observations by measuring the scattered and reflected solar radiation in limb and nadir geometry (*Sinnhuber et al.*, 2005).

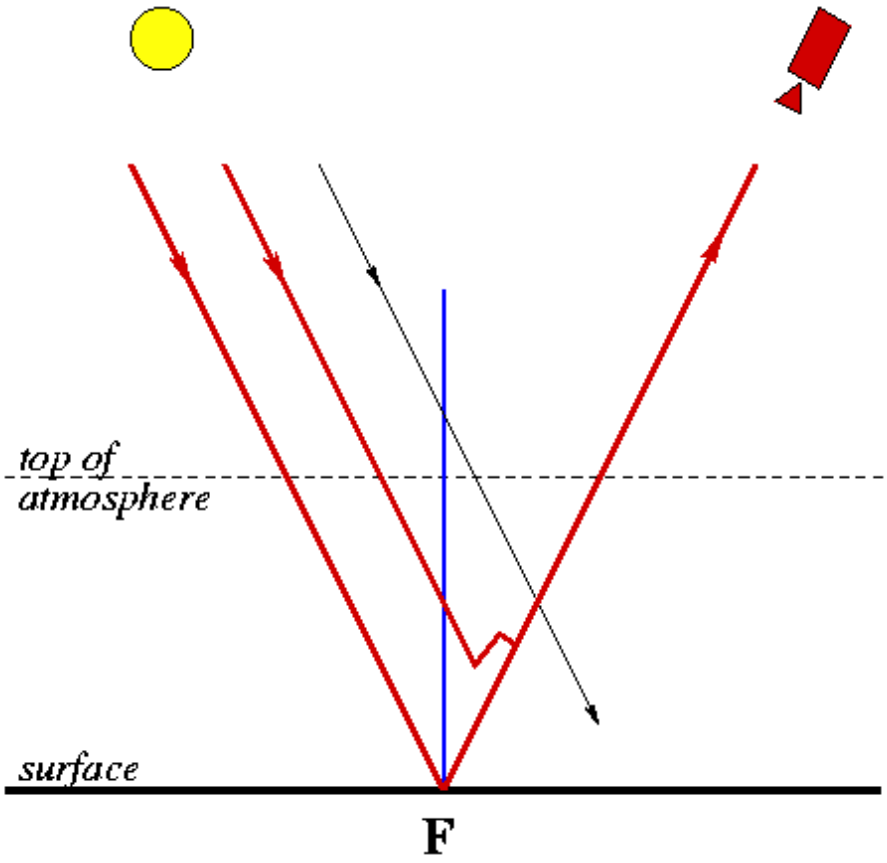

Figure 3.2: Schematic representation of the slant path (thick red lines) of incoming sunlight through the earth's atmosphere to the satellite. A part of the light reaching the satellite is reflected by the earth's surface, another part is scattered higher in the atmosphere. The thick blue line represents the "vertical column" (*van Geffen and Roozendael*, 2006)

It was launched in March 2002 as a joint project of Germany, the Netherlands and Belgium. It measures atmospheric absorption in spectral bands from the ultraviolet to the near infra-red (240 nm - 2380 nm), providing knowledge about the composition, dynamics and radiation balance of the atmosphere. SCIAMACHY has three different viewing geometries: nadir, limb, and sun/moon occultation which yield total column values as well as distribution profiles in the stratosphere and (in some cases) the troposphere for trace gases (including BrO) and aerosols.

In limb mode, looking forward and starting at the Earth horizon the atmosphere is scanned tangentially over a 1000 km swath. At the end of

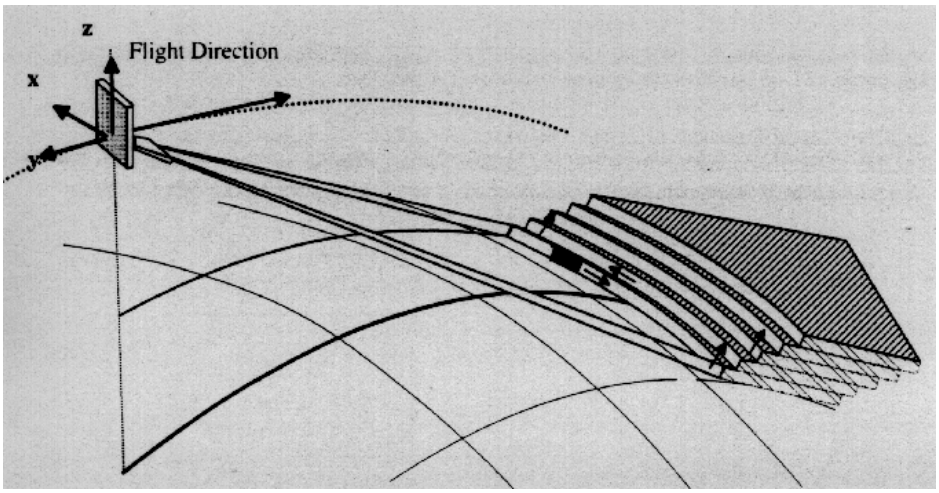

Figure 3.3: SCIAMACHY Limb viewing geometry

each azimuth scan, the elevation is increased by 3 km. This scan pattern is reproduced until the maximum altitude of 100 km is reached (Fig.3.3).

SCIAMACHY BrO profiles retrieved by Universities of Bremen (*Rozanov et al.*, 2005), Heidelberg, and Harvard (*Sioris et al.*, 2006) are available for comparison with the validation measurements. Unfortunately the two first retrievals differ from the Harvard retrieval significantly. Sometimes the Harvard retrieval reveals twice higher BrO values. To investigate possible reasons for the disagreement between the vertical distributions of BrO retrieved from the SCIAMACHY limb measurements and subsequently improve existing retrieval algorithms the project BOOST (Bromine Oxide in the lOwer STratosphere, web-page: http://www.iup.physik.uni-bremen.de/boost/) is organized by Dr. A. Rozanov from the University of Bremen.

Balloon-borne BrO profiling is performed using the solar occultation technique. Since 1996 stratospheric BrO has been measured by balloon-borne DOAS instruments (*Ferlemann et al.*, 1998). In addition to the spectrometers observing direct sunlight, a small UV/visible spectrometer has been operated in limb geometry observing scattered sunlight on-board the balloon gondola since 2002 (*Weidner et al.*, 2005). The inferred BrO abundances correspond well with the data inferred from direct sun measurements. The BrO evaluation is performed in the wavelength range from 346 nm to 360 nm as recommended by *Aliwell et al.* (2002). The precision and accuracy of the technique is $\pm 4\%$ and $\pm 12\%$, respectively. Profile information of stratospheric BrO was obtained by a least-squares profile invertion technique (*Rodgers*, 2000).

Another DOAS balloon-borne instrument is Systeme d'Analyse par Ob-

servation Zenithale (SAOZ) employed by Centre National de Recherche Scientifique - Service d'Aeronomie (France). BrO is measured by solar occultation in the 320-400 nm UV spectral range during the afternoon ascent of the balloon at SZAs lower than 90° and at the beginning of sunset from float altitude up to 92°-93° SZA. The measurements are repeated every 30s resulting in a vertical sampling of about 200m during the balloon ascent. Profile retrievals are carried out using the onion peeling technique. The major systematic error comes from the uncertain estimation of the residual BrO column above float altitude. A constant BrO mixing ratio of 14±2pptv is generally assumed. Systematic errors due to the BrO cross-section's uncertainty and its temperature dependence estimated at +5/-10%. A full description of the instrument and the retrieval algorithm can be found in *Pundt et al.* (2002).

3.2 The chemical conversion resonance fluorescence technique

The only established in-situ technique for BrO and ClO detection is the chemical conversion resonance fluorescence (CCRF), which is employed in the ClO/BrO balloon-borne instrument as well as in the Jülich aircraft instrument HALOX.

This technique was developed at Harvard University, Cambridge, Massachusetts (USA). As very first measurements three simultaneous observations of atomic chlorine (Cl) and the chlorine monoxide radical (ClO) are reported which encompass the altitude interval between 25 and 45 kilometers (*Anderson et al.*, 1977). The first BrO measurements were performed by the same scientific group on May 20, 1986 from Palestine, Texas (USA). An upper limits of BrO was detected only. It was observed to be less than 15 pptv between 35 and 24 km altitude (*Brune and Anderson*, 1986). Later an aircraft version of this instrument was developed. It was installed on the US high-altitude aircraft ER-2 and further improved (*Stimpfle et al.*, 1999).

Later, balloon instruments were developed at University of California (USA) at Irvine (UCI) and in the Research Center Jülich (Germany) in 1995. The Jülich instrument was built in collaboration with the UCI. The Jülich ClO/BrO instrument has performed the very first measurements of halogen radicals in the Arctic stratosphere at altitudes higher than those the ER-2 can reach. In 2001, its improved version called HALOX (HALogen OXides) was developed to enable measurements on-board the Russian M55-"Geophysica" aircraft. In addition to ClO and BrO, HALOX can detect the chlorine monoxide dimer $ClOOCl$.

Figure 3.4: TRIPLE shortly before the launch in Kiruna on 6 March 2003. ClO/BrO-instrument is in the forefront

The TRIPLE instrument has performed a number of successful flights since 1995. All of them were performed on-board the TRIPLE gondola (Fig.3.4), which is able to carry 3-4 instruments: the cryogenic whole air sampler (BONBON) of University of Frankfurt, the Jülich Lyman-α fluorescence hygrometer (FISH), and the ClO/BrO resonance fluorescence instrument were on-board for all flights. In addition the dual cell ozone photometer, an ECC (electrochemical concentration cell) ozone sonde, or a tunable diode laser absorption spectrometer (TDL) were on-board for some flights.

The principle of the CCRF technique is shown in Fig.3.5. Excess nitric oxide (NO) is added to the air stream at the entrance of the measurement duct. It generates halogen atoms by a fast chemical reaction with the halogen monoxides:

$$ClO + NO \rightarrow Cl + NO_2 \tag{3.2}$$

$$BrO + NO \rightarrow Br + NO_2 \tag{3.3}$$

These atoms are then subsequently detected by resonance fluorescence in the vacuum ultraviolet (VUV). VUV-radiation is generated by plasma discharge lamps containing traces of the corresponding halogen atoms in helium. The bromine lamps radiate at wavelengths of 131.7/131.8 nm (doublet). The chlorine lamps emit at 118.9 nm. The lamps are fabricated in the Research Center Jülich (*Vogel*, 1998).

Figure 3.6 shows the bromine atomic transitions in the UV. Although there are more transitions to the ground state, the doublet 131.7/131.8 nm is chosen due to a minimum of the oxygen absorption at these wavelengths. Nevertheless, the oxygen absorption there is 70 times

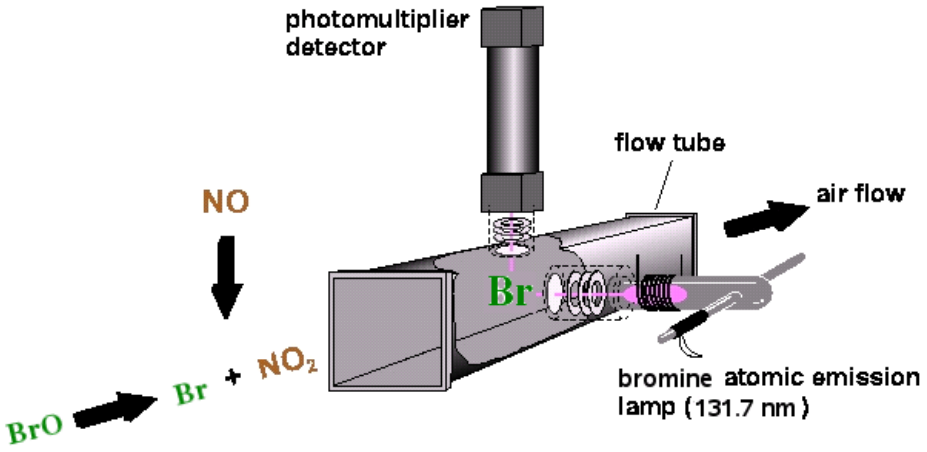

Figure 3.5: Schematical view of the chemical conversion resonance fluorescence technique in the vacuum ultraviolet

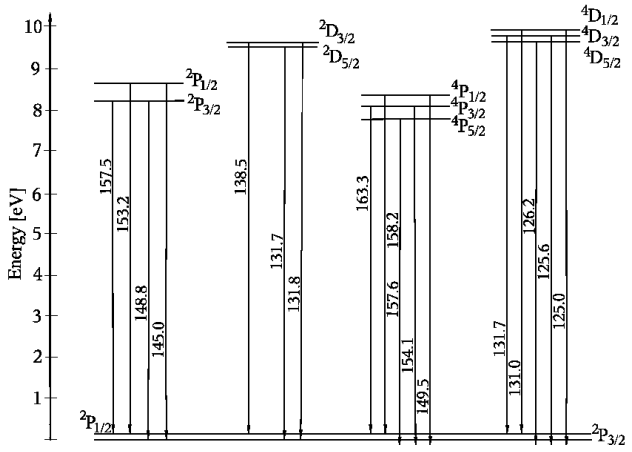

Figure 3.6: Energy state diagram for the bromine atom. The transitions' wavelengths are in nm (transitions from http://physics.nist.gov/PhysRefData/Handbook/Tables/brominetable6.htm)

higher than at 118.9 nm (chlorine emission line). To isolate the doublet an air filter is used, which significantly suppresses the oxygen emission lines between 135 and 160 nm. The air filter is a cell equipped with a SrF_2-window (which cuts all lines shorter than 128 nm) and purged by synthetic air. The pressure in the air filter is regulated by choosing appropriate in- and outlet flow restrictors. One air filter is placed immediately in the face of the lamp, the second one - in front of the photomultiplier. Figure 3.7 shows the bromine spectrum of a specific lamp (Br049) taken without and with the air

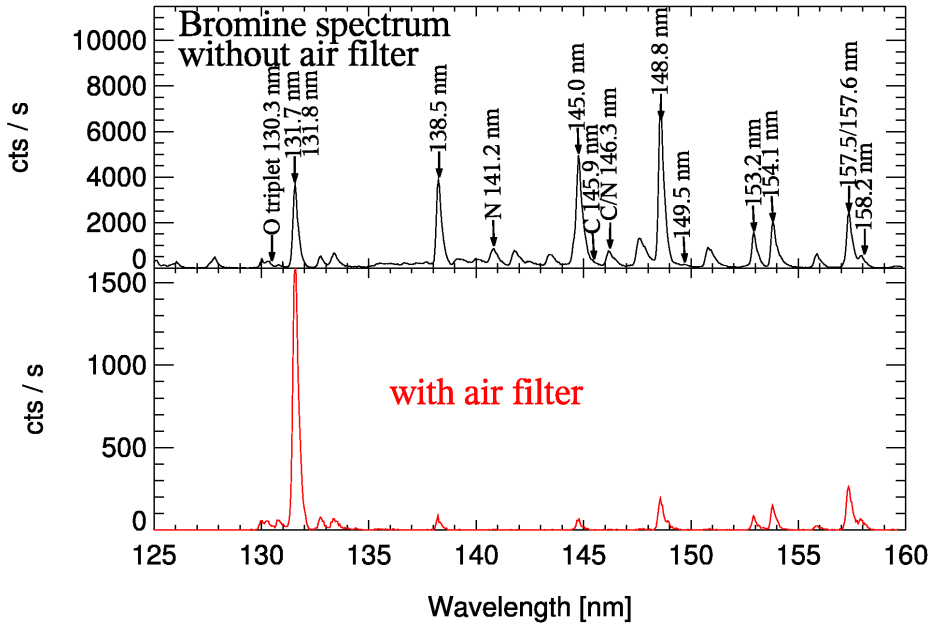

Figure 3.7: Emission spectra of bromine lamp Br049; black line: without air filter; red line: with air filter. Apart from the bromine lines, there are contamination lines from oxygen, carbon, and nitrogen atoms. In the short-wave part of the spectra the SrF_2-window effect can be seen: all lines below 128 nm are eliminated from the spectrum. Due to the oxygen absorption properties, all lines except 131.0 and 131.7/131.8 nm are strongly absorbed by the filter.

filter. It can be seen that most of the lines apart from 131.0 and the doublet 131.7/131.8 nm are absorbed or strongly suppressed by oxygen. Additional absorption in the measurements duct eliminate all other "impurity" lines.

The light from the lamps excites appropriate halogen atoms. These excited atoms re-emit the light in all directions (Fig.3.8). Without halogen atoms in the flow tube, there will be no radiation from them, so the light from the lamps will just come across the tube and there will be background signal only detected by the photomultiplier tube (PMT). This background signal consists of the Rayleigh scatter (on oxygen and nitrogen molecules present in the flow tube) and chamber scatter (on the walls of the flow tube). Razor blades strongly suppress scattering of radiation from the walls. The light in the direction perpendicular to that of the beam from the lamp is the evidence of the halogen atoms presence (as centers of secondary light emission) in the measurement duct. The instrument is run in cycling mode, in which the NO addition is turned on and off periodically (usually every 10s).

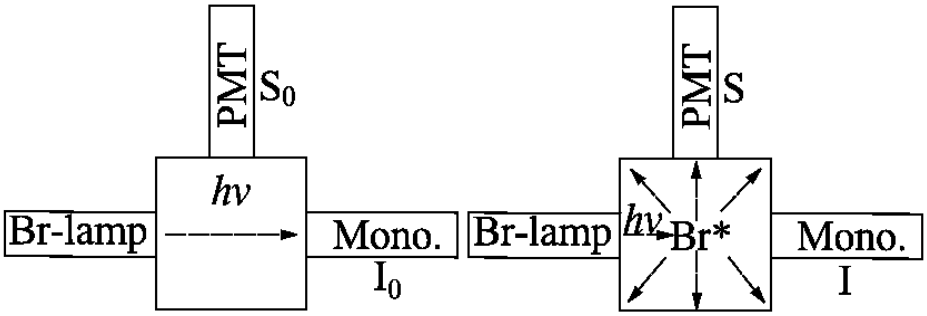

Figure 3.8: The resonance fluorescence principle. Left: there are no bromine atoms in the system. PMT registers the background signal S_0; the monochromator - the intensity of the bromine doublet 131.7/131.8 nm. Right: there are bromine atoms in the system. The lamp light is absorbed by these atoms and re-emitted isotropically. PMT registers the signal S; the monochromator - the signal I

This allows to measure the effective signal (signal caused by halogen atoms + background, see (3.4)) and the background alone alternately.

$$S_{tot} = S_{Cl/Br} + S_{Rayleigh} + S_{chamber}, \tag{3.4}$$

where S_{tot} is a total signal, consisting of signal caused by halogen atoms $S_{Cl/Br}$, Rayleigh scatter $S_{Rayleigh}$ (light scatter on oxygen molecules), and chamber scatter $S_{chamber}$ (light reflected from the walls of the measurement duct). The difference between the signals with NO on and off is a measure of the amount of Cl or Br atoms present for a given pressure and temperature.

Despite of many similarities in detection of ClO and BrO, there are a couple of important differences, which make BrO detection particularly difficult. First of all the volume mixing ratio (VMR) of ClO usually is much higher than that of BrO. Besides, there is strong absorption of VUV-light by oxygen. But oxygen absorption at 118.9 nm (Cl emission line) has accidentally it's minimum (absorption cross section is $1.4 \times 10^{-20} \frac{cm^2}{molecule}$), and at 131.7 nm ($Br$ emission line) - unfortunately not (the absorption cross section there is $10^{-18} \frac{cm^2}{molecule}$). That is why the oxygen absorption generates much more problems for the BrO measurements. as a consequence during BrO measurement analysis the signal has to be averaged over several tens of minutes to obtain signal to noise ratios of at least 2. This integration time increases with decreasing altitude due to increasing oxygen density. Figure 3.9 illustrates this effect.

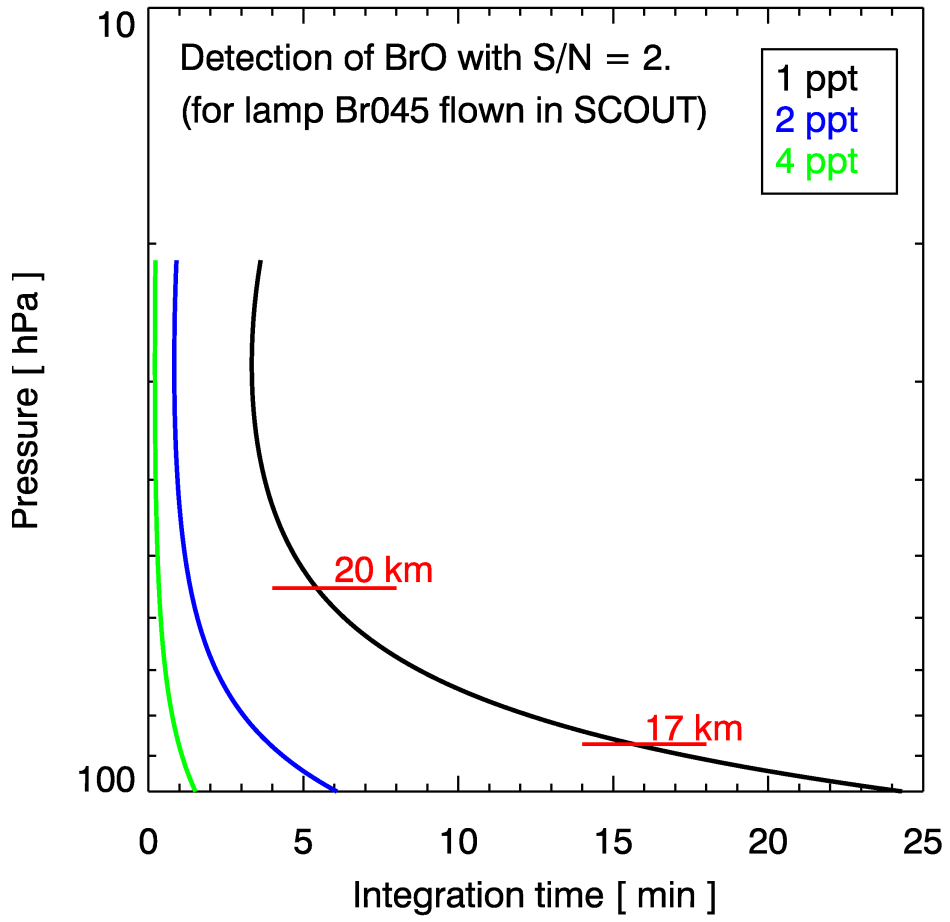

Figure 3.9: Integration time needed to detect given mixing ratios of BrO calculated for realistic lamp parameters of Br045

3.2.1 The reactions in the measurement duct

There are so-called back reactions in the measurement duct converting halogen atoms (X) into compounds like XNO, XNO_2, XO, XO_2 or $XONO$. As a consequence not all Cl and Br remain in the atomic form until they reach the detection module. To make a correct calculation of ClO and BrO mixing ratio from the amount of Cl and Br it is necessary to know precisely the so called conversion efficiency. This parameter shows which fraction of the chlorine and bromine monoxides does remain in atomic form until passing by the detection axes. For this purpose one has to take into consideration the chemical reactions occurring in the measurement duct after NO addition. These reactions are listed below ($X = Cl, Br$). After each reaction the rates of concentration change is noted in square brackets for $X = Br$. These

rates were calculated by means of reaction constants taken from *Sander et al.* (2003) for temperature 200 K, pressure 100 hPa, NO and O_3 mixing ratios of 2 ppm, and NO_2 mixing ratio of 1 ppb.

$$XO + NO \rightarrow X + NO_2 \quad [234s^{-1}] \tag{3.5}$$

$$X + NO + M \rightarrow XNO + M \quad [2.2s^{-1}] \tag{3.6}$$

$$X + NO_2 + M \rightarrow XNO_2 + M \quad [1.5 \cdot 10^{-2}s^{-1}] \tag{3.7}$$

$$X + O_3 \rightarrow XO + O_2 \quad [2.3s^{-1}] \tag{3.8}$$

$$X + O_2 + M \rightleftarrows XO_2 + M \quad [7.6 \cdot 10^{3}s^{-1}] \tag{3.9}$$

$$NO + O_3 \rightarrow NO_2 + O_2 \quad [1.2 \cdot 10^{-2}s^{-1}] \tag{3.10}$$

$$X + NO_2 + M \rightarrow XONO + M \quad [1.5 \cdot 10^{-2}s^{-1}] \tag{3.11}$$

The reactions (3.5) provide desirable conversions of BrO into Br. The remaining reactions (3.6)-(3.11) convert Br into other compounds not detectable by the resonance fluorescence. That is why the conversion efficiency is always lower than 100%.

The conversion efficiency depends on the temperature and pressure (the reactions' rate constants depend on them), on the ozone mixing ratio, on the amount of NO added, and on the distance of the detection axes from the NO-injector (the longer the distance, the more time there is for the back reactions to take place; there is, however, a limit, as $XO + NO$ also needs some time to react). Taking all these factors into consideration, the conversion efficiency can be calculated by means of the FACSIMILE program (*Curtis and Sweetenham*, 1987). For example, dependence of the conversion efficiency on the distance from the NO-injector for different intensities of the NO-flow is shown in Fig.3.10.

Fortunately in case of the BrO conversion the back reactions do not play an important role. It is easy to choose appropriate amounts of NO added to obtain a "plateau" independent on the distance from the NO-injector. Before a measurements campaign the optimal amount of NO to be added into the measurement duct is found by means of the FACSIMILE model. And vice versa, during the data analysis the conversion efficiency can be calculated for every moment of the flight from known pressure, temperature, flow speed, NO-flow intensity, and ozone mixing ratio.

By periodically varying the NO flow as well as the air flow speed through the measurement duct, the validity of the modelled conversion efficiency can be checked. The NO flow is varied during each NO-on cycle (usually 10s) by means of a mass flow controller. Standard settings are 6s at about 3 sccm (Standard Cubic Centimeters per Minute) purified NO, and then 2s

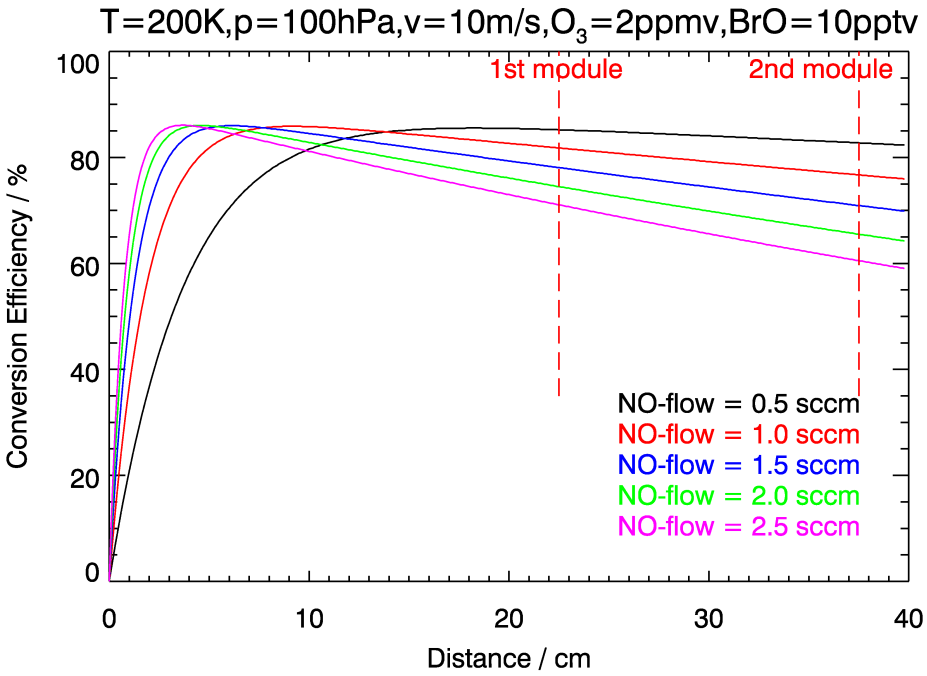

Figure 3.10: Efficiency of the conversion of BrO to Br in the flow tube of the ClO/BrO-instrument in dependence on the distance from the NO-injector for different NO-flows (in sccm). The modeling was performed for conditions with pressure p of 100 hPa, temperature $T = 200$ K, flow speed $v = 10$ m/s, ozone mixing ratio = 2 ppmv, BrO mixing ratio = 10 pptv, and NO_2 mixing ratio = 100 pptv. The positions of the BrO detection modules are marked by red dashed lines

each at about 0.5 sccm and 0.2 sccm, respectively. The air flow speed is also varied: after 10 min at nominal speed (around 12 $\frac{m}{s}$) the pump (a modified turbo charger) is stepped up and down by about 20% for 2 minutes each, respectively, yielding a 14 minutes pump cycle. More details for the balloon instrument can be found in *Woyke* (1998).

3.2.2 The quality check of the BrO profiles

During all three validation balloon flights three consecutive measurement modules (one for ClO and two for BrO) were used. There were two modules for BrO detection, because these flights were focused on the SCIAMACHY BrO profile validation. Also the HALOX aircraft instrument has two BrO detection modules mounted in two independent measurement ducts. These configurations enable internal comparisons between data measured in paral-

lel. All detection modules are independently calibrated before and after each flight.

An internal BrO comparison of two detection modules of the balloon instrument is unfortunately available only for the flight on 6 March 2003, since during the two other flights the second BrO modules failed due to lamp or detector problems. This comparison demonstrates, however, good agreement (Fig.3.11). Error bars denote statistical errors from signal averaging.

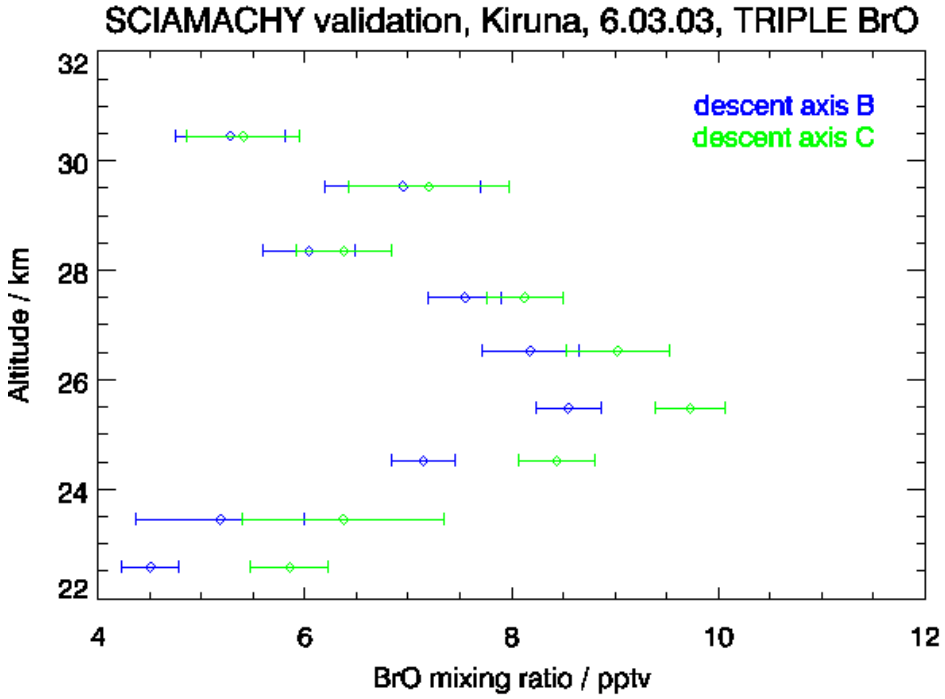

Figure 3.11: Result of the internal comparison of the BrO detection modules B and C mounted one after another on the TRIPLE

The general accuracy, however, derived from the calibration and other error sources is at least 30%. If the latter error is applied, agreement between two modules is within error bars. Good agreement confirms the correctness of the kinetic correction for the atmospheric BrO determination from the measured bromine atom concentration.

3.2.3 Calibration

To calculate the concentration of the Br atoms from the VUV light intensity detected at the photomultipliers (PMTs) it is essential to know the calibration constant. The calibration constant is the ratio of the resonance fluorescence signal to the BrO concentration. This parameter depends on: lamp

properties (in particular, changes of MgF_2-windows, through which the light leaves the lamp) and on the properties of the detection module (i.e. the measurement duct's inner surface). Therefore the calibration constant may be different for different lamps and may also vary over time. These possible drifts of the calibration constant make it necessary to perform the calibration before and after every campaign. The scheme of the calibration bench is shown in Fig.3.12.

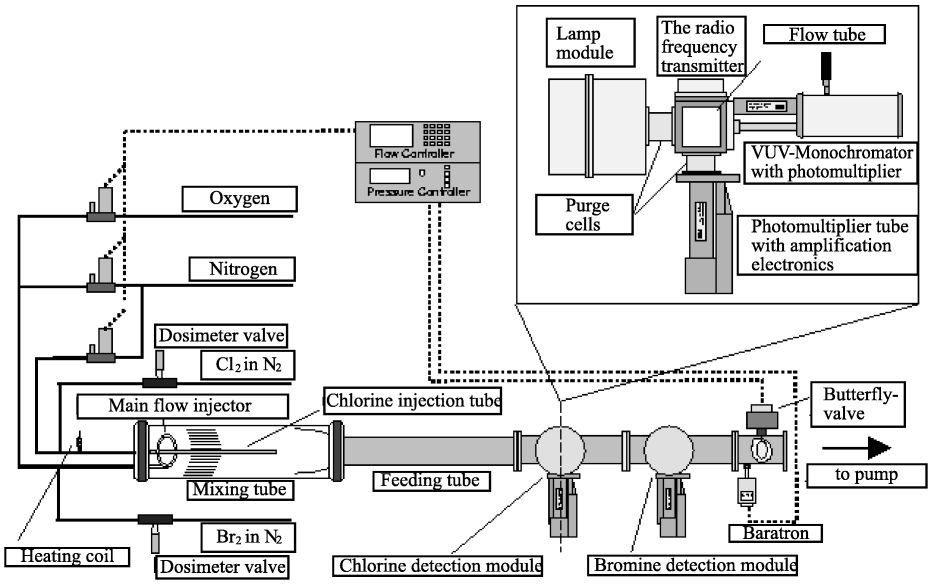

Figure 3.12: Schematic view of the bench for the calibrations of the ClO/BrO-instrument

The determination of the bromine calibration constant by means of an absorption measurement similar to the chlorine calibration (*Brune et al.*, 1989a; *Woyke*, 1998) is not possible due to the unknown absorption cross-section of Br on the 131.7 nm wavelength. Besides, the preparation of a mixture with exactly known BrO volume mixing ratio to determine the Br absorption cross-section is very difficult. That is why the bromine calibrations are based on the chlorine calibration.

The calibration bench is designed in such a way to provide appropriate pressure and flow speed conditions, as they are present during a stratospheric flight. The nitrogen and air flow are regulated by means of mass flow controllers. Pressure is regulated by a butterfly-valve placed before the vacuum pump.

To generate atomic chlorine a gaseous mixture of nitrogen and molecular chlorine is directed over a red-hot tungsten filament, where molecular chlorine

is thermally dissociated into atoms. Then this mixture is homogeneously added to the main gas flow through an injection tube. The resulting chlorine mixing ratio is in the range of several ppbv. Switching the tungsten filament on and off, a periodic chlorine atoms addition into the calibration system is possible.

It is very essential that the mixing tube and the chlorine injection tube ensure homogeneous mixing of gases and laminar flow. For the wall loss minimization the system is coated with Teflon.

For the bromine calibration two detection axes (the same as during the flights) are mounted onto the calibration bench one after another. The first axis contains the chlorine lamp, the second axis the bromine one. A VUV-monochromator (McPherson, Model 234/302VM, resolution $\lambda/\Delta\lambda \approx 600$) is connected to the chlorine axis for controlling of the Lyman-α fraction in the light flux of the chlorine lamp (Lyman-α is the emission line of atomic hydrogen at 121.6 nm; this line contributes significantly to the chlorine lamp radiation due to impossibility to completely remove all hydrogen impurities during lamp manufacturing). The bromine calibration is performed under a constant flow of chlorine atoms. Molecular bromine is added to the flow in an amount large enough to completely titrate the chlorine. For the bromine calibration a nitrogen-bromine gaseous mixture is periodically added to the calibration system through a valve into the main gas flow. The following reaction occurs:

$$Cl\bullet + Br_2 \rightarrow BrCl + Br\bullet \tag{3.12}$$

This reaction is very quick and generates the same number of Br atoms as that of Cl atoms in a few milliseconds. The calibration is based on the fact that the number of appearing bromine atoms is equal to the number of chlorine atoms present at the beginning of the reaction (3.12): $[Cl] = [Br]$. In other words, the chlorine concentration detected without bromine addition is equal to the bromine concentration detected during the addition of bromine.

An example of the changes in the signals from both chlorine and bromine axes during the addition of Br_2 are shown in Fig.3.13.

After bromine addition the chlorine signal decreases down to its background value. Simultaneously, the bromine signal increases due to the resonance fluorescence of the bromine atoms. The differences in the signals are:

$$\Delta S^{Cl} = S_0^{Cl} - S^{Cl} = C_{cal}^{Cl} \cdot [Cl] \tag{3.13}$$

$$\Delta S^{Br} = S^{Br} - S_0^{Br} = C_{cal}^{Br} \cdot [Br] \tag{3.14}$$

The bromine calibration constant is calculated from the ratio $\frac{\Delta S^{Br}}{\Delta S^{Cl}}$ under the

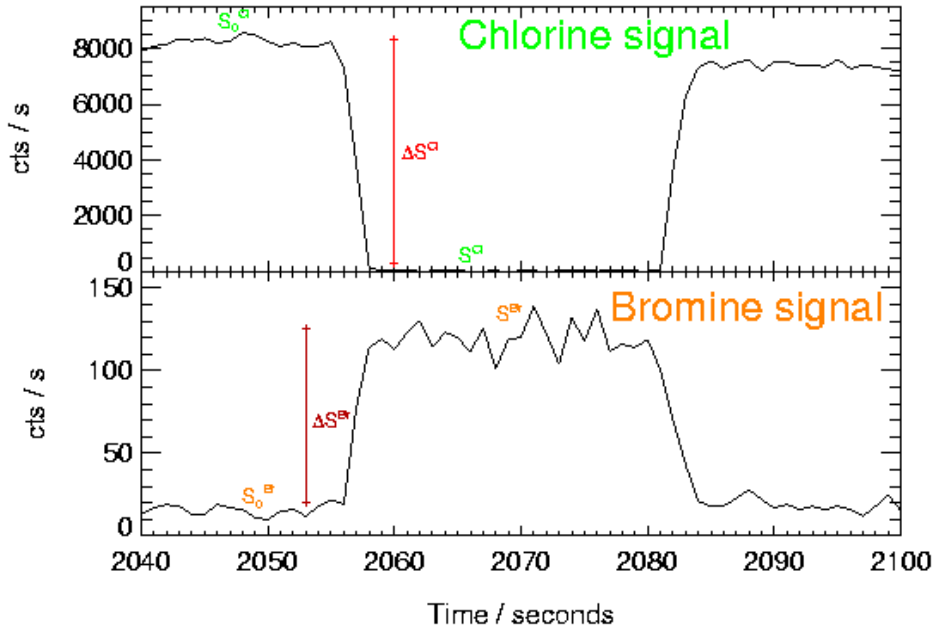

Figure 3.13: Temporal variation of the detector signals during the bromine calibration at 20hPa

assumption that $[Cl] = [Br]$:

$$(C_{cal}^{Br})_{Air} = \frac{\Delta S^{Br}}{[Br]} \approx (C_{cal}^{Cl})_{Air} \cdot \frac{\Delta S^{Br}}{\Delta S^{Cl}} \tag{3.15}$$

$(C_{cal}^{Cl})_{Air}$ is calculated using the measurements of $\frac{\partial S}{\partial p}$ (dependence of the chlorine background signal on the pressure) and Lyman-α (see (*Woyke*, 1998) for details). $(C_{cal}^{Cl})_{Air}$ is based on the Cl atom absorption coefficient at 118.9 nm which was measured by *Schwab and Anderson* (1982) to a accuracy of $\pm 10\%$. Including all other error sources C_{cal}^{Cl} has an error of around 13%.

A normalization of the calibration factor is performed by means of the background signal:

$$K^{Br} = \frac{C_{cal}^{Br}}{S_{bgr}} \tag{3.16}$$

During laboratory bromine calibrations the normalized calibration factor K^{Br} is determined for different pressures (in the pressure range from 10 to 100 hPa). The set of K^{Br}-values obtained for different Br-lamps as well as at UCI is shown in Fig.3.14. The different detection modules calibrations reproduce in essence the same calibration curve, which has been measured in the laboratory of Darin Toohey (at that time University of Irvine, USA)

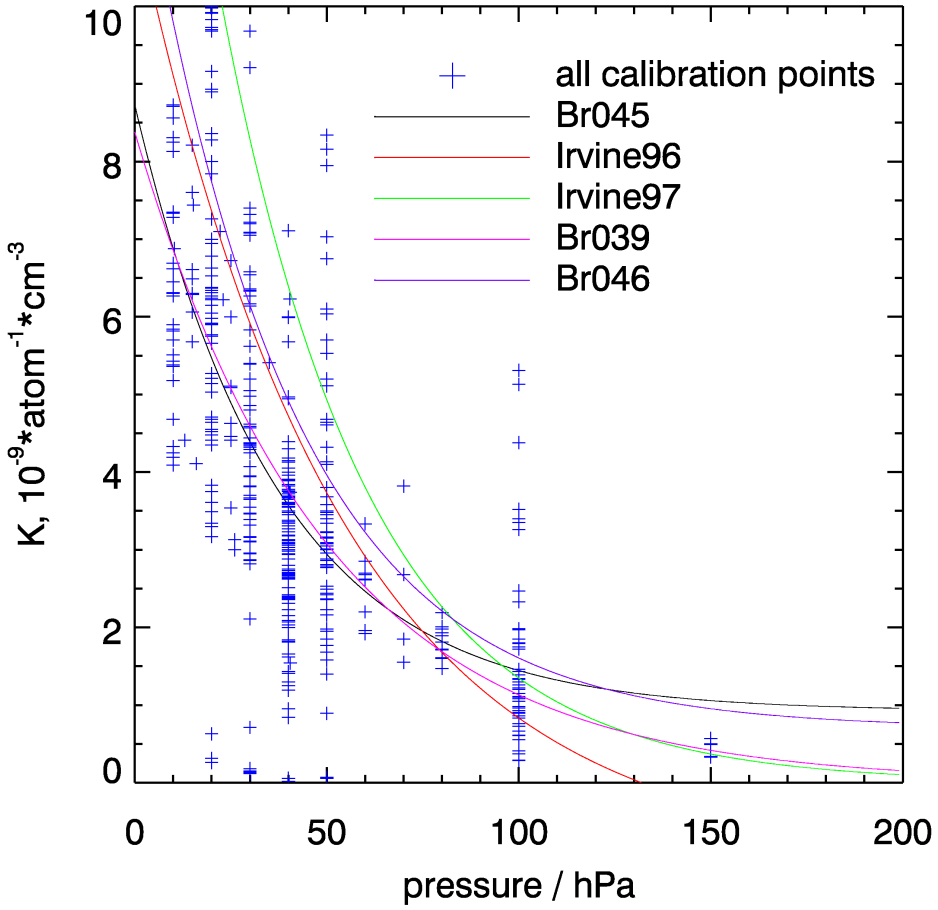

Figure 3.14: The bromine calibration factors for all Br-lamps employed in TRIPLE. The fitted curves for Br039, Br045, and Br046 bromine lamps are shown as well, along with the calibrations curves obtained at UCI in 1996 and 1997 years.

(*McKinney et al.*, 1997). The latter was obtained for the balloon instrument and, hence, for the pressure range 5-80hPa. In case of the HALOX instrument, the interesting pressure range is 50-150 hPa (limited by the maximal flight altitude of M55-"Geophysica" and the density of O_2). That is why, the calibration curves obtained in Jülich and Irvine differ so much at pressures higher than 100hPa. The fitted curves for both Jülich (for the different lamps) and Irvine calibrations can be described by the following formulae:

$$K^{Br} = -10^{-9} + e^{-18.2-0.019 \cdot pressure[hPa]} \text{ for Irvine'96 curve;} \quad (3.17)$$

$$K^{Br} = e^{-17.8-0.026 \cdot pressure[hPa]} \text{ for Irvine'97 curve;} \quad (3.18)$$

$$K^{Br} = e^{-18.5974-0.02 \cdot pressure[hPa]} \text{ for Br039 lamp;} \quad (3.19)$$

$$K^{Br} = 9.21 \cdot 10^{-10} + e^{-18.7-0.027 \cdot pressure[hPa]} \text{ for Br045 lamp;} \quad (3.20)$$

$$K^{Br} = 7.01 \cdot 10^{-10} + e^{-18.3-0.0256 \cdot pressure[hPa]} \text{ for Br046 lamp} \quad (3.21)$$

For data analysis the calibration factor has to be recalculated for stratospheric temperatures and pressures. This recalculation is performed with the help of the following formula yielding the calibration constant for the flight conditions C^{Br}_{flight}:

$$C^{Br}_{flight} = S^{flight}_{bgr} K^{Br} \frac{T_{Lab}}{T_{flight}} \sqrt{\frac{T^{Br-lamp}_{Lab} + T_{Lab}}{T^{Br-lamp}_{Flight} + T_{flight}}}, \quad (3.22)$$

where T_{Lab} and T_{Flight} are the temperatures in the calibration laboratory and in the flight; $T^{Br-lamp}_{Lab}$ and $T^{Br-lamp}_{Flight}$ - the corresponding temperatures in the bromine lamp (see *Vogel* (1998)) for details.

C^{Br}_{flight} is accurate to $\pm 25\%$ (2σ). The BrO retrieval from the TRIPLE and HALOX measurements is performed by means of signal averaging over long time intervals (up to 15 minutes). Therefore, there are statistical error attributed to averaging procedure. The overall accuracy of the TRIPLE BrO measurements is of $\pm$30-35%, which includes the error of the fligt calibration constant and the statistical averaging error.

More detailed descriptions of the balloon-borne and aircraft versions of the CCRF instruments follow.

3.3 TRIPLE ClO/BrO instrument

In the balloon-borne instrument the probed air is sucked by means of a Roots pump through the measurements duct (Fig.3.15). The duct has a square cross-section of 5×5 cm. The velocity of the air flow can be regulated by means of the pump power variation. The reagent nitric oxide is then added into this flow through injectors at three different flow rates in a (usually) 20 s cycle during which NO is added for 10 s, and the background is measured for 10 s as well. Bromine atoms produced by this chemical conversion are then detected with resonance fluorescence, and the photomultiplier detector signal is stored, together with diagnostic data, by the on-board computer system.

ClO and BrO are measured by means of three detection axes mounted one after another. The first axis in all flights was a Cl module, the second and third were Br modules.

The bromine detection axis consists of a resonant light source set ("bromine lamp") at a right angle to a photomultiplier. The light beam from the

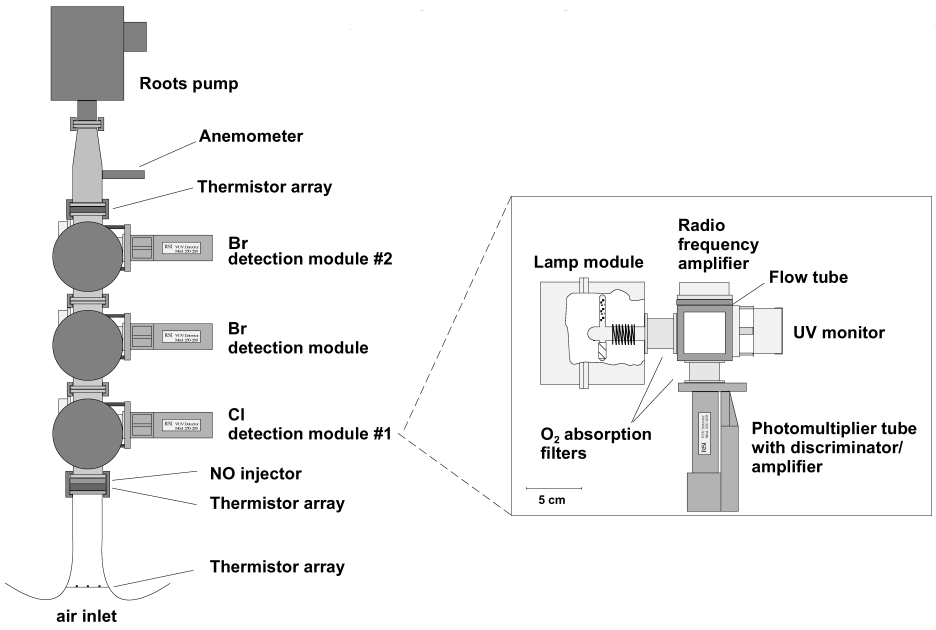

Figure 3.15: TRIPLE ClO/BrO-instrument configuration

lamp and the detector field of view cross the flow tube, intersecting in the center. Razor blade light traps are placed opposite the lamp and detector, and an UV-monitor behind the lamp monitors the ultraviolet flux from the lamp. The lamp itself is stabilized by optical feedback to an infrared monitor controlling the amount of bromine released into the helium plasma from a palladium bromide source arm attached to the lamp body.

Besides that, the measurement duct is equipped with three thermistor arrays (placed at its beginning, between the second and third axes, and at the very end of the duct). These arrays measure the flow temperatures in the central part of the flow, as well as near duct's walls. This allows to obtain an information about flow characteristics (is flow turbulent or laminar, etc.) during a post-flight data analysis. An anemometer for the measurements of the flow velocity is mounted at the end of the measurement duct before the pump system.

During a flight, the balloon instrument is controlled by the on-board control and data acquisition system, which switches the instrument on, when the ambient pressure crosses a pre-established pressure limit, switches the detection modules on, switches NO addition on and off, changes the pump power, etc. During a flight there is a possibility to receive and monitor data from the instrument ("telemetry"), and to transmit commands to the instrument ("telecommands"). This allows to reveal incorrect instrument

performance and restart it in case of any problems (pump overheating, etc.).

3.4 HALOX instrument

After the series of successful measurements by the TRIPLE balloon instrument its aircraft version was designed and built also in the Research Center Jülich (Fig.3.16). The new instrument was named HALOX (HALogen OX-

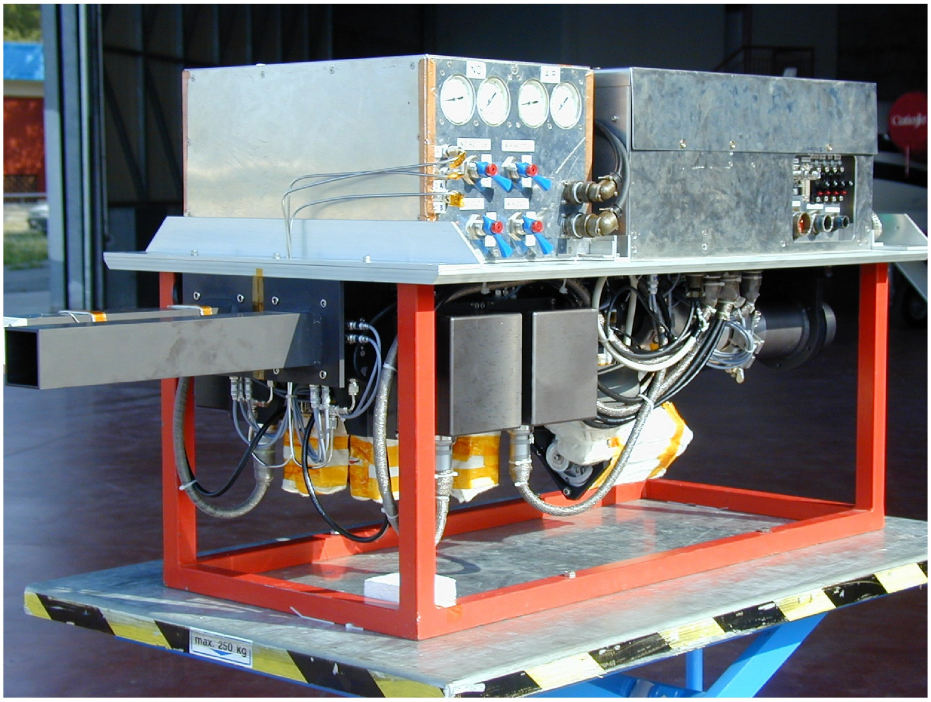

Figure 3.16: HALOX instrument

ides). In September 2001 it was integrated into the Russian high-altitude aircraft M55-"Geophysica". After that it has taken part in several field campaigns. At present it is the worldwide only operational aircraft instrument of this type. Several changes in the HALOX design were undertaken in comparison with the balloon instrument.

HALOX was built with two parallel measurement ducts (Fig.3.17). Two detection axes are mounted on each of them.

As it was mentioned in Section 3.2, one of the most serious problems for bromine detection is the absorption of the UV-radiation on 131.7 nm by atmospheric oxygen. Therefore one pressure reducing duct (Axis B) was implemented for the HALOX instrument. It consists of a 8 mm nozzle inlet and a pump at the end of the duct.

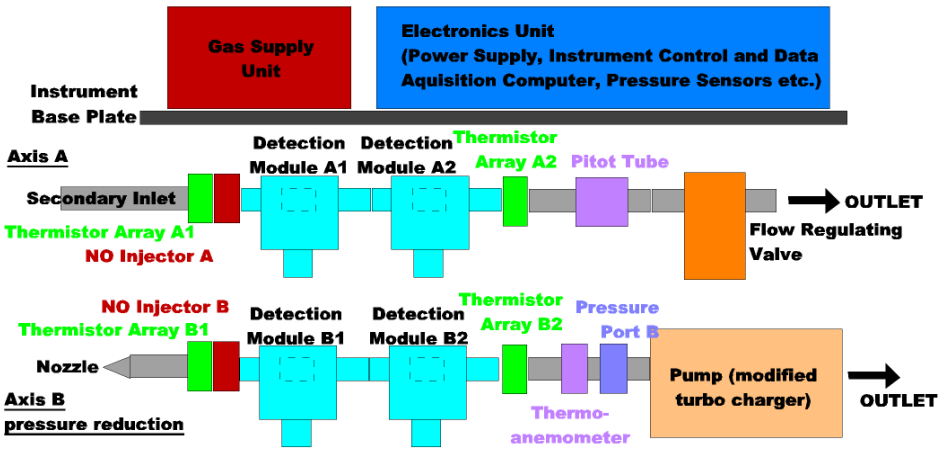

Figure 3.17: Schematical setup of the HALOX instrument

The air flow in the other channel (hereinafter Axis A) is assured by the flow in a direction opposite to the aircraft flight. Due to the high speed of the "Geophysica" precautions have to be taken for Axis A to prevent too rapid air flow through the Axis (it would have as a consequence not sufficient time for conversion of BrO into Br) and to prevent possible turbulence in the measurement duct (in this case there would be excessive contacts of the air flow with the walls, that would lead to Br loss). That is why the following construction was designed: at first the ambient air flows into a primary inlet. It is decelerated there. Significant fraction of this air leave this space through the primary outlet without coming into the measurement duct. The central part of the primary flow does not have any contacts with the walls. This part is then led into the secondary inlet and the measurement ducts. The flow speed in Axis B is controlled by pump power variation and nozzle diameter. In Axis A there is a butterfly-valve at its end enabling flow speed regulation. This butterfly-valve receives the readings from a thermoanemometer in the Axis and in dependence on the flow speed the valve changes its opening to maintain the desirable flow speed.

CHAPTER 4

Flights Description of TRIPLE and HALOX

TRIPLE has performed more than 10 successful flights since 1995. This thesis reviews the last three balloon flights as well as the HALOX flights listed in Table 4.1 below. More details about the flights are given in Appendix B. This chapter gives an overview of the geophysical and meteorological conditions of all balloon and aircraft measurements utilized in this thesis work.

Table 4.1: List of TRIPLE and HALOX flights. TRIPLE flights are indicated by (∗)

Campaign	**Location**	**Latitude**	**Time**
ENVISAT valid.(∗)	Aire-sur-l'Adour	mid-lat.	24.09.2002
EUPLEX	Kiruna	Arctic	15.01.-11.02.2003
ENVISAT valid.	Kiruna	Arctic	28.02.-16.03.2003
ENVISAT valid.(∗)	Esrange	Arctic	6.03.2003
ENVISAT valid.(∗)	Esrange	Arctic	9.06.2003
TROCCINOX	Araçatuba	tropics	18.01.-7.03.2003
SCOUT-O3	Darwin	tropics	4.11.-17.12.2005

4.1 The balloon flight at Aire-sur-l'Adour on 24 September 2002

The mid-latitude flight at Aire-sur-l'Adour, France, was performed on 24 September 2002. The CNES (Centre national d'études spatiales - French

space agency) balloon division headquarters is situated there. The geographical coordinates of the place are 43.71°N, 0.25°W. The flight profile as well as the temperature and the SZA at the position of the balloon are shown in Fig.4.1. The trajectory of the balloon is shown by the blue line in Fig.4.2.

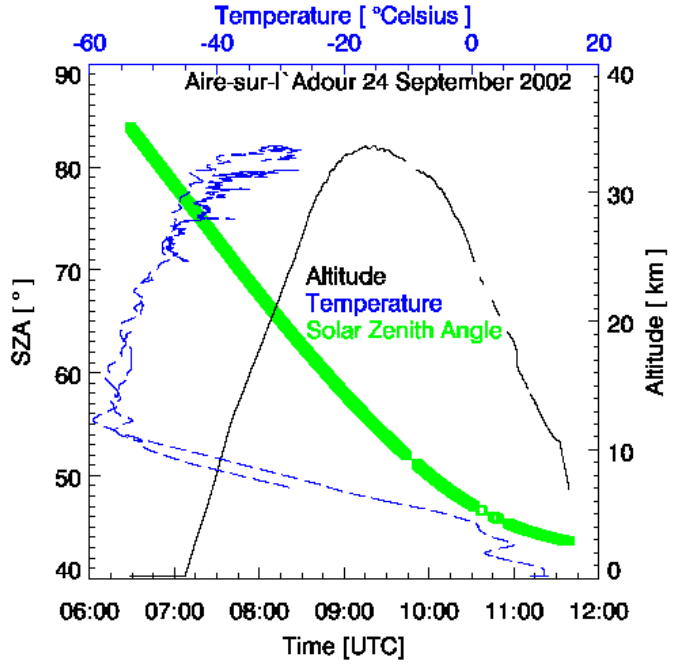

Figure 4.1: Flight profile, temperature and SZA at balloon position for the flight on 24 September 2002 at Aire-sur-l'Adour

Due to the eastward direction of the balloon trajectory the SZA was decreasing faster than for the fixed balloon position.

During this flight the tropopause was found to be at $\sim$ 12 km. The launch was at 7:07 UT. At this moment the SZA was 77°. The highest flight altitude of $\sim$ 34 km was reached at 9:21 UT after 2 hours 14 minutes.

All three balloon flights were dedicated to the ENVISAT validation. The ENVISAT orbit has a period of $\approx$100 minutes, flying over Europe every day at $\sim$8:00 - 10:00 UT and at $\sim$18:00 - 20:00 UT (*Zandbergen et al.*, 2003). This fact determined the times of the balloon flights.

At around 10:00 UT the balloon started to descend. The descent speed was controlled by means of a valve on top of the balloon. At 11:32 UT the instrument was separated from the balloon using the telecommand and continued its descent by three parachutes to ensure its soft landing before the Pyrenees mountain range. Due to the relatively weak Br-lamp used during the flight the first BrO point was extracted at 21 km during ascent. Sig-

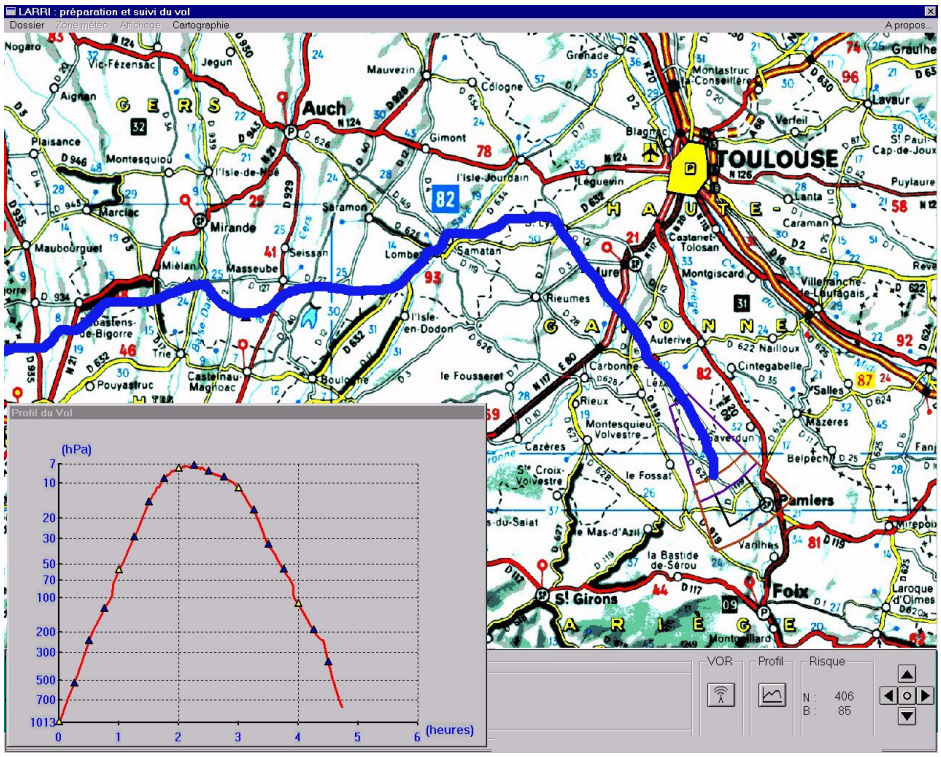

Figure 4.2: Balloon trajectory during the flight on 24 September 2002 at Aire-sur-l'Adour

nal/noise ratio was not sufficient for reliable BrO detection at lower altitudes. Measurements were performed during ascent only, because of an instrument pump breakdown (overheating) soon after the highest altitude was reached. Despite of numerous attempts to resume pump operation (that is why the descent part of the flight profile in Fig.4.1 is dash-like) it could unfortunately not be restarted.

4.2 The balloon flight at Esrange on 6 March 2003

While the first flight was performed in autumn in mid-latitude, the next one was beyond the polar circle. It occurred in winter in Esrange (a rocket range and research center of the Swedish Space Corporation). Its geographical coordinates are 67.9°N, 21°E. The altitude profile and the corresponding SZA are shown in Fig.4.3. The instrument was launched on 6 March 2003 at 6:03 UT. The SZA at the launch time was 88°. At 8:02 UT the maximum

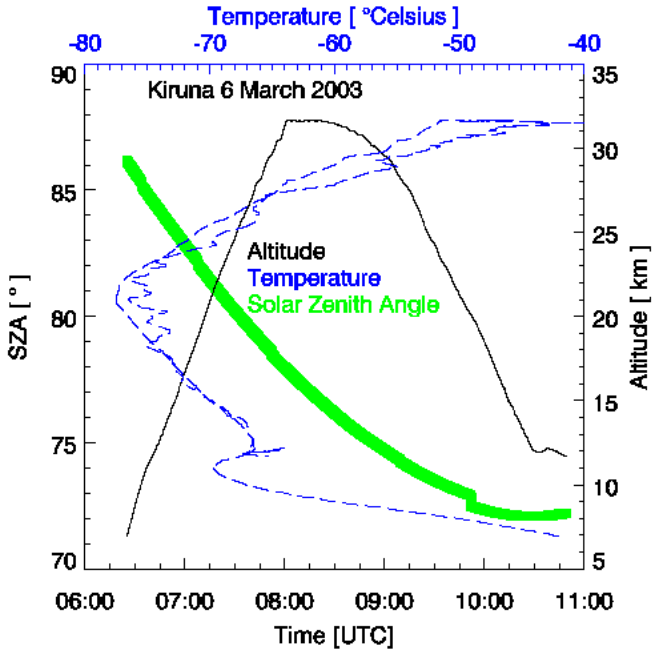

Figure 4.3: Flight profile, temperature and SZA at balloon position for the flight on 6 March 2003 at Esrange

altitude of $\sim$ 32 km was reached 1 hour 59 minutes after the launch. Untill this moment the SZA had decreased down to 77.8°. After a short float (about 20 minutes) the balloon started its valve-controlled descend at 8:21 UT. And then the instrument was separated from the balloon at 10:50 when SZA was 73.5°. Taking the temperature profile into consideration, the tropopause was situated at $\sim$ 10 km. On this day there was, however, the so called second tropopause at $\sim$ 21 km. This phenomenon is an interesting but regular feature in the cold polar vortex.

The trajectory of the balloon is shown by the blue line in Fig.4.4.

The polar vortex position at a potential temperature of 475 K and its temperature on this day is represented in Fig.4.5. The vortex position is shown for 00:00 UT. In Fig.4.5 (right) one can see that the cold pool was exactly above Esrange with the minimum temperature at that day as low as 194 K. At 475 K ($\sim$ 20 km) the polar vortex was well-above Esrange, at 400 K ($\sim$ 16 km) the potential vorticity over Esrange was quite low indication a location outside the polar vortex. The fact that the balloon entered the vortex between 16 and 20 km altitude means the instrument observed both air masses inside and outside the vortex. BrO measurements started at 9.5 km at 6:30 UT and SZA = 86°.

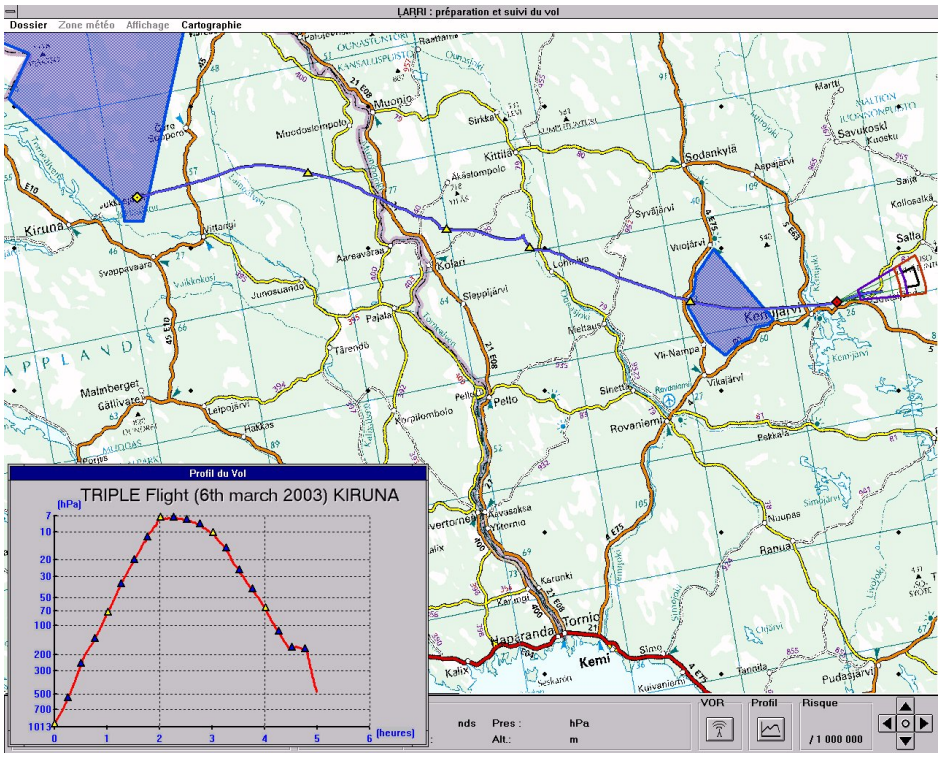

Figure 4.4: Balloon trajectory during the flight on 6 March 2003 at Esrange

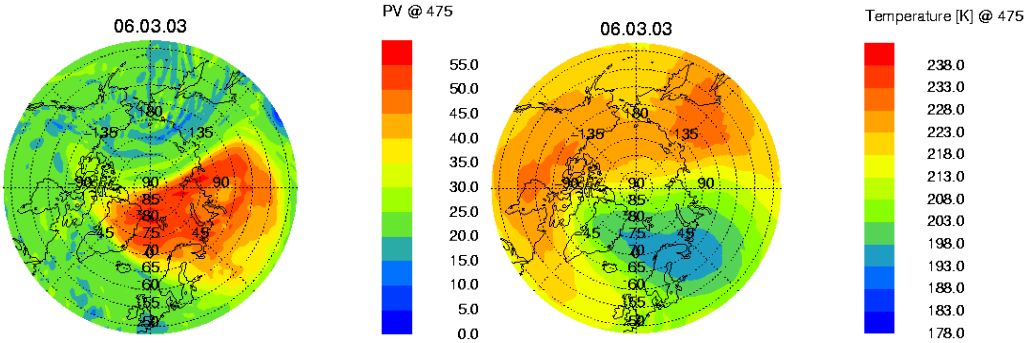

Figure 4.5: The northern hemispheric polar vortex on 6 March 2003 at 00:00 UT for the potential temperature level of 475 K ($\sim 20km$). The potential vorticity (PV) as well as the temperature are shown by means of colour codes. PV is in PV-units ($10^{-6} \cdot K \cdot m^2 \cdot kg^{-1} \cdot s^{-1}$)

4.3 The balloon flight at Esrange on 9 June 2003

The flight was launched on 9 June 2003 during midsummer at 4:56 UT and SZA = 66.9° at Esrange (67.9°N, 21°E). The altitude profile and the corre-

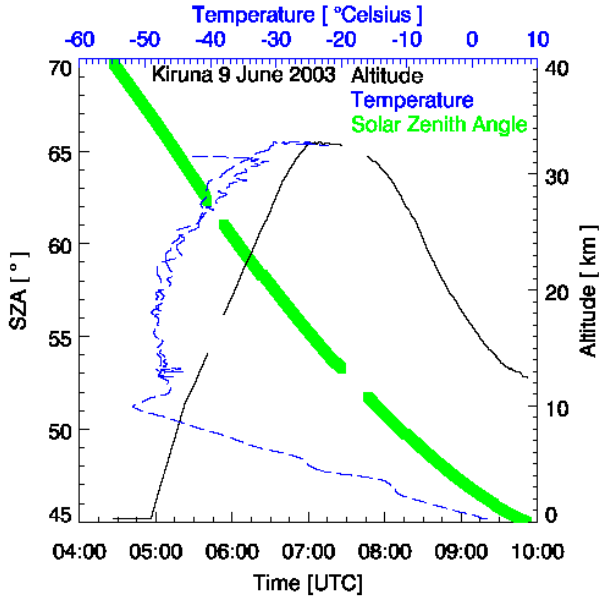

Figure 4.6: Flight profile, temperature and SZA at balloon position for the flight on 9 June 2003 at Esrange

sponding SZA are shown in Fig.4.6.

After two hours, the float altitude of $\sim$ 33 km was reached at 7:01 UT and SZA = 55°. After a short float (about 25 minutes) the balloon started its valve-controlled descend at 7:24 UT. And then the instrument was separated from the balloon at 9:52 when SZA was 45°. From the temperature profile, the cold point tropopause height is estimated to be at $\sim$ 10 km.

The lowest altitude, at which BrO was detected, is $\sim$ 18 km.

The tropospheric and stratospheric winds blew at the day of the flight in opposite directions. That is why the trajectory of the balloon turned out to be very compact. There were only about 20 km between the launch place and the place of balloon landing. The trajectory of the balloon in Fig.4.7 is indicated as thick blue line.

4.4 The EUPLEX and ENVISAT validation aircraft flights

The EUPLEX (European Polar Stratospheric Cloud and Lee Wave Experiment) Arctic aircraft campaign took place in January-February 2003 in Kiruna, Sweden (67.9°N 20.2°E). EUPLEX was organized to clear up the following key questions of Arctic stratospheric ozone depletion: How do PSCs

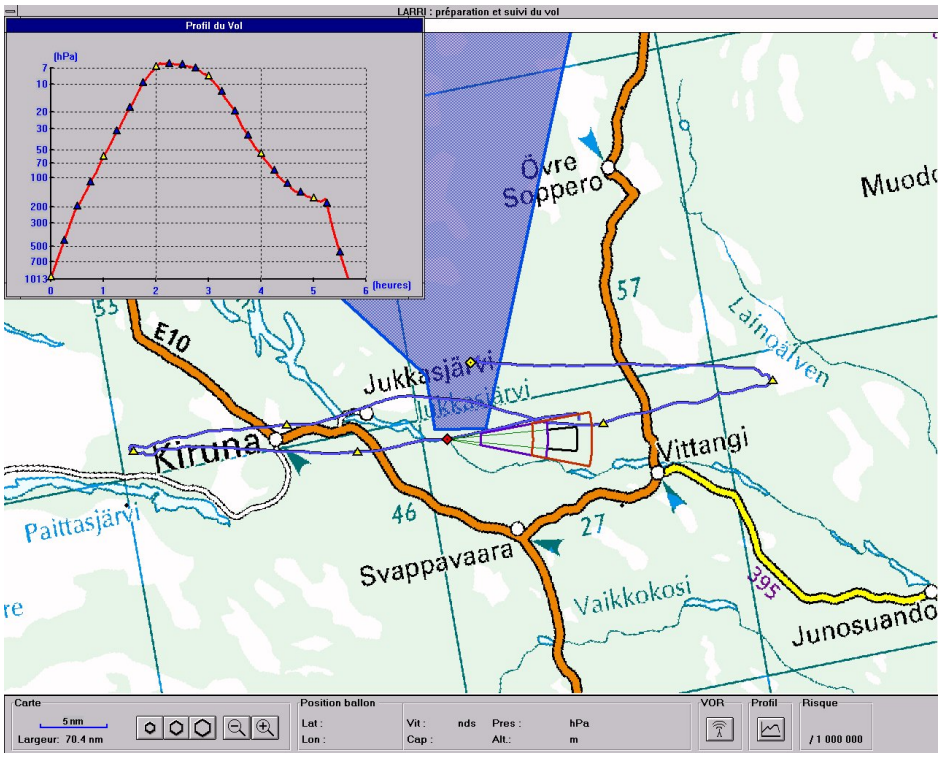

Figure 4.7: Balloon trajectory during the flight on 9 June 2003 at Esrange

form? How can observed denitrification and dehydration be explained? Are observed halogen activation rates consistent with the current theory of heterogeneous activation on PSC particles? What is the relative importance of synoptic and Lee wave PSCs for chlorine activation and Arctic ozone loss? Can observed ozone loss rates be explained by the currently accepted ozone loss cycles given simultaneously observed ClO, BrO, and NO/NO_y mixing ratios?

EUPLEX was directly followed by the ENVISAT validation campaign in late February - early March 2003. All flights carried out within the campaign are listed in Table 4.2.

The flights trajectories are shown in Fig.4.8. The flights sampled quite a big area from Spitzbergen to southern Scandinavia and from the Norwegian sea to the Barents sea. Flight profiles as well as SZAs, and temperatures during the flights are shown in Figures B.1 - B.3 in Appendix B.

The tropopause height estimated from the temperature profiles was ~ 10 km at the beginning of the campaign rising up to ~ 12 km at its end. The

Table 4.2: Flights overview of the EUPLEX campaign

Date	**Purpose of flight**
15 Jan 03	Quasi-Lagrangian flight through lee-wave clouds to study: • Microphysical properties of PSCs • Local-scale chlorine activation
19 Jan 03	Survey flight into the polar vortex to study: • Denitrification/renitrification • synoptic-scale chlorine activation • synoptic scale ozone loss • mixing near vortex edge
23 Jan 03	Ditto
26 Jan 03	Ditto
30 Jan 03	• Self MATCH flight • ClO_x partitioning and chemistry at high SZAs
02 Feb 03	Flight within ENVISAT aerosol validation
06 Feb 03	Flight into the cold pool during threshold conditions for PSC formation to study: • composition of liquid and solid PSCs • formation of NAT particles
07 Feb 03	Ditto
08 Feb 03	like 15 Jan 2003
09 Feb 03	like 06/07 Feb 2003
11 Feb 03	Flight within ENVISAT aerosol validation
28 Feb 03	Flight within ENVISAT validation
2 Mar 03	Flight within ENVISAT validation
8 Mar 03	Flight within ENVISAT validation
12 Mar 03	Flight within ENVISAT validation
16 Mar 03	Flight within ENVISAT validation

negative temperature gradient with altitude above the tropopause was observed during all flights (see Appendix B). It is in agreement with conditions during the balloon flight on March 6, 2003 in Esrange near Kiruna, where a second tropopause was found to be at $\sim$ 21 km.

The polar vortex positions for each flight day are shown in Figures B.4 - B.5 in Appendix B. During the Arctic winter 2002 - 2003, the vortex at 475 K was established by 10 December 2002, and did not break down before April 2003 (*Christensen et al.*, 2005). December 2002 was characterized by very low temperatures (*Tilmes et al.*, 2003). Around mid-January 2003, however, the vortex became perturbed, and during 19-23 January the vortex

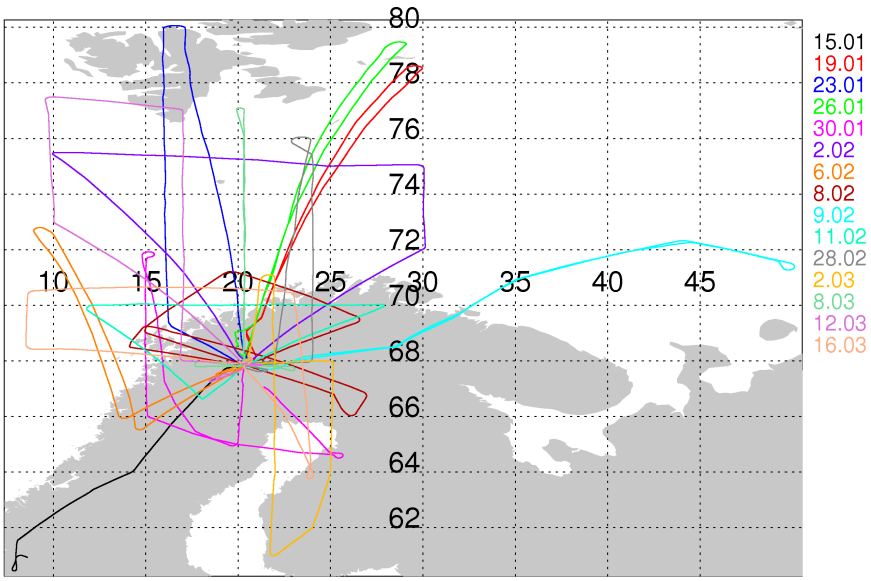

Figure 4.8: EUPLEX campaign flight trajectories. See Table 4.2 for details of the flights

was split into two parts. In early February 2003, the vortex became more symmetrical, only to experience another splitting around 20 February into two parts that reunited again on 22 February (there were not any EUPLEX flights during this period). The vortex eventually broke down around mid-April 2003. Polar vortex temperatures are shown in Figures B.6 - B.7 in Appendix B. Large-scale maps with flight trajectories and PVs are given in Figures B.8 - B.12 in Appendix B.

4.5 The TROCCINOX aircraft flights

The research project TROCCINOX (Tropical Convection, Cirrus and Nitrogen Oxides Experiment) investigated the impact of tropical deep convection on the distribution and the sources of trace gases, cloud and aerosol particles focusing on processes in the upper troposphere and lower stratosphere. The fully instrumented Russian research aircraft M55-"Geophysica" probed the large scale structure of the upper troposphere and lower stratosphere during transfer flights to and from Brazil. In co-operation with Brazilian partners the aircraft operations were co-ordinated with ground-based and space borne systems. The TROCCINOX field campaign was performed during January and February 2005, locally based in São Paulo State. The "Geophysica" was operated out of Araçatuba airport. All flights carried out within the campaign are listed in Table 4.3.

Flights trajectories are shown in Fig.4.9 (transfer flights) and Fig.4.10 (local flights). The flights were performed above southern Brazil (parts of two flights were above the Atlantic ocean near the Brazilian coast) probing air masses within more than 1500 km in zonal direction and about 1000 km in meridional direction.

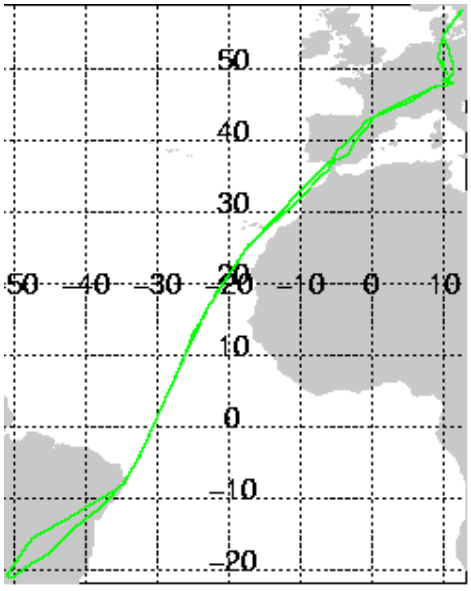

Figure 4.9: The trajectories of the transfer flights for the TROCCINOX campaign. The MARSCHALS test flight trajectory (Oberpfaffenhofen - southern Sweden) is also shown

Table 4.3: Flights overview of the TROCCINOX campaign

Date	**Purpose of flight**
18 Jan 2005	Oberpfaffenhofen, instrument test
20 Jan 2005	Transfer, Oberpfaffenhofen - Seville
23 Jan 2005	Transfer, Seville - Sal Island
23 Jan 2005	Transfer, Sal Island - Recife
27 Jan 2005	Transfer, Recife - Araçatuba
1 Feb 2005	West-East survey along 21°W, lightning NO_X accumulation, stratospheric inflow in tropical tropopause layer (TTL)
4 Feb 2005	thundercloud probing
5 Feb 2005	thundercloud probing
8 Feb 2005	West-East survey, TTL characterization
12 Feb 2005	East bound survey with dive, TTL characterization
15 Feb 2005	West-East track with dive, ENVISAT validation
17 Feb 2005	ENVISAT validation
18 Feb 2005	tropical convection characterization
24 Feb 2005	Transfer, Araçatuba - Recife
27 Feb 2005	Transfer, Recife - Sal Island
27 Feb 2005	Transfer, Sal Island - Seville
2 Mar 2005	Transfer, Seville - Oberpfaffenhofen
7 Mar 2005	MARSCHALS (Millimeter-wave Airborne Receiver for Spectroscopic CHaracterization of Atmospheric Limb-Sounding) test flight into the Arctic polar vortex

Flight profiles as well as SZAs, and temperatures during the flights are shown in Figures B.13 - B.15 in the Appendix B. The tropopause height estimated from the temperature profiles was $\sim$ 16-17 km. A test flight was performed on January 18, 2005 over Oberpfaffenhofen, so the position of the polar vortex is of interest for this day, because sometimes the southernmost vortex edge can reach as far as Italy (e.g. on February 9, 2003). After the M55-"Geophysica" return to Oberpfaffenhofen, the MARSCHALS instrument test flight was performed on 7 March 2005. At that day the polar vortex edge reached down to 50°N. Therefore, a flight within the polar vortex could be performed starting from Oberpfaffenhofen. The positions of the vortex on 18 January 2005 and 7 March 2005 are shown in Fig.4.11. Its temperatures are given in Fig.4.12. It is seen that the vortex was very far from Germany on 18 January 2005. Besides that, the stratosphere in the

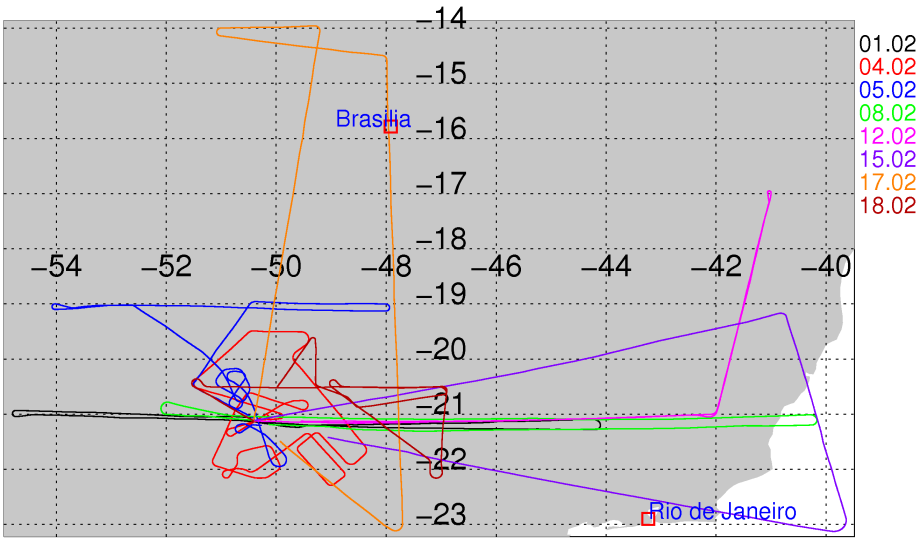

Figure 4.10: TROCCINOX campaign local flights trajectories. See Table 4.3 for details of the flights.

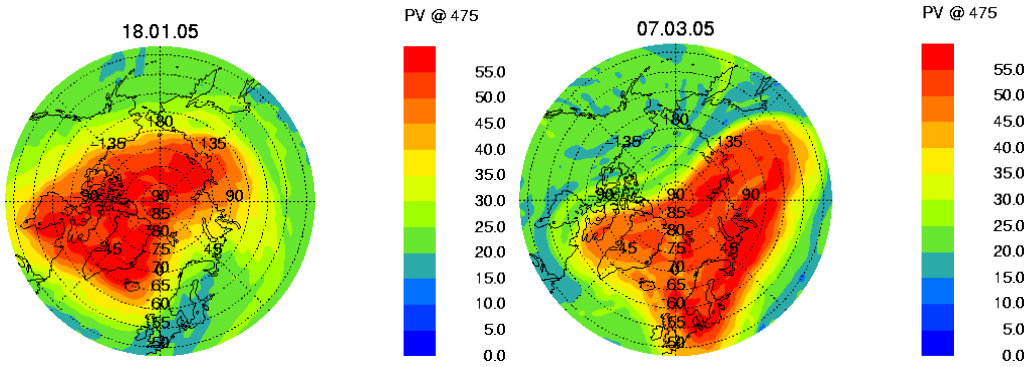

Figure 4.11: The northern hemispheric polar vortex on 18 January and 7 March 2005 both at 00:00 UT for the potential temperature level of 475 K

region of the test flight was rather warm on that day, while on 7 March the temperatures in the flight region were about 10 K colder. Flight trajectories for 18 January and 7 March 2005 together with PV values for these days are shown in Fig.4.13.

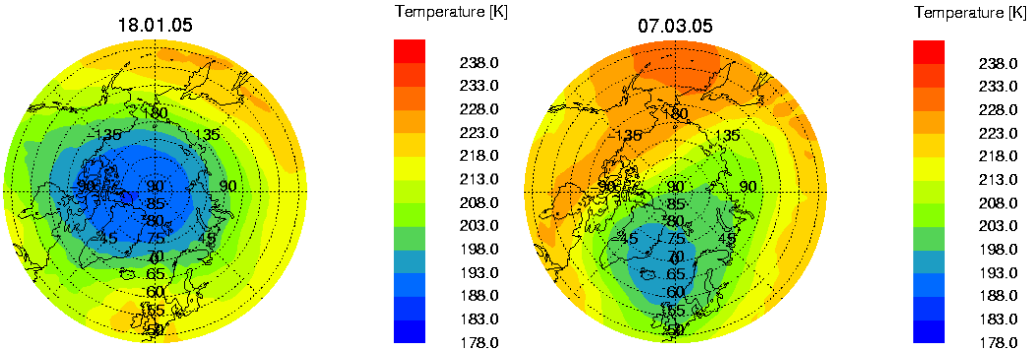

Figure 4.12: Temperatures of the Arctic polar vortex on 18 January and 7 March 2005 at 00:00 UT for the potential temperature level of 475 K

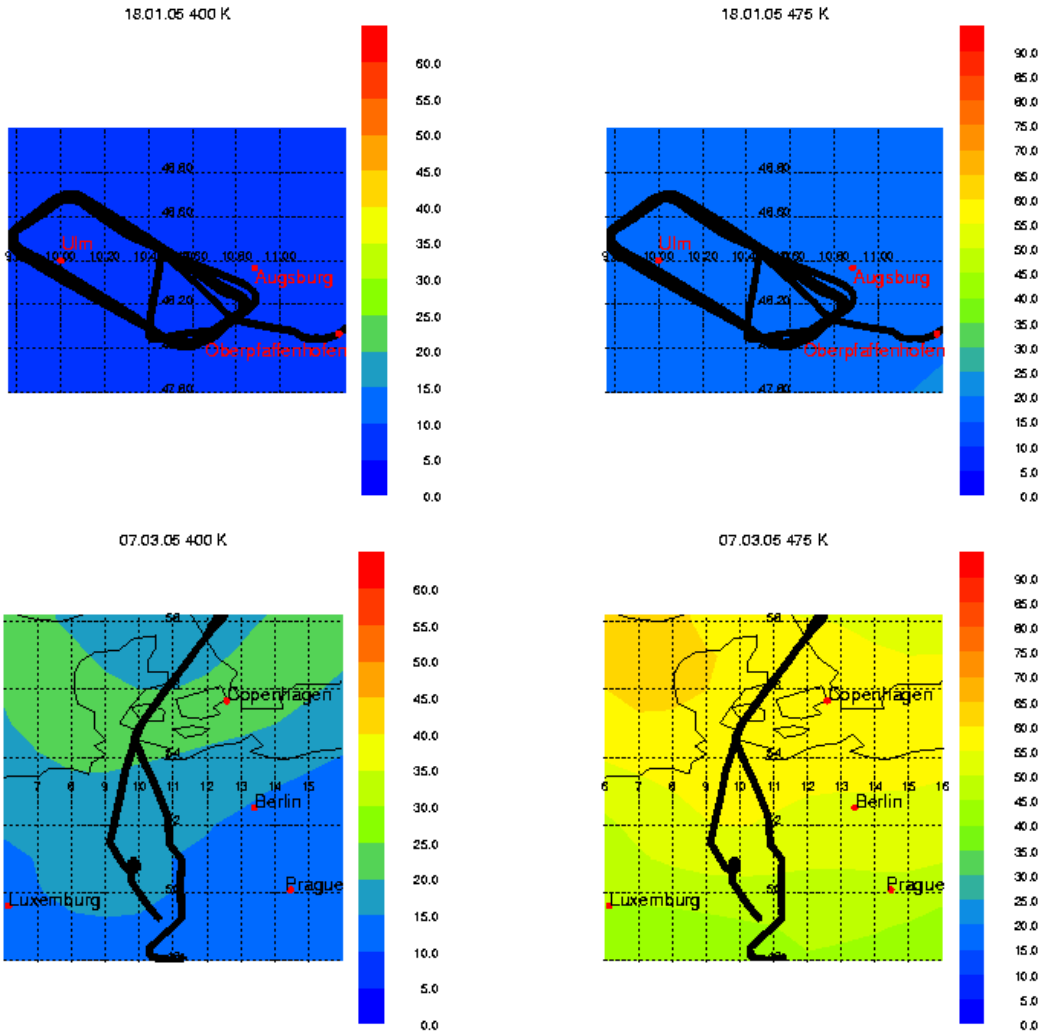

Figure 4.13: Flight trajectories and potential vorticity of the flights on 18 January and 7 March 2005. The trajectories are shown by thick black lines. The potential vorticity is shown by means of colour code in PV units for two potential temperature levels of 400 and 475 K. Note that the scale for PV is changed from the left to the right panels

4.6 The flights within the CRISTA-NF test campaign

Additional opportunity to carry out *BrO* measurements on-board M55-"Geophysica" was given in the frame of the test campaign in July 2005 (TC5). Two new instruments were tested: MARSCHALS, mentioned already above; and CRISTA-NF (CRyogenic Infrared Spectrometers and Telescope for the Atmosphere - New Frontiers). The campaign site was Oberpfaffenhofen, where the Flight Facility of Deutsches Zentrum für Luft- und Raumfahrt (German Aerospace Center, DLR) is situated. Its geographical position is 48.1°N 11.3°E. The campaign was quite short: only two flights were performed. Flight trajectories are shown in Fig.4.14. During these two flights

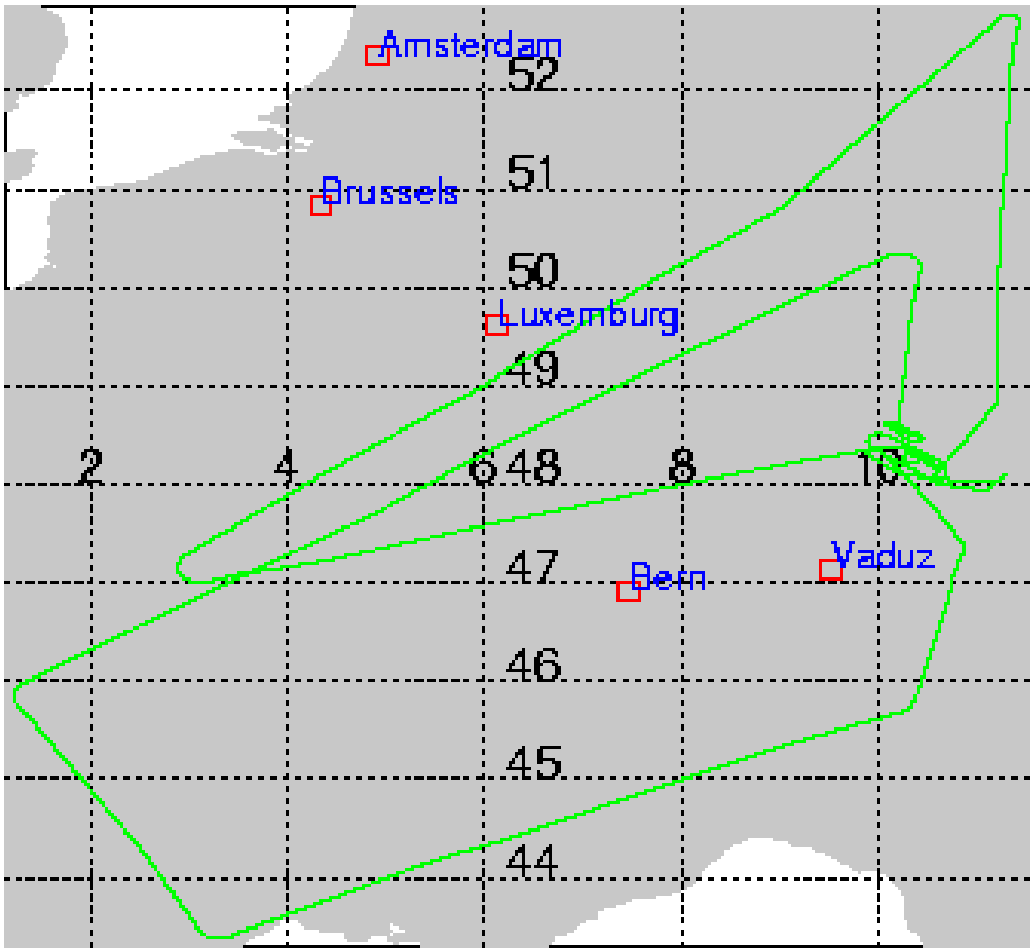

Figure 4.14: Flights trajectories during the TC5 campaign

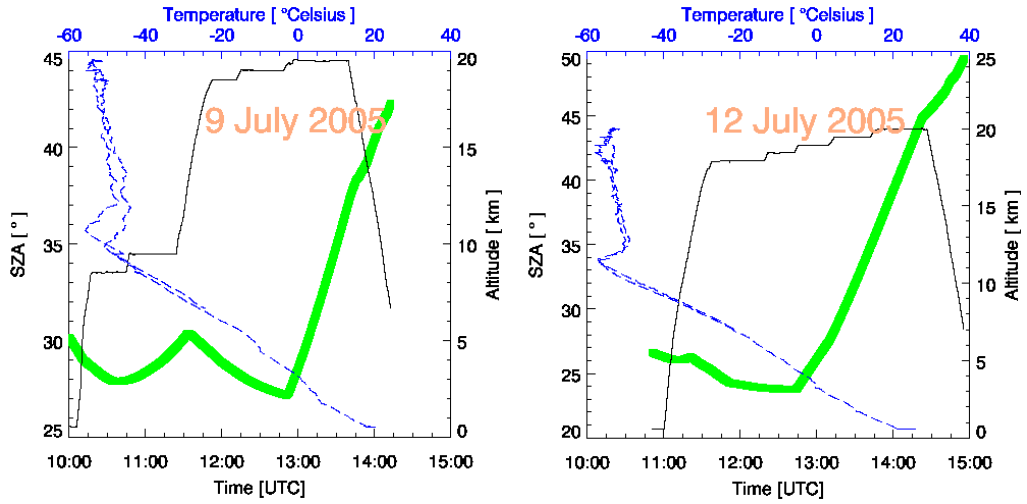

Figure 4.15: Flight profiles, temperatures and the SZAs for the TC5 campaign

M55-"Geophysica" flew above Germany, Austria, Italy, and France. Flight profiles as well as SZAs, and temperatures during these flights are shown in Fig.4.15. The tropopause height estimated from the temperature profiles was $\sim$ 11 km.

4.7 SCOUT-O3 aircraft flights

To observe how water and chemical species are lifted by strong thunderstorms, and to understand how they can reach the stratosphere in this way the SCOUT-O3 (Stratosphere-Climate Interactions with Emphasis on the Upper Troposphere and Lower Stratosphere) campaign was organized. One particular storm system that was studied in detail was the so called Hector, which occurs almost daily during November and December over the Tiwi Islands north of Darwin, Australia (11°S 131°E).

All flights carried out within the campaign are listed in Table 4.4.

.

The campaign was based at the Royal Australian Air Force base in Darwin, Australia (12.5°S, 130.8°E). Flight trajectories are shown in Figures 4.16 (transfer flights) and 4.17 (local flights). The flight patterns covered the area of more than 750 km in East-West direction and almost 1500 km in North-South direction. The flights were performed above northern Australia,

Table 4.4: Flights overview of the SCOUT-O3 campaign

Date	**Purpose of flight**
31 Oct 2005	Oberpfaffenhofen, instrument test
4 Nov 2005	Transfer, Oberpfaffenhofen - Larnaca
4 Nov 2005	Transfer, Larnaca - Dubai
8 Nov 2005	Transfer, Dubai - Hyderabad
9 Nov 2005	Transfer, Hyderabad - U Taphao
12 Nov 2005	Transfer, U Taphao - Brunei
12 Nov 2005	Transfer, Brunei - Darwin
16 Nov 2005	Hector survey
19 Nov 2005	Hector survey
23 Nov 2005	North-South survey
25 Nov 2005	Hector survey
28 Nov 2005	Hector survey (aborted)
29 Nov 2005	North - South survey
30 Nov 2005	Hector survey
30 Nov 2005	after Hector survey
5 Dec 2005	south survey flight specifically adjusted to three remote sensing instruments MIPAS, CRISTA and MARSCHALS
9 Dec 2005	Transfer, Darwin - Brunei
10 Dec 2005	Transfer, Brunei - U Taphao
13 Dec 2005	Transfer, U Taphao - Hyderabad
14 Dec 2005	Transfer, Hyderabad - Dubai
16 Dec 2005	Transfer, Dubai - Larnaca
17 Dec 2005	Transfer, Larnaca - Oberpfaffenhofen

Tiwi Islands, and Arafura sea of the Pacific Ocean. The tropopause height estimated from the temperature profiles was $\sim$ 17 km (Figures B.16 - B.18 in Appendix B).

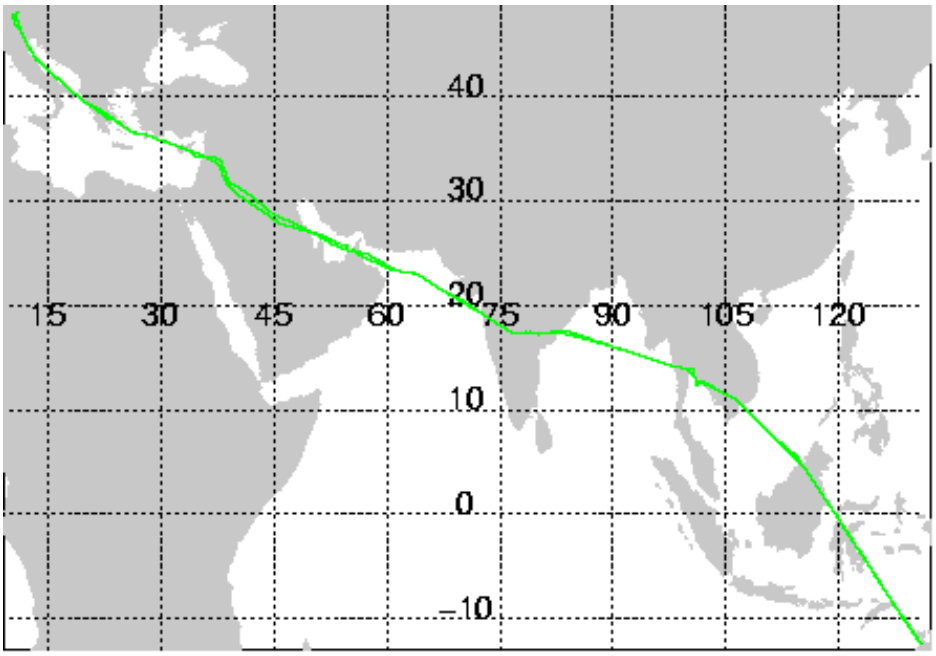

Figure 4.16: The trajectories of the transfer flights for the SCOUT-O3 campaign

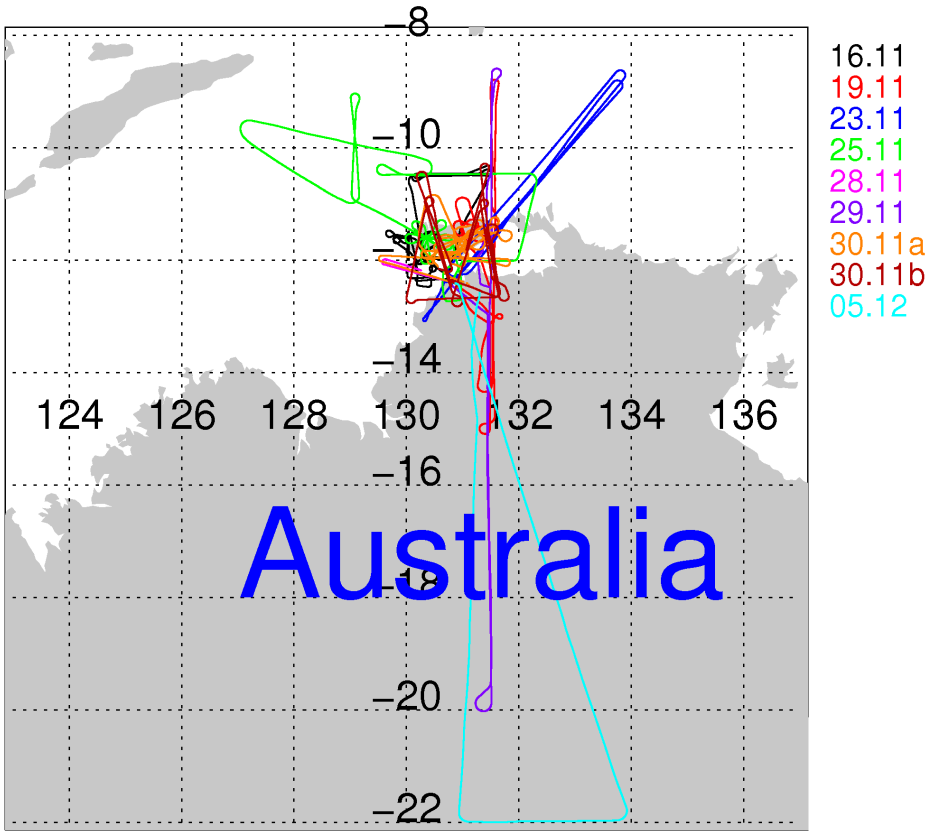

Figure 4.17: SCOUT-O3 campaign local flights trajectories. See Table 4.4 for details of the flights.

CHAPTER 5

Modelling with CLaMS

This chapter describes the photochemical model CLaMS that was employed in this work and presents results of the CLaMS simulation for the balloon flight on June 9, 2003.

5.1 Eulerian and Lagrangian approaches to the modelling

The abbreviation CLaMS means Chemical Lagrangian Model of the Stratosphere. CLaMS is a chemical transport model (CTM) that was developed at the Research Center Jülich and is described elsewhere (*McKenna et al.*, 2002b,a; *Grooß et al.*, 2002; *Konopka et al.*, 2003). It is based on the Lagrangian concept, that means that chemical processes are evaluated for so called "air parcels" that are transported with the wind and therefore change their location. The trajectories of the air parcels are determined from meteorological analysis (e.g. from ECMWF (the European Centre for Medium-Range Weather Forecast) (*Simmons et al.*, 1989)).

Most CTMs are based on the Eulerian method. Following this method the atmosphere is divided into a grid of cells. The content of every cell is supposed to be homogeneous. Then the chemical reactions are run in these cells. For each time step it is calculated which fraction of the air from a particular cell has drifted into one of the neighboring cells due to atmospheric dynamics. After that the air parcels are distributed newly according to the grid of cells. This procedure implies mixing of air parcels (so called "numerical diffusion") which may not reflect the real mixing process. In other words the Eulerian

method employs a fixed grid, which does not allow for features smaller than the fixed spatial resolution of the grid.

On the contrary CTMs employing the Lagrangian method calculate trajectories of chosen air parcels at first. Then the chemistry taking place along the trajectories is determined.

Figure 5.1 shows the principal modules incorporated in the 3-D CLaMS

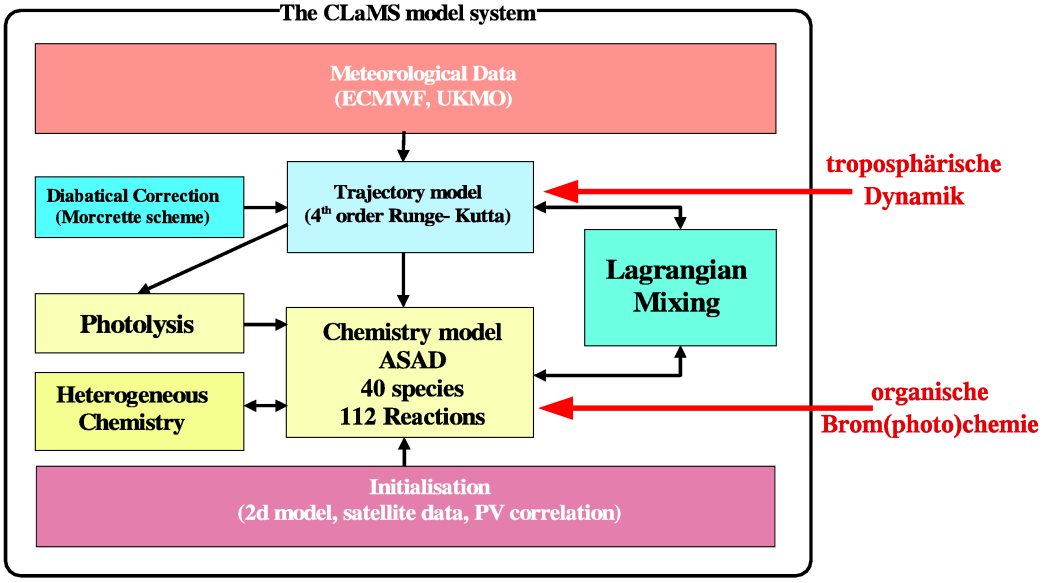

Figure 5.1: CLaMS model scheme

CTM. The advantage of CLaMS is that it can be applied in a flexible manner due to its modular structure. For this work CLaMS is used as a box-model, that means that chemistry (including photolysis and heterogeneous chemistry) is calculated for the individual air parcelsalong their trajectories without the use of the mixing. Such a Lagrangian model as CLaMS is an ideal tool for making comparisons between model calculations and balloon or aircraft measurements, because it is possible to use just backward or forward trajectories from the flight path instead of the complete 3-D grid in the Eulerian model. Therefore CLaMS is ideally suited to calculate the photochemical evolution of compounds like BrO in order to account for the temporal mismatch of different measurements.

The trajectory composition can be realized in either forward or reverse direction in time (so called backward or forward trajectories). This means the identification of the temperatures, pressures, and solar zenith angles in the air parcel probed by an instrument for a certain time period before or after the measurement. The initialization has to be determined, this means

the concentrations of all chemical compounds important for the simulation have to be set for the start time of the simulation. After that the chemical calculations start. Namely, it is calculated how the system does evolve under certain meteorological conditions (back or forward trajectories) from the beginning to the end of the period in question. Unlike the trajectory calculations, the chemical calculations are conducted forward only due to irreversibility of chemical processes.

5.2 Simulation of the dynamics and chemistry with CLaMS

The calculations of the air parcel trajectories in CLaMS base on wind and temperature fields taken from meteorological analysis. These fields are calculated by means of a meteorological model. In particular, ECMWF data sets used here have a meridional and zonal resolution of 1.125°, a temporal resolution of 6 hours, and a vertical one of approximately 1-2 km.

The vertical coordinate of the model in the stratosphere is the potential temperature Θ. Due to the vertical stability of the stratosphere (see Appendix A) vertical winds can be neglected in isentropic coordinates for many modelling tasks in this region of the atmosphere. So the information about the horizontal winds is sufficient. However, the adiabatic descent of the air masses has to be taken into consideration for polar regions and long-term simulations. For this purpose the new quantity $\frac{d\Theta}{dt}$, the temporal change of the potential temperature Θ, has to be introduced. For that an improved and numerically more efficient version (*Zhong and Haigh*, 1995) of the Morcrette radiation scheme (*Morcrette*, 1991) originally developed for use in the ECMWF model is employed in CLaMS. The trajectories are calculated from the ECMWF wind data by a Runge-Kutta scheme with a 30-min time step.

CLaMS uses a comprehensive set of reactions occurring in the stratosphere (*McKenna et al.*, 2002a), including full chlorine and bromine chemistry, 36 chemical species, and 115 reactions (including 27 photolysis and 11 heterogeneous reactions). The heterogeneous reaction rates depend on composition and state of aggregation of the surfaces where the reactions occur. These rates and the microphysics of liquid and solid aerosol are calculated using the scheme developed by *Carslaw et al.* (1995). The particle phases considered in these simulations are liquid ternary $H_2SO_4/HNO_3/H_2O$ solution aerosols, solid sulphuric acid tetrahydrate (SAT), nitric acid trihydrate (NAT), and water ice particles. In CLaMS two different scenarios are considered. For the default case, NAT formation is forbidden and only liquid

aerosols exist, forming supercooled ternary solution droplets (STS) below the NAT formation temperature (around 195 K in the low stratosphere), while in the alternative condensation scenario, NAT is formed from the STS droplets upon cooling when an HNO_3 supersaturation with respect to NAT of 10 is reached ($\sim$ 3 K supercooling).

5.3 Trajectory calculation

An ideal validation of the SCIAMACHY instrument would be to probe the same air mass as SCIAMACHY by some other instrument. In reality this condition is, however, unreachable. To overcome all these difficulties the so called "trajectory hunting technique" (THT) was developed (*Danilin et al.*, 2002).

At the first stage, backward and forward trajectories are calculated for each point of the balloon measurements. The length of the trajectories is arbitrary. Usually, it is a one-day trajectory for the photochemical correction purposes, and up to 10 days for detailed investigation of air mass origin (it is essential to keep in mind that longer trajectories have naturally larger uncertainties). In this work, the balloon measurements are origination points of the trajectories. So the balloon is called "hunter". The SCIAMACHY profiles' locations are the "targets". From a practical reason, it is better to launch trajectories from the locations of the infrequent measurements (in our case, from the balloon points) and to hunt in the more dense field of the SCIAMACHY measurements.

At the second stage of the THT it is checked whether the air parcels probed by the balloon pass within a reasonable temporal-spatial distance of any SCIAMACHY measurements of a few days around the balloon measurements. If so, the hunting for this trajectory is successful and it is a subject of comparison with the corresponding SCIAMACHY point. The complete information concerning the SCIAMACHY measurements (the overpass time, measurement duration, size and location of ground pixels) are taken from the website of the SCIAMACHY Operations Support Team (SOST) (http://atmos.caf.dlr.de/projects/scops/).

Examples of the THT are given Figures 5.2 - 5.4. In these figures the matching SCIAMACHY overpasses are marked. The match criterion is the same as it was chosen for the ozone Match experiment (*von der Gathen et al.*, 1995): a time difference between the satellite measurement and the trajectory has to be less than 1 hour, and the spatial distance between them has to be shorter than 500 km. For comparison, the footprint size of the SCIAMACHY swath is 960×200 km.

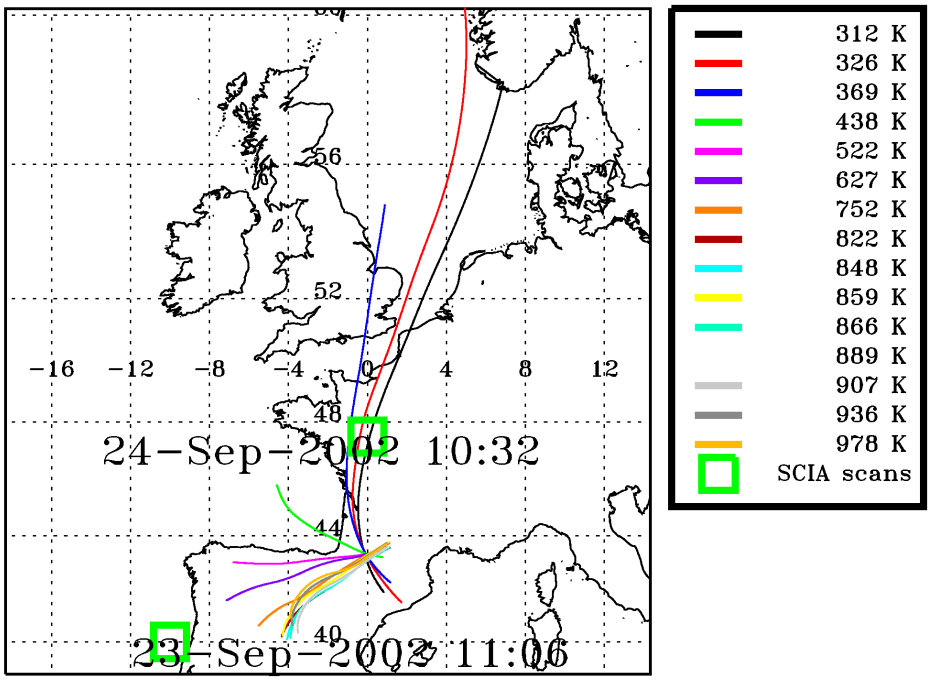

Figure 5.2: One day backward air mass trajectories for the TRIPLE ascent observations at Aire-sur-l'Adour, France, on September 24, 2002. The trajectories are shown in different colours for different altitudes given in potential temperature units. The swathes of SCIAMACHY are shown by means of green squares. Note that the swathes size is not scaled. Overpass times are given near the squares as well.

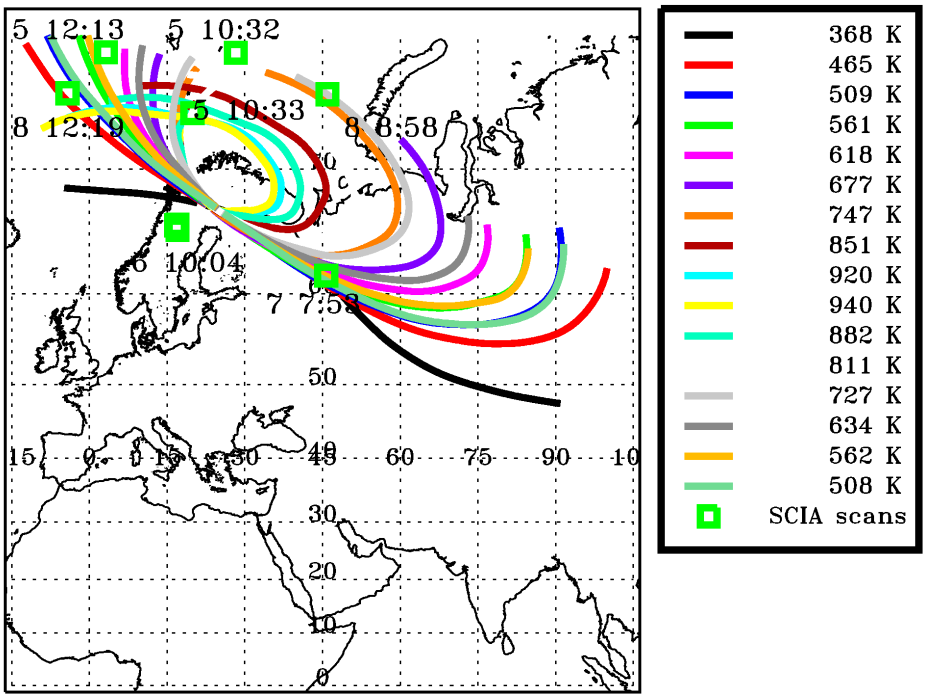

Figure 5.3: One day backward and two days forward air mass trajectories for the TRIPLE observations at Esrange, Sweden, on March 6, 2003. The trajectories are shown in different colours for different altitudes given in potential temperature units. The swathes of SCIAMACHY are shown by means of green squares. Note that the swathes size is not scaled. Overpass times are given near the squares as well (day number and UTC only).

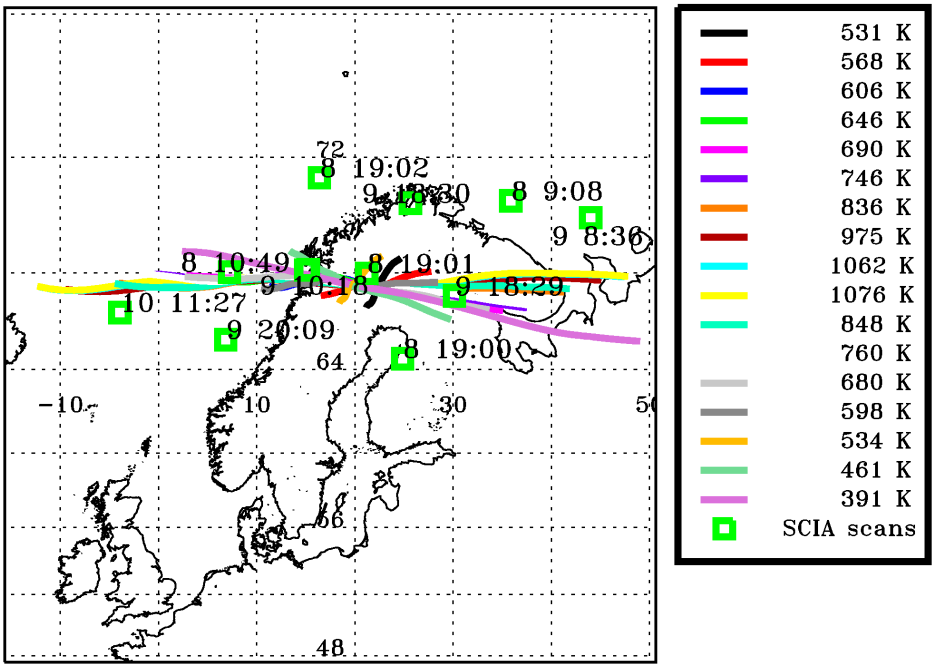

Figure 5.4: One day backward and one day forward air mass trajectories for the TRIPLE observations at Esrange, Sweden, on June 9, 2003. The trajectories are shown in different colours for different altitudes given in potential temperature units. The swathes of SCIAMACHY are shown by means of green squares. Note that the swathes size is not scaled. Overpass times are given near the squares as well (day number and UTC only).

To check the reliability of the calculated trajectories so called offset trajectories were calculated as well. They started at the same time as the "original" trajectories but the starting points were shifted by 3° both in latitude and longitude. In this way there were 4 offset trajectories for every central trajectory. An example of such a backward 20 days long trajectory family for the flight on June 9, 2003 for two different altitudes is shown in Fig.5.5. There was not any significant divergence of the trajectory families

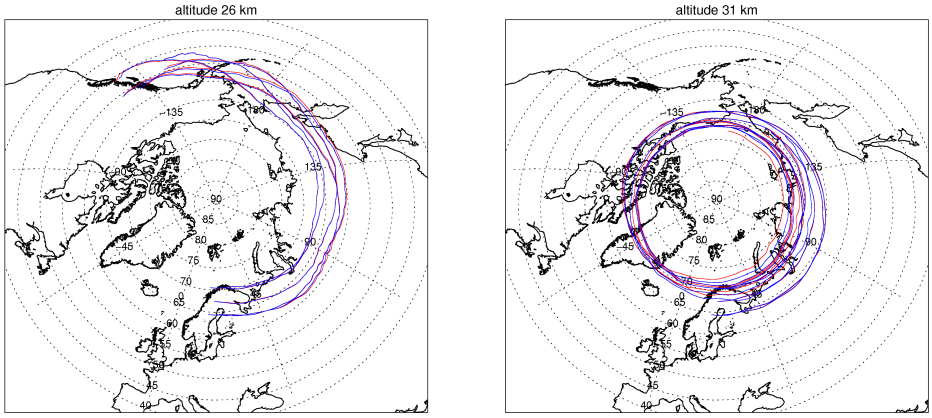

Figure 5.5: Central and offset back trajectories (see text) calculated for the ascent (red lines) and descent (blue lines) locations of the balloon flight on June 9, 2003, in Esrange, Sweden

in this case.

5.4 A case study: the balloon flight on June 9, 2003

An agreement between measurements and model results confirms that our understanding of stratospheric chemical processes is correct. A disagreement reveals, in turn, "weak" points in our knowledge.

Therefore an attempt to reproduce the measured BrO profile of the balloon flight on June 9, 2003, in Esrange, Sweden was performed by means of CLaMS.

Despite of rather similar photochemical conditions, quite different volume mixing ratios were observed during the ascent and descent parts of this balloon flight. The same phenomenon occurred in the flight on March 6, 2003. No operational malfunctions of the instrument were found. The low BrO during the ascents can be probably attributed to loss of BrO radicals

on the surface of the balloon, gondola or instrument itself. Whereas during the descents the probed air is uncontaminated by such effects. That is why from now on only the descent profile will be considered.

5.4.1 Initialization procedure

Two sources were used for initialization of species which were considered in the simulation. The first one are the measurements of the BONBON instrument on-board the TRIPLE gondola. It is a cryogenic whole air sampler (*Schmidt et al.*, 1987). The whole air samples are collected cryogenically in evacuated and conditioned sample bottles cooled with liquid neon and are analyzed by gas chromatography using an electron capture detector. The vertical profiles of the most important CFC species, Halons, as well as SF_6, CH_4, and N_2O can be obtained using BONBON. The second initialization data source is the Halogen Occultation Experiment (HALOE) on the Upper Atmosphere Research Satellite (UARS) (*Russell et al.*, 1993). This instrument measures ozone and other species using the solar occultation technique. It observes daily profiles at multiple longitudes along two latitude circles determined by the satellite's orbit. HALOE observes 15 sunrise and 15 sunset profiles per day at lower latitudes; the latitude range was 29.83°N - 74.25°N in May and 61.07°N - 64.47°N in the end of June 2003.

The CLaMS simulation described here starts on 20 May 2003 (20 days before the flight date) and is performed on 13 isentropic levels (384.4, 409.8, 465.7, 502.8, 538.1, 576.1, 615.3, 667.9, 721., 779., 845.6, 881.9, and 913 K). This set of theta levels corresponds to the altitudes where BONBON has taken samples. The inorganic bromine was initialized with the help of the BONBON data. Total bromine was set to 18.4 ppt (see Text below). For every point probed by BONBON a 20-days backward trajectory was calculated.

The initialization for ozone is taken from HALOE. Unfortunately HALOE measurements are quite sparse. That is why we tried two approaches for the initialization: a "temporal initialization" and a "spatial initialization". For the temporal initialization the closest HALOE scan to the midnight of May 20 was chosen and its values were taken to initialize the model. There is a gap in HALOE data between May 12 and 21, though. Therefore the HALOE values from May 21 were used. For the spatial initialization all HALOE scans performed in May - June 2003 were examined to reveal the closest spatial ones of them for each Θ-level and their values were used for the initialization (Fig.5.6). Both initializations have their own profiles so we decided to carry out simulation runs for both in order to test the sensitivity of the model to different initializations. To initialize the chemically inert tracer CH_4 HALOE

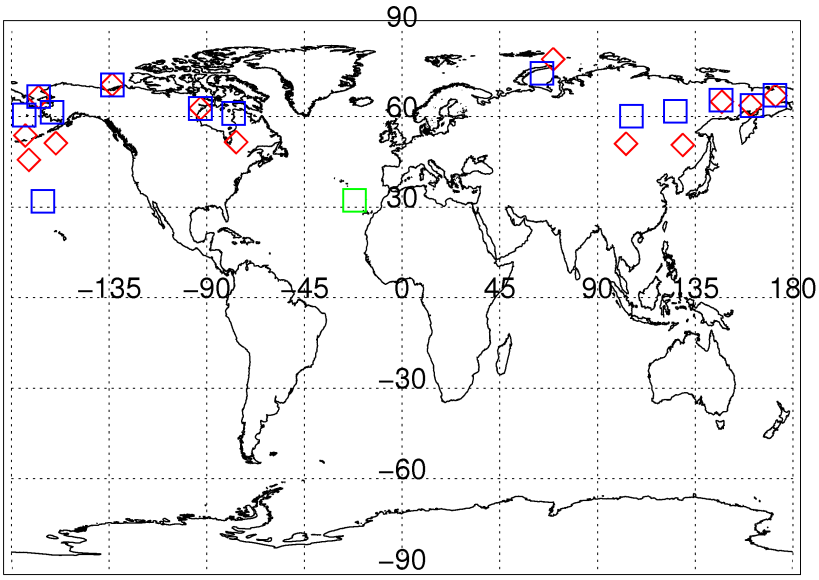

Figure 5.6: The spatial and temporal initialization for the CLaMS run. The red diamonds mark the positions of air parcels on different theta levels on May 20, 2003 at 0:00 UTC which were then probed by TRIPLE on June 9, 2003. The green square shows the geolocation of the closest in time HALOE scan on May 21, 2003, at 20:17 UTC. The volume mixing ratios obtained during this scan were used as "temporal" initialization. The blue squares mark HALOE scans performed in May-June 2003, which are closest to the locations of the TRIPLE measurements. These volume mixing ratios were taken as "spatial" initialization.

data were used as well. The same principle as for ozone was applied.

The so called family concept is used in CLaMS. This means that certain chemical species are grouped together into chemical families. The intrafamily conversion rates are typically much faster than the net rate of change of a given family. The chemical families defined in CLaMS are $O_x(= O_3 + O(^1D) + O(^3P))$, $NO_x(NO + NO_2 + NO_3)$, $ClO_x(= Cl + ClO + 2Cl_2O_2)$, and $BrO_x(= Br + BrO)$. For long model runs one can initialize just one family member with the sum of the entire family. This does not cause any error, because after a few steps the species are distributed within a family due to relatively fast chemistry.

From the NO_x family HALOE detects NO and NO_2 only. Their sum was taken as the initial value for NO_2, while NO was initialized as zero due to the short photochemical lifetime. As for O_3 and CH_4 there are two versions of initialization: the "spatial" and the "temporal" ones. H_2O and HCl were also initialized with the help of HALOE. All "temporal" and "spatial" initial profiles, as well as the HALOE profiles used for initialization are shown in Fig.5.7.

To initialize the bromine family a tracer correlation between Br_y and CH_4 determined by *Grooß et al.* (2002) was used. This correlation was ascertained for spring conditions, so it can be used as a good approach for the late spring conditions. For this correlation, all measurements at mid-latitudes to high latitudes made by the ACATS (the Airborne Chromatograph for Atmospheric Trace Species) instrument on-board the American research aircraft ER-2 and by the cryogenic whole air sampler BONBON were analyzed. The correlation was found to be very tight. With the polynomial fit to these data

$$[Br_y, ppt] = 44.3 - 106.3[CH_4, ppm] + 155[CH_4, ppm]^2 - \\ - 92.83[CH_4, ppm]^3 + 17.8[CH_4, ppm]^4 \quad (5.1)$$

the CH_4 measured by BONBON on the balloon flight on 9 June 2003 was used to calculate the mixing ratio of total inorganic bromine Br_y. The CH_4 from BONBON and Br_y, as well as the correlation curve between CH_4 and Br_y from (5.1) are shown in Fig.5.8. The simulation was started in the nighttime. Taking the above mentioned family concept employed in CLaMS into consideration, $BrONO_2$ as the main night reservoir was initialized by Br_y, while the other bromine species (HBr, Br, $HOBr$, BrO, $BrCl$, and Br_2) were initialized to zero.

The remaining chemical species are of less importance for the chemical simulations and were initialized using the corresponding Mainz 2-D photochemical model results (*Gidel et al.*, 1983; *Grooß*, 1996).

To check the sensitivity of the model towards the partitioning within

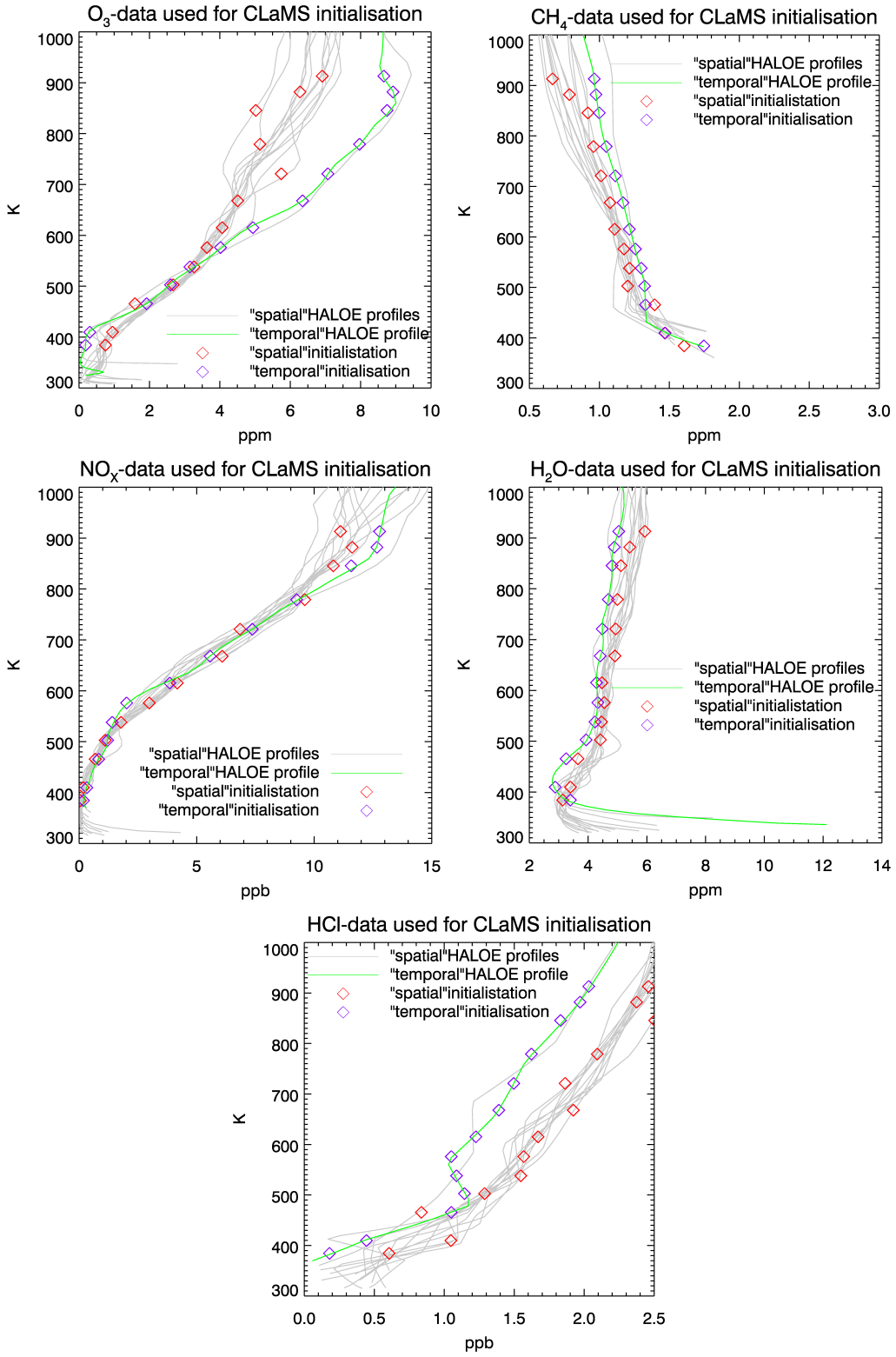

Figure 5.7: O_3, CH_4, NO_x, H_2O, and HCl initializations on 20 May 2003 for 13 theta levels. There are 13 profiles for each species from the best spatially collocated HALOE scans (shown in grey). For every theta level the value from the closest corresponding profile is taken as the "spatial" initialization. The resulting spatial initialization profile is shown by red diamonds. The best temporally collocated HALOE profile is shown in green

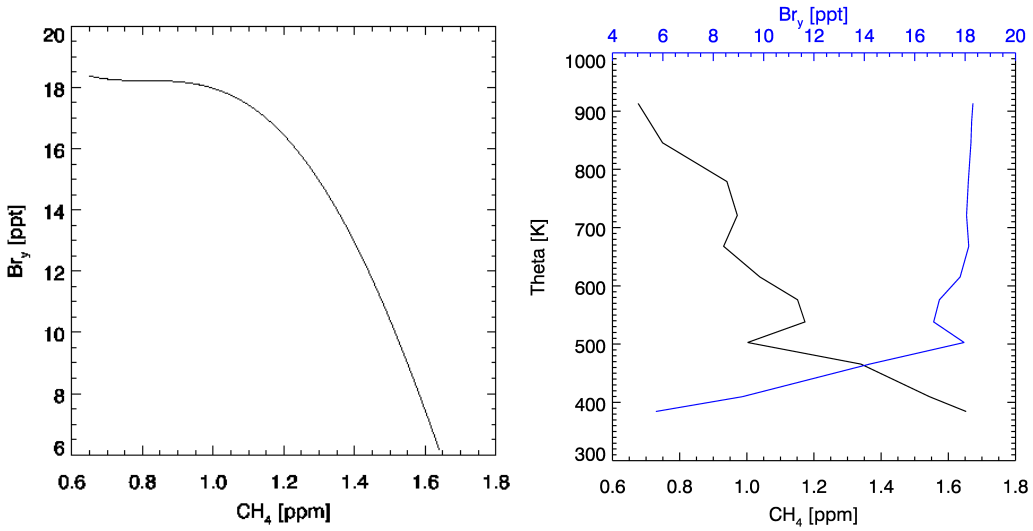

Figure 5.8: The CH_4/Br_y correlation (left panel) and the initialization derived by means of this correlation and BONBON CH_4 observation (right panel).

the chlorine family and towards NO_2 three additional initialization cases were created. The first one was the same as the standard case, but volume mixing ratios of chlorine nitrate $ClONO_2$ were halved and the mixing ratio of hydrochloric acid HCl was doubled. The second and third initialization cases were the same as the standard one as well, but volume mixing ratios of nitric oxide NO_2 were doubled in the second case and halved in the third case, respectively.

5.4.2 Model results

The results of the CLaMS simulation and the BrO profile obtained during the descent of TRIPLE on 9 June, 2003, are shown in Fig.5.9. In general, very good agreement is found. Deviations of the simulated values from the observation are well within the error bars.

The differences in the temporal and spatial initialization had a limited effect on the CLaMS results: the largest difference of 13% between the CLaMS simulations was found at the lowest theta level of 384 K, where the BrO volume mixing ratio itself was very low. The average difference was found to be only 3%.

Changing of the partitioning within the chlorine family (doubling of HCl and halving of $ClONO_2$) has generated a maximum increase of 4% in BrO compared to the standard run. This can be understood since the families

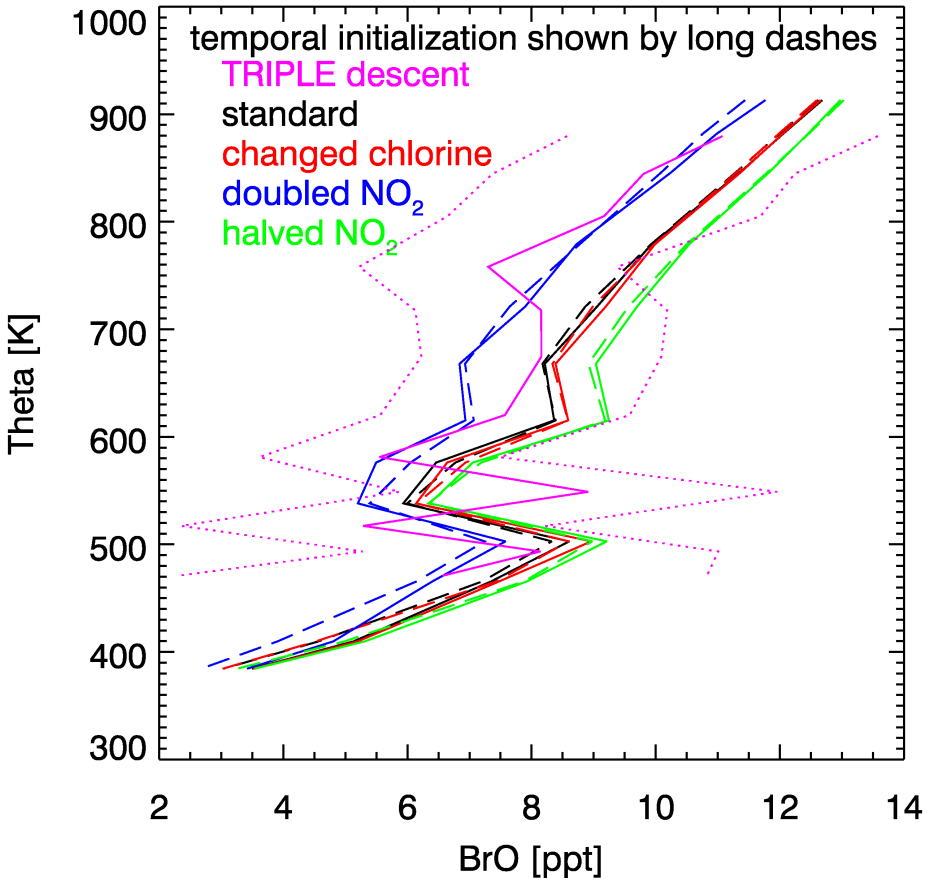

Figure 5.9: Comparison between the ClO/BrO-instrument measurements and CLaMS simulations for the TRIPLE balloon flight on 9 June 2003. The range of measured BrO uncertainty (1σ) is shown by dotted lines. There were two ways of initialization: the "spatial" and the "temporal" (see text). Results of the simulations with the temporal initialization are shown by long dashed lines. Besides that, two additional initialization cases were made: with the partitioning within the chlorine family changed and with doubled and halved NO_2. The first case is shown in blue, the second one in green

are coupled via the $BrO + ClO$ reaction only and changing the partitioning within the Cl_y family has only a minor effect on the very low BrO mixing ratios.

In contrast to this, variation of the NO_2 amount had an obvious influence on the BrO profile: doubling of NO_2 left more BrO in form of its reservoir $BrONO_2$ decreasing the simulated BrO profile by 2-17% depending on the potential temperature. Reduction of nitric oxide by 50% consequently increases the simulated bromine monoxide profile by 1-10%. Variations introduced by NO_2 changes are, however, much smaller than the error bars.

In general, the standard run of CLaMS tends to overestimate the measured BrO profile by 12%. However, this discrepancy is within the measurement error of the TRIPLE instrument. In other words, this means that the measured BrO, the initialization made using BONBON CH_4 data and the correlation from *Grooß et al.* (2002), as well as chemistry employed by CLaMS are consistent and realistic.

Not only the final result of the simulation is of interest. During the 20-days long simulation air parcels were experiencing different solar zenith angles. This enables to reveal the dependence of BrO on SZA. The simulated diurnal variation is shown in Fig.5.10 At lower theta levels BrO decreases more or less monotonically with increasing SZA tending to zero at SZA$\sim$92°. Whereas at the highest altitudes it has a more step-like behavior, having a "horizontal plateau" at SZAs lower than 85°, but decreasing very abruptly starting from 90° and staying above zero a bit further than at lower altitudes.

Beside that, the partitioning within the bromine family for day- and nighttimes is of special interest. Chemical partitioning has a major influence on the efficiency of a particular halogen in ozone destruction. The best way to illustrate this statement is to compare the fluorine, bromine, and chlorine families. In the case of fluorine, as soon as it is released from fluorine source gases in the stratosphere it forms the very tightly bound and therefore stable hydrogen fluoride HF (*Rowland and Molina*, 1975). Hence, the amount of ozone destructing F and FO is extremely low, and therefore fluorine has a negligible impact on ozone. Chlorine forms not only the hydrogen compound, but also chlorine nitrate $ClONO_2$. These species, however, can be converted either to chlorine Cl_2 or $HOCl$, which is then photolytically destructed to Cl atoms, and can destroy ozone (called therefore active chlorine). The partitioning between active chlorine and chlorine reservoir species is determined by chemical and physical conditions in the stratosphere, first of all by presence of polar stratospheric clouds, etc.

Bromine is not as strongly bound to its reservoirs as chlorine. That is why the fraction of active bromine is higher than its chlorine counterpart since $BrONO_2$ as well as HBr photolyse much faster than the corresponding

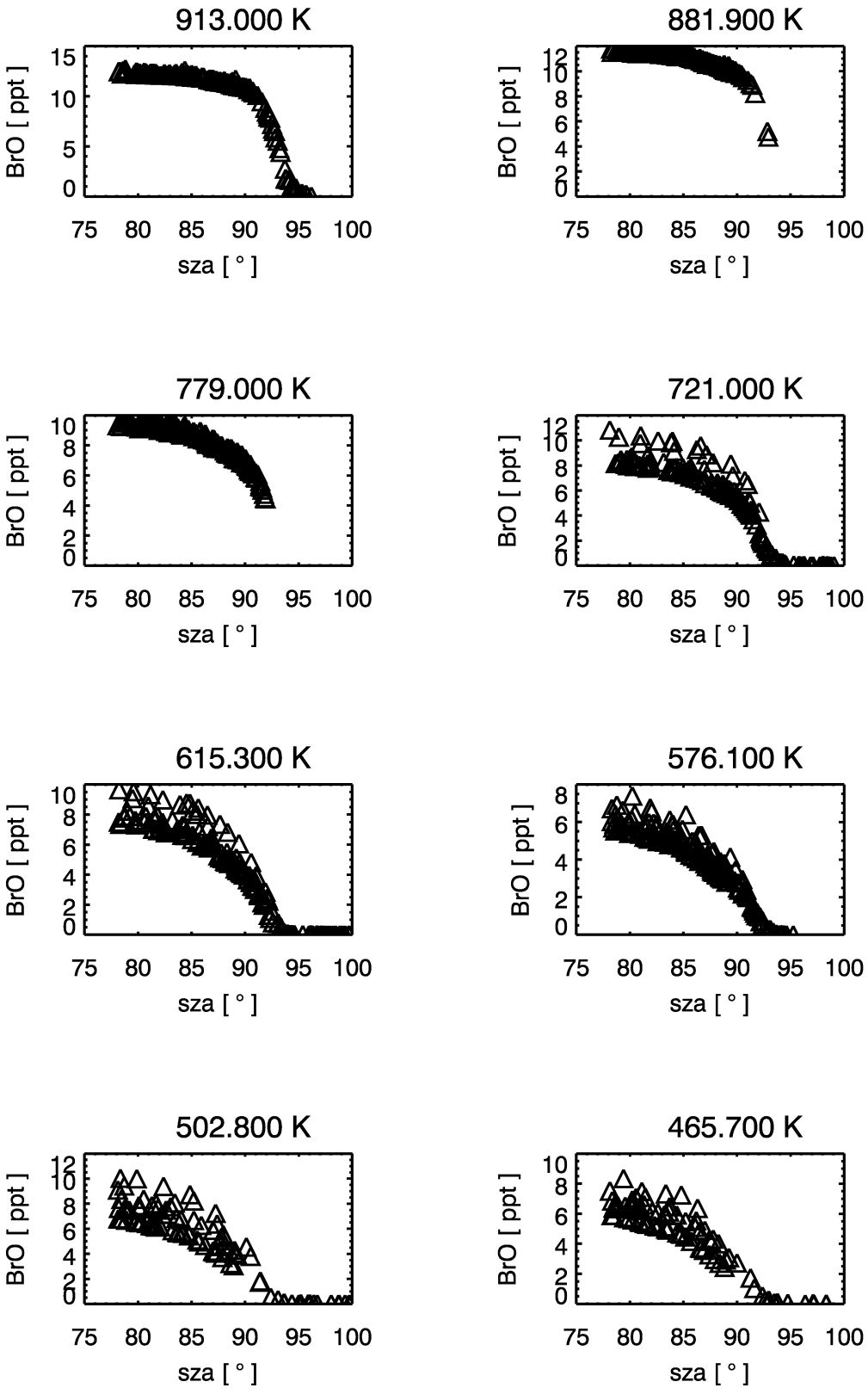

Figure 5.10: *BrO* as a function of solar zenith angle as simulated by CLaMS both for sunrises and sunsets for different potential temperatures.

chlorine species. The partitioning between bromine species is still subject of speculation, because only bromine monoxide has been observed more or less regularly. Therefore simulations as the one presented here allow to gain some insight about this subject. The day- and night partitioning within the bromine family based on the backward trajectories for the TRIPLE balloon flight on 9 June 2003 is presented in Fig.5.11. The partitioning presented here

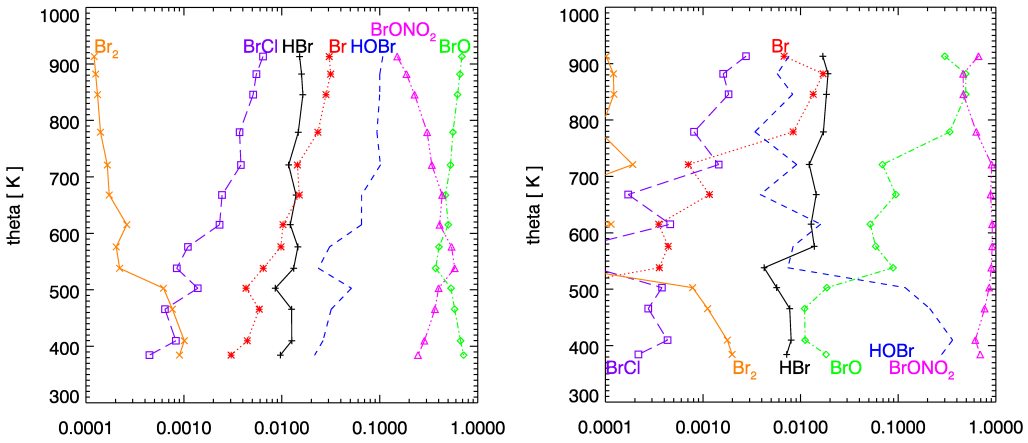

(a) Day (b) "Night"

Figure 5.11: The calculated day- and nighttime partitioning within the bromine family. The calculation is based on the backward trajectories for the TRIPLE balloon flight on 9 June 2003. Only those parts of the trajectories, where the solar zenith angle was lower than 60°, were taken into consideration for the daytime partitioning calculation; for the nighttime partitioning only parts with SZA greater than 90° were chosen.

is not representative for every season and region. The conditions experienced by air parcels were rather specific: most air parcels were under the influence of sun light during all 20 days, since polar day had already started in the latitude range under investigation. Therefore the probed conditions should be rather sensible to the photolysis of the reservoirs (especially $BrONO_2$). The fact that BrO is reproduced quite well within the CLaMS simulation gives confidence into the implemented CLaMS photochemistry.

For the calculation of the nighttime partitioning only parts of the trajectory with SZA greater than 90° were chosen. It would have been better to limit "night" by 95° instead of 90°, but as it was said, some air parcels at high altitudes (750 K) never experienced SZA higher than 90°.

Generally the most abundant bromine species in the sunlit lower and middle stratosphere is BrO. In our case, however, there was an exception between about 520 and 600 K, where bromine nitrate was more prevalent.

According to the CLaMS simulations at 540 K approximately 40% of Br_y is in the form of BrO rising to about 75% at 385 and 915 K. The main source of BrO is the photolysis of $BrONO_2$

$$BrONO_2 + hv \rightarrow Br + NO_3 \tag{5.2}$$

followed by

$$Br + O_3 \rightarrow BrO + O_2 \tag{5.3}$$

In the sunlit lower stratosphere the main destruction of BrO occurs by reaction with NO_2

$$BrO + NO_2 \rightarrow BrONO_2 \tag{5.4}$$

Thus, taking Reaction (5.4) into account, the above-mentioned drop in the BrO fraction between 520 and 600 K can be attributed to enhanced NO_2 there (Fig.5.12). This happened because of polar vortex remnants at this Θ-level (*Grooß et al.*, 2006). The measured BrO reveals, however, slightly enhanced value at this altitude, which we currently are unable to explain.

In total darkness, however, BrO represents less than a few percent of Br_y.

$BrONO_2$ is the second most abundant compound in the sunlit lower stratosphere. It represents approximately 55% of the total Br_y at about 540 K rapidly decreasing upwards down to about 15% at 920 K. Whereas in the night-time Br_y is almost completely in the form of $BrONO_2$.

$HOBr$ is supposed to be the third most abundant bromine compound in the daytime lower stratosphere making up 2-10% of Br_y (with the fraction increasing with altitude). In the night-time the fraction of $HOBr$ reaches 30% at 400 K.

According to our current understanding, generally only a small percentage of Br_y in the lower stratosphere is in the form of HBr: less than 2% independent on SZA.

Br constitutes 0.3% in the sunlit lowermost stratosphere rising to 3% at 900 K, virtually disappearing at night-time.

$BrCl$ constitutes much less than 1% of Br_y both in day- and night-time. This is the case, however, only when ClO is low as the case under the conditions of our case study. Under activated Cl conditions in the polar vortex $BrCl$ becomes a major night-time reservoir for Br_y.

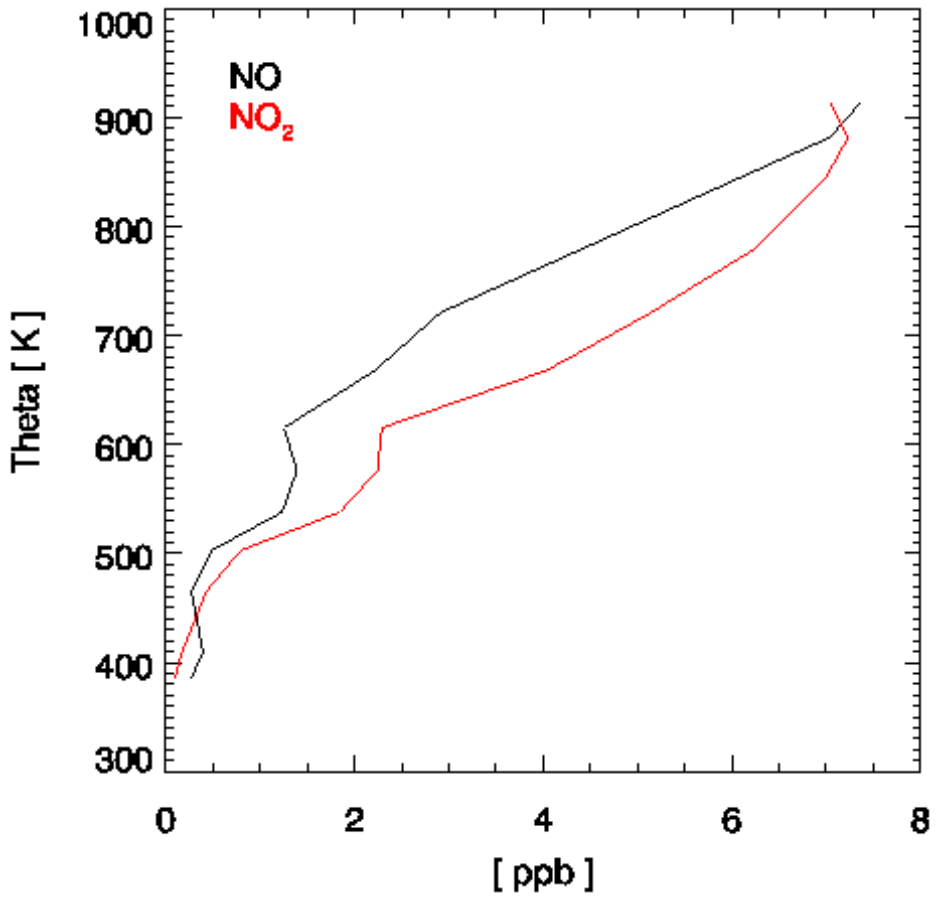

Figure 5.12: NO and NO_2 from the CLaMS simulation for the TRIPLE balloon flight on June 9, 2003, 12:00 UT

CHAPTER 6

Results of BrO measurements and its comparison with the SCIAMACHY profiles

SCIAMACHY measurements require appropriate validation, i.e. the estimation and improvement of the satellite data quality by means of its comparison with independent measurements obtained by other well-established instruments which are co-located in time and space as closely as possible.

6.1 BrO profile retrievals from SCIAMACHY

Up to now no operational processor for BrO retrievals could be established by ESA. Only scientific retrievals from independent groups are available. SCIAMACHY BrO profiles retrieved by two groups were used for comparison with the TRIPLE measurements: these are the groups from Universities of Bremen (Alexei Rozanov) and Heidelberg (Sven Kühl). One more group, at the University of Harvard, makes BrO retrieval from the SCIAMACHY data as well. However, firstly there are no profiles from this group for the TRIPLE flight days; secondly, comparison of the tropical HALOX BrO profile with that retrived by this group reveals significant discreapancy. Therefore only profiles from Bremen and Heidelberg were used for comparisons with the TRIPLE.

These two groups use different retrieval algorithms. The Bremen group uses the Uni Bremen retrieval processor version CDI-(V 1.2.17-2) (www.iup.physik.uni-bremen.de/scia-arc) as described by *Rozanov et al.* (2005), and the temperature dependent BrO absorption cross-sections from *Fleischmann et al.* (2004). The BrO retrieval is possible in the altitude range

from about 15 to about 30 km with a precision of about 30-50% for a single profile and an estimated systematic error of 10-20% or at least 1 pptv (including a contribution due to remaining pointing uncertainty).

The group of Sven Kühl from University of Heidelberg uses a two-step method to retrieve the stratospheric distribution of BrO. In the first step, slant column densities (SCDs) for BrO are derived from the SCIAMACHY limb spectra by the DOAS method. Secondly, the trace gas SCDs are converted into vertical concentration profiles applying radiative transfer modelling. The inversion is performed by an optimal estimation method.

6.2 Photochemical correction of the BrO profiles measured by TRIPLE

A validation flight with a perfect collocation between the satellite swath and the balloon-borne instrument is almost impossible (see Sec. 5.3). As a consequence, there always is a certain difference between photochemical conditions under which satellite and balloon-borne instruments obtain their profiles for validation purposes. These differences have to be taken into consideration, when one deals with BrO validation, since the BrO concentration depends on photochemical conditions (see Sec. 5.4.2). Once it has been assumed by trajectory studies that the observed air masses are comparable (see Sec. 5.3), it is possible to correct the BrO profile measured by a balloon-borne instrument for the SZA of the satellite measurement by means of photochemical modelling. For this purpose the diurnal variation of BrO for the day and location of the measurement has to be modelled. The model has to be initialized in such a way to reproduce the BrO measured by TRIPLE. Then the BrO value for the SZA of the SCIAMACHY scan is taken to compare with the SCIAMACHY BrO limb value.

For this photochemical correction the CLaMS model (see Sec. 5.1) was employed. CLaMS BrO simulation for the balloon flight on June 9, 2003 revealed very good agreement with the measured BrO. Since the simulation was 20 days long including, in that way, day and night conditions, it gives confidence in correctness of the photochemistry employed by CLaMS. Such a long time for the simulation was chosen because of rather specific photochemical conditions during the period of the simulation: a polar day has already started at the beginning of June. That is why, to test correctness of photochemical evolution of bromine species simulated by CLaMS longer simulation time was needed in order to "reach" the period with "normal" day/night changing.

To perform the model runs for the TRIPLE BrO profiles correction the air mass trajectories were calculated as follows: each trajectory was started at 23:00 UTC on the day before the flight (September 23, 2002, March 5, 2003, and June 8, 2003). Trajectories were chosen so to cross the TRIPLE position during the measurement. All trajectories were calculated to be 24 hours long. If the end values of the chemical species did not differ markedly from the initial ones, this was taken as an indication of the convergence of the model.

Initial values for the simulation of the flight in Aire-sur-l'Adour on September 24, 2002 were taken:

- for O_3, HNO_3, and H_2O from the MIPAS (The Michelson Interferometer for Passive Atmospheric Sounding) satellite instrument on-board ENVISAT;

- for NO_2 and CH_4 from the MIPAS balloon instrument, which has performed its flight from Aire-sur-l'Adour on the same day with TRIPLE, but in the evening;

- for ClO_x from the Mainz-2D model. The partitioning was, however, recalculated by means of an independent CLaMS run;

- for all species within the bromine family zero was taken as initial value apart from $BrONO_2$, which was initialized by BrO values measured by TRIPLE. This approach, however, leads to obvious underestimation of modelled BrO, because not 100% of the bromine family appear as BrO during daytime. The underestimation factor for each altitude level was calculated later on. A second model run was performed for each modelling case, where the $BrONO_2$ initialization was increased by the underestimation factor. Finally, the third model run was done for each modelling case, where the end values of the bromine family species from the second run were taken as initial values for the third run. This did not, of course, change the sum of the bromine family, but in this way the Br_y partitioning was adjusted to the model photochemistry.

- other species were initialized with the help of the Mainz-2D model.

Initialization for the Kiruna flight on March 6, 2003 was the same as for the flight in Aire-sur-l'Adour, apart from the following differences:

- O_3 was initialized with the values measured by the ozone sonde on-board TRIPLE;

- NO_2 and HNO_3 were taken from the LPMA (Laboratoire de Physique Moléculaire pour l'Atmosphère et l'Astrophysique) balloon instrument, which had flown two days before the TRIPLE flight;
- CH_4 was taken from the BONBON (Cryogenic whole air sampler) instrument on-board TRIPLE;
- H_2O was taken from the FISH (Fast In-Situ Stratospheric Hygrometer) instrument on-board TRIPLE.

For the Kiruna flight on June 9, 2003 CLaMS was initialized as follows:

- O_3 from an ozone sonde launched one hour later than TRIPLE;
- NO_2, HNO_3, and H_2O were taken from the MIPAS satellite instrument (8 June 2003, 22:11 UT, 65.7°N 7.4°E) ;
- CH_4 as for the March flight was taken from BONBON;
- ClO, Cl_2O_2, and the bromine family were initialized as described for the flight in Aire-sur-l'Adour.

Modelling results for the important species are shown in Figures 6.1-6.3, where diurnal cycles on different theta levels are shown by means of different colours. For the most abundant species the start and end VMRs agree very well indicating that the model photochemistry has equilibrated. The BrO VMRs as measured by TRIPLE are exactly reproduced.

All BrO profiles measured by TRIPLE as well as their photochemically corrected versions are shown in Fig.6.4. As it can be seen from Fig.6.4 for the three described TRIPLE flights the photochemical correction does not cause substantial changes to the measured profiles. This follows from the fact that BrO exhibits a quite constant plateau during day time. In other words, if measurements have SZA smaller than about 80°, they can be more or less directly compared, since the photochemical correction brings negligible change compared to the error bars of the measurements.

6.3 Comparison of TRIPLE balloon-borne and SCIAMACHY BrO profiles

As it was mentioned above, up to now SCIAMACHY BrO profiles retrieved by the Universities of Bremen (*Rozanov et al.*, 2005), Heidelberg, and Harvard (*Sioris et al.*, 2006) are available for comparison with the validation

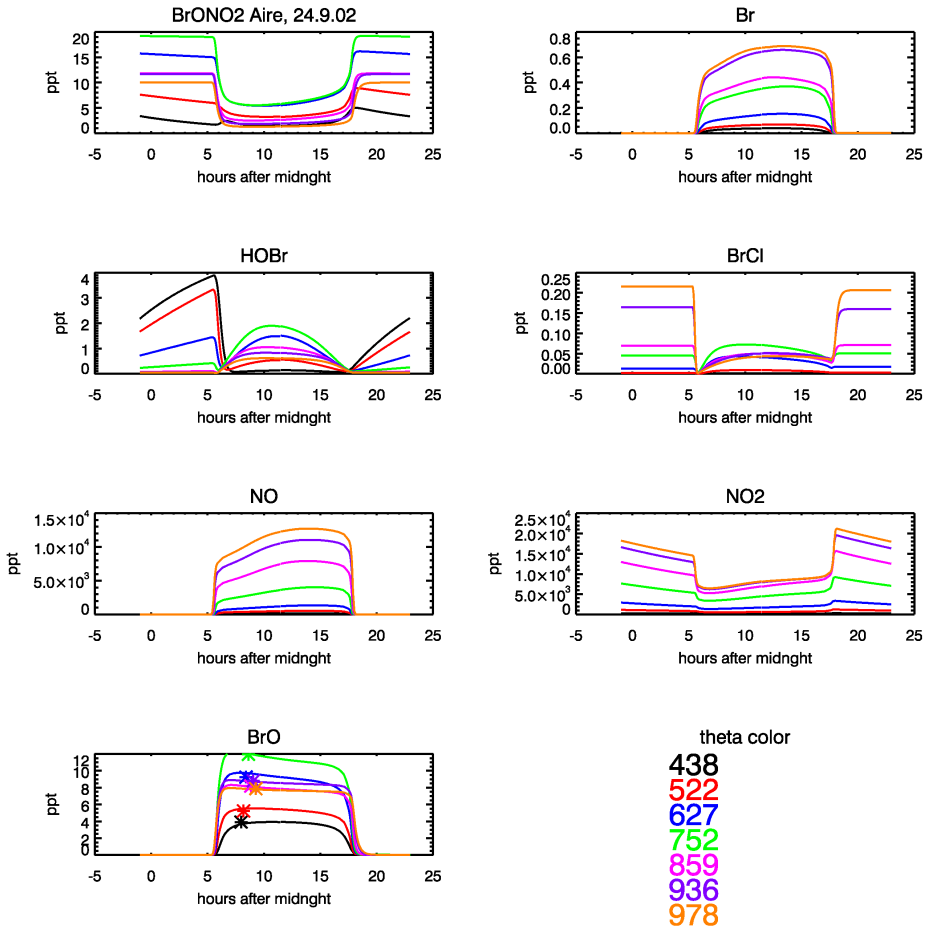

Figure 6.1: Diurnal cycles of substantial chemical species for the mid-latitude conditions on 24 September 2002 as simulated by CLaMS. Results for different theta levels are shown by different colours. On the *BrO* panel VMRs measured by TRIPLE are additionally shown by asterisks

measurements. The parameters and results of all TRIPLE measurements are available on the internet-site http://www.iup.physik.uni-bremen.de/boost/, which serves as discussion forum for optimization the validation in general. Further comparisons will be performed by means of back- and forward trajectory hunting (see Section 5.3) and appropriate photochemical correction.

SCIAMACHY *BrO* limb profiles, which are ready to compare with TRIPLE, are those taken on September 24, 2002, March 6, 2003, and June 9, 2003 (all three balloon flights, performed by TRIPLE, since SCIAMACHY is in the orbit).

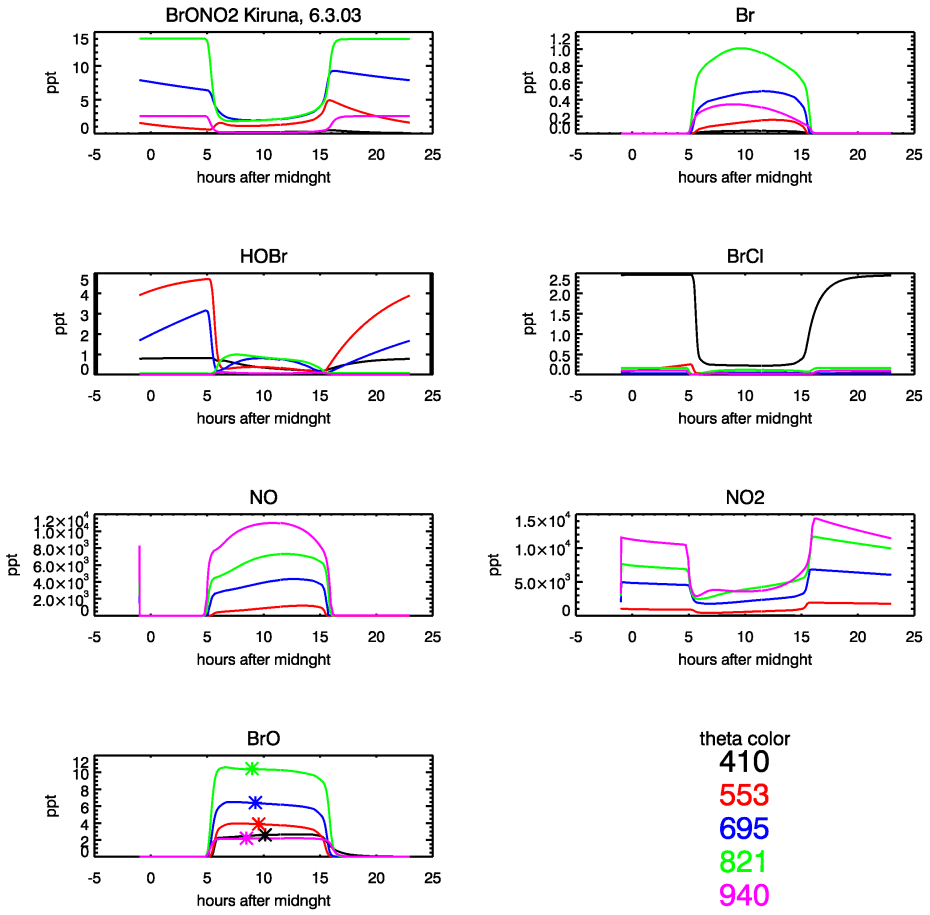

Figure 6.2: Diurnal cycles of substantial chemical species for the high latitude conditions on 6 March 2003 as simulated by CLaMS. Results for different theta levels are shown by different colours. On the *BrO* panel VMRs measured by TRIPLE are shown as well by asterisks

The dates and locations of TRIPLE measurements as well as the corresponding SCIAMACHY swathes, the geophysical regimes and the SZA for both type of measurements are given in Table 6.1. For every point measured by the balloon-borne instrument backward and forward trajectories were calculated. Based on these calculations one SCIAMACHY swath was chosen for each flight for back- and forward trajectories as a best match. So there are four SCIAMACHY profiles (Bremen and Heidelberg versions for best back- and forward matches) to compare with each balloon-borne instrument profile. The essential information about these SCIAMACHY swathes (orbit number, time, spatial distance to air parcels probed by the balloon-borne instrument,

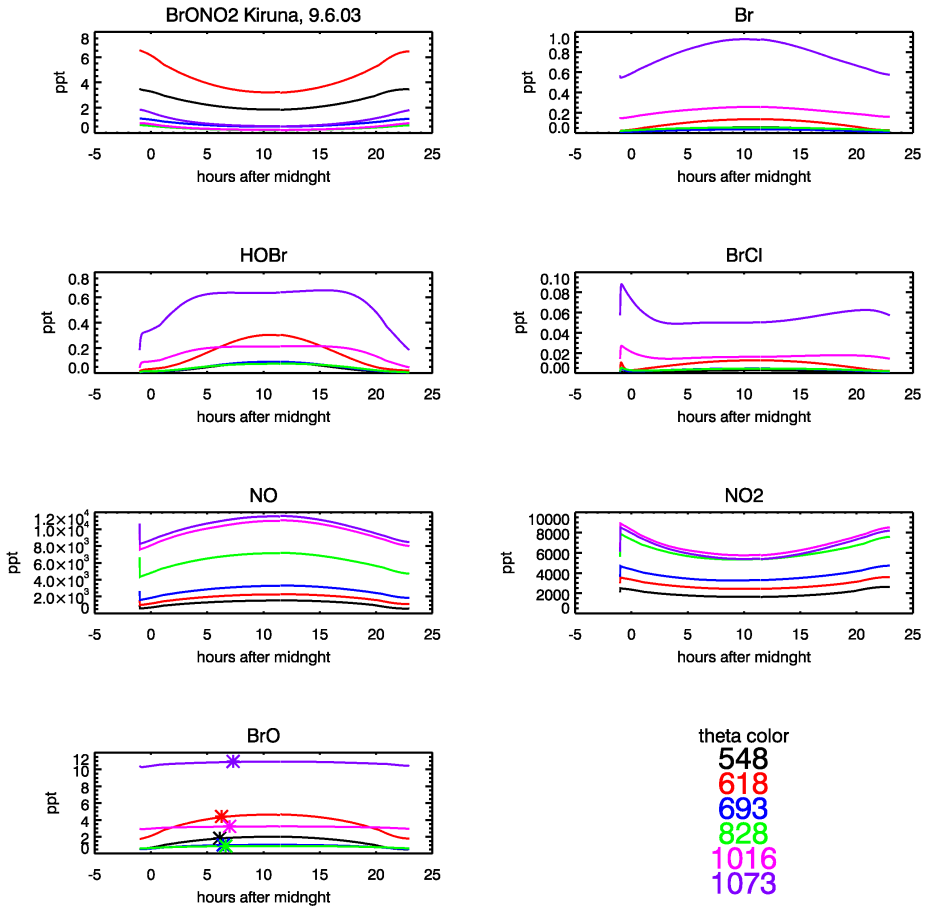

Figure 6.3: Diurnal cycles of substantial chemical species for the high latitude polar day conditions on 9 June 2003 as simulated by CLaMS. Results for different theta levels are shown by different colours. On the *BrO* panel VMRs measured by TRIPLE are shown as well by asterisks

altitude range of matched air masses) are listed in Table 6.1 as well.

The SCIAMACHY profiles presented here were the most up to date versions from the BOOST web page http://www.iup.physik.uni-bremen.de/boost/. Comparisons of the preliminary SCIAMACHY *BrO* profiles with the TRIPLE *BrO* (among other balloon-borne instruments) have been already published in (*Rozanov et al.*, 2005) and (*Dorf et al.*, 2006).

Fig.6.5 shows the comparison of *BrO* profiles measured by SCIAMACHY (retrieved both by Bremen and Heidelberg groups) and by TRIPLE. On each figure the TRIPLE *BrO* profile photochemically corrected to the SZA of the SCIAMACHY measurement (apart from the backward match for the flight

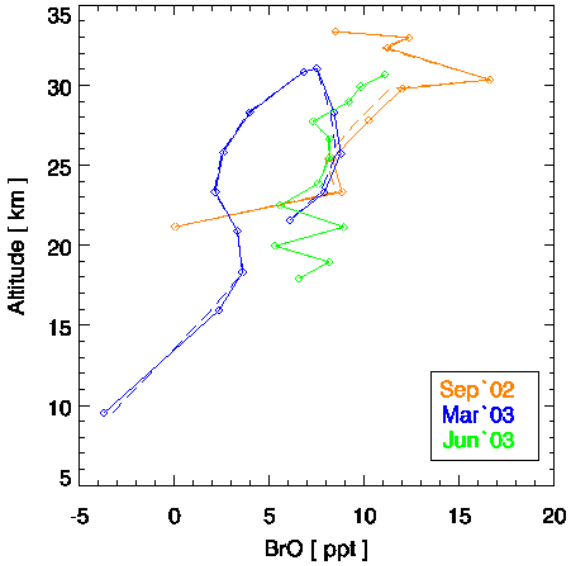

Figure 6.4: *BrO* profiles measured by TRIPLE during the three validation balloon flights. Profiles photochemically corrected to the SZA of the corresponding SCIAMACHY measurement are shown by means of dashed lines.

Table 6.1: Summary of TRIPLE *BrO* measurements and ENVISAT / SCIAMACHY overpasses

Date Time [UTC]	**Location**	**Geophys. Cond. SZA range**	**Satellite coincidence Orbit, Date, Time [UTC], SZA**	**Altitude range [km]**	**Spatial mismatch [km]**
24 Sep 2002 8:11-10:07	Aire-sur-l'Adour 43.7°N 0.3°W	mid-lat autumn 49°-66°	2954, 23 Sep 2002, 11:06, 44.5° 2968, 24 Sep 2002, 10:32, 50°	21-29 16-33	303-781 380-585
6 March 2003 6:32-9:44	Esrange 67.9°N 21.1°E	high lat. winter 73°-85°	5288, 5 Mar 2003, 12:13, 82.6° 5301, 6 Mar 2003, 10:04, 72.5°	16-28 5-31	8-900 387-496
9 June 2003 7:56-9:08	Esrange 67.9°N 21.1°E	high lat. spring/ summer 45°-49°	6652, 8 Jun 2003, 19:01, 81.5° 6661, 9 Jun 2003, 10:18, 45.6°	5-31 5-34	20-557 107-197

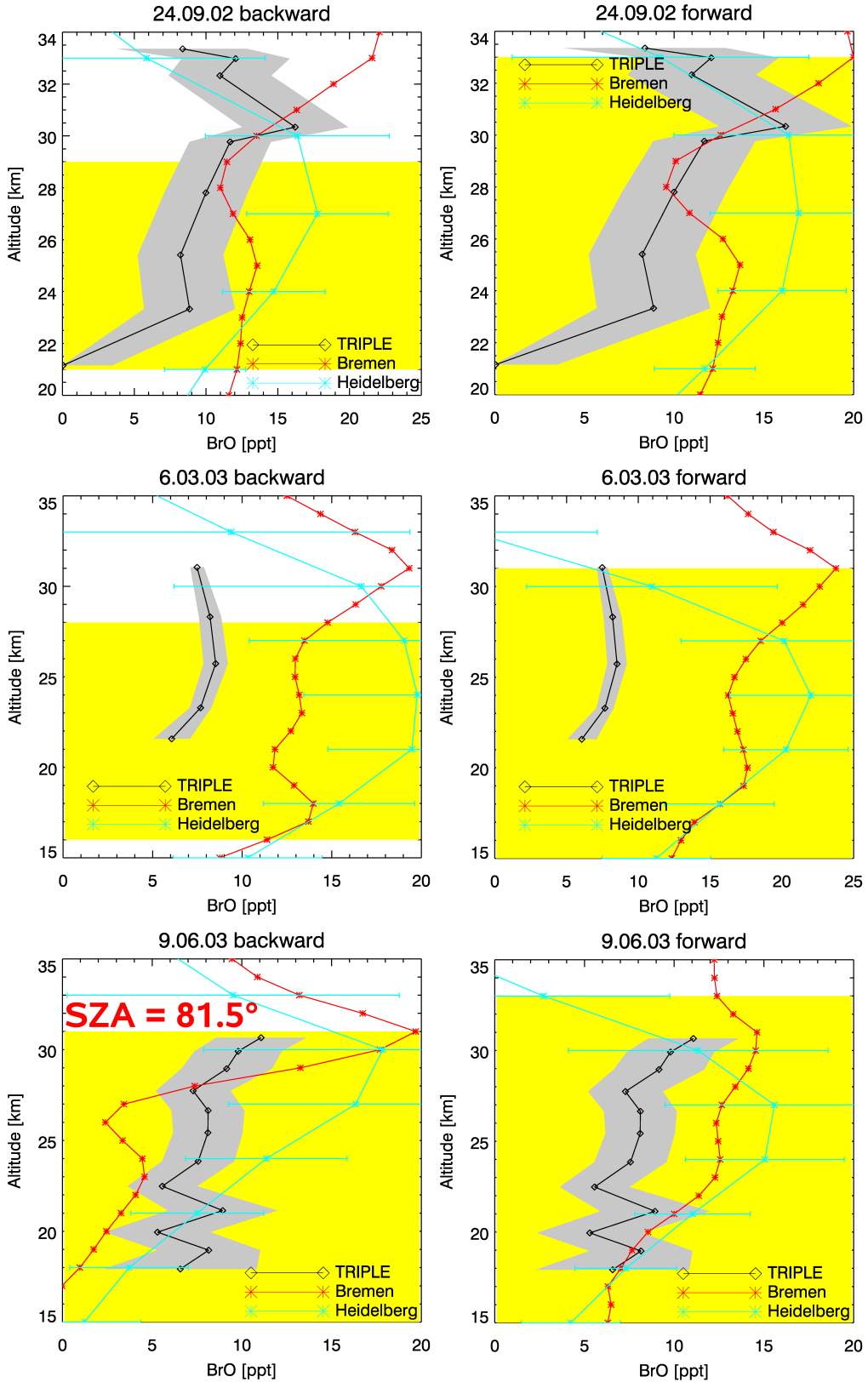

Figure 6.5: Comparison of BrO profiles measured by TRIPLE (black) and SCIAMACHY (red and cyan). For better visibility the retrieved BrO VMRs are connected by solid lines. The yellow marked area indicates the altitude region where according to the trajectory model SCIAMACHY and TRIPLE have probed the air masses according to the match criteria (see Text for details).

on 9 June 2003, where SCIAMACHY SZA was very high (81.5°)) is shown. Corresponding SCIAMACHY BrO limb profiles retrieved by the Bremen (red profiles) and Heidelberg (cyan profiles) groups are shown as well. For the Bremen BrO profiles the error bars are not shown. They are about 30-50%.

The BrO retrieval from the TRIPLE measurements is performed by means of signal averaging over long time intervals (up to 15 minutes). The statistical averaging error is indicated in Fig.6.5 by means of the grey marked area. The accuracy of the TRIPLE BrO measurements is ±30% (not reflected in the plots). That is why, in the cases where the statistical error does not exceed 30%, one has to use this value as the error.

At high altitudes the pump can not quite maintain the fast air flow in the measurement duct. This and the low pressure (less than 10hPa) could cause increased loss of Br atoms on the walls, and consequently, potential underestimation of the BrO VMR by the CCRF method.

The TRIPLE mid-latitude measurements on September 24, 2002 were performed between SZA of 49.3° and 65.6°, whereas the SZA of the SCIAMACHY measurement was 44.5° for the backward match and 50° for the forward match. Since satellite and balloon measurements were taken in the morning well after sunrise, and the diurnal variation of BrO in this SZA interval is rather small (see Fig.5.10), the correction applied to TRIPLE BrO is less than 6% for both the backward and forward matches. The spatial distance between air masses probed by TRIPLE and by SCIAMACHY ranges from 303 to 781 km for the backward match and from 380 to 585 km for the forward match. But despite of this reasonable match the SCIAMACHY profiles show on average much larger values (40-100% higher than TRIPLE) and there is no agreement within the given error bars below 26 km. Above this altitude there is a noticeable difference between the Bremen and Heidelberg BrO profiles both in absolute value and in the shape. While the Bremen profile experiences a decrease in BrO VMR between 26 and 28 km, then monotonically increasing with altitude, the profile of Heidelberg reaches its maximum around 27 km, rapidly decreasing after that. Nevertheless the Heidelberg SCIAMACHY values agree well with TRIPLE BrO within the error bars of the individual instruments in the range 30-33 km.

TRIPLE high latitude measurements on March 6, 2003 were performed under SZA between 73.1° and 85.5°. The SCIAMACHY backward match scan was done under 82.6° and the forward one - under 72.5°. TRIPLE profiles were photochemically corrected to match SZAs of SCIAMACHY, the correction, however, did not exceed 19%, with an average correction of 3%. The spatial distance between air masses probed by TRIPLE and by SCIAMACHY ranges from 8 to 900 km for the backward match and from

387 to 496 km for the forward match. Again there is a difference between SCIAMACHY profiles retrieved by the Bremen and Heidelberg groups. Both profiles reach their maxima, then decreasing with altitude. This maximum lies, however, at 30 km in the Bremen profile and at 24 km in the profile from Heidelberg. Obviously there is no agreement at all between SCIAMACHY and TRIPLE BrO for this flight, apart from the highest point in the TRIPLE profile (around 31 km), which agrees at least within the error bars with the Heidelberg version of SCIAMACHY BrO. SCIAMACHY reveals much higher BrO values (30-60% for the backward match and up to 70% higher for the forward match) for this day.

The TRIPLE spring high latitude measurement on June 9, 2003 was performed in polar day conditions under SZA of 45.4°-49°. SCIAMACHY performed a backward match scan under SZA 81.5°, which is quite different from the SZA of the TRIPLE measurements. It can be seen that the Bremen BrO profiles for backward and forward matches differ quite noticeable. That is why the backward match BrO profile has to be taken in consideration with regard to this fact. The forward match of SCIAMACHY was performed under SZA of 45.6°. The photochemical correction to this value of SZA was negligible (less than 1%), but it is encompassed in Fig.6.5. The spatial distance between air masses probed by TRIPLE and by SCIAMACHY ranges from 20 to 557 km for the backward match and from 107 to 197 km for the forward match. The backward match profiles of SCIAMACHY reveal rather different values for the altitude range between 21 and 27 km. While the Bremen retrieval shows around 3 ppt of BrO, the Heidelberg BrO increases from 7 to 16 ppt in this altitude range. Below 21 km and above 27 km the two SCIAMACHY retrievals agree within the error bars. Between 18 and 22 km the TRIPLE and Heidelberg BrO agree very well. Above these altitudes the Heidelberg BrO is higher, nevertheless, it coincides with TRIPLE BrO within the measurement error. Below approximately 28 km Bremen BrO is lower (down to 80% at 18 km), and above - higher (40% at 31 km) comparing to TRIPLE BrO. SCIAMACHY forward match profiles retrieved by both groups agree well up to 31 km, where Heidelberg BrO starts to decrease very rapidly. Agreement between Heidelberg and TRIPLE BrO is within the error bars, apart from the point at 24 km, where Heidelberg retrieval suggests BrO to be about 50% higher than that measured by TRIPLE. Bremen BrO agrees with TRIPLE perfectly up to 21 km altitude. Above it the Bremen BrO is 20-50% higher than that measured by TRIPLE.

Overall, the TRIPLE BrO is significantly lower than that retrieved by Bremen and Heidelberg groups from the SCIAMACHY measurements. Below approximately 30-31 km the Heidelberg profiles tend to reveal slightly higher values of BrO, remaining, however, in reasonable agreement with the

Bremen profiles within errors. Above 31 km things change: here the Heidelberg BrO decreases rapidly with increasing altitude and is lower than retrieved using the algorithm of the Bremen group.

On average, the Bremen and Heidelberg SCIAMACHY retrievals reveal around 43% higher BrO VMRs compared to the TRIPLE BrO. Only to a very small extent these discrepancies can be explained by mismatches between the TRIPLE and SCIAMACHY measurements. Taking backward and forward matches into consideration separately, it can be concluded that SCIAMACHY forward matches agree slightly better with TRIPLE BrO, than backward matches (discrepancies are 41% for forward matches against 46% for backward ones), which could be attributed to a better spatial agreement of the forward matches with air masses probed by TRIPLE (in average 325 km for forward matches and 515 km for backward ones).

It is significant to mention that the SCIAMACHY retrievals do not agree with each other very well which points to problems in the retrieval procedures. Both retrievals show very similar general shapes which may be caused by a-priori dependence. Besides that, the Bremen profiles always show much more "features" in the profile shape than Heidelberg which may be due to oscillations in the procedure.

The TRIPLE profiles were checked and seem consistent with photochemical models, however, the profiles retrieved from the SCIAMACHY measurements are systematically higher than the in-situ measurements. This is also observed when comparing TRIPLE with DOAS balloon profiles (see Fig.6.9) and seems to be a general problem that should be dealt with in future campaigns.

6.4 BrO measured by HALOX on-board M55-"Geophysica" aircraft

HALOX instrument took part in a number of measurement campaigns performed using the Russian aircraft M55-"Geophysica". The highest flight altitude of "Geophysica" aircraft does not exceed 21 km or 50hPa. On this altitude our measurements indicate BrO VMRs of generally less than 6 ppt (see Fig.6.5). Due to these low VMRs and low sensitivity of the BrO measurements at these pressure levels BrO detection in the lower stratosphere is very difficult.

To obtain a reasonable signal to noise ratio the detector signal has to be averaged for long time up to half an hour (see Fig.3.9). In addition, not every part of the flight can be used for analysis, since during climbs and dives the

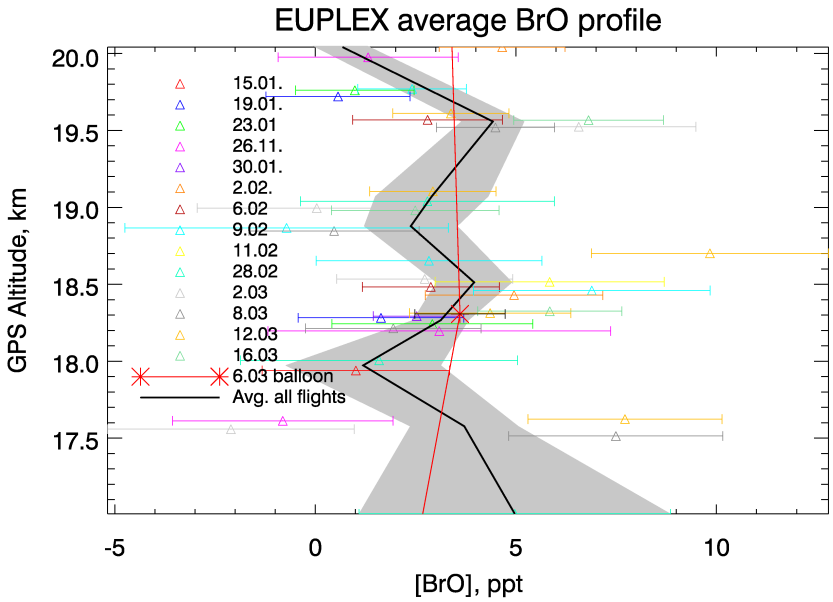

Figure 6.6: Results of the BrO measurements during the Arctic EUPLEX campaign in January-March 2003. Points from individual flights are shown by means of different colours. The averaged BrO profile is shown by the black line. The grey area shows the average profile error.

signal is quite disturbed due to turbulence in the measurement duct. That is why for usually 4-5 hours long M55-"Geophysica" flights a maximum of 4-5 BrO data points can be measured. Therefore BrO measurement results for every campaign are averaged into one profile as long as no significant variation over different flights are present. In case of the tropical campaigns a profile is averaged employing data from different geophysical locations (see Figures 6.6-6.8). The mean profiles were calculated using weighted averages of the data points. The mean value was calculated using the following formula:

$$\mu = \frac{\Sigma(\frac{x_i}{\sigma_i^2})}{\Sigma(\frac{1}{\sigma_i^2})} \tag{6.1}$$

where each measured BrO data point x_i in the sum is weighted inversely by its own variance σ_i^2. The uncertainty of the mean σ was calculated as

$$\sigma_\mu^2 = \frac{1}{\Sigma(\frac{1}{\sigma_i^2})}. \tag{6.2}$$

Since BrO does not vary significantly during one campaign or even different campaigns in similar geophysical regimes, the BrO observations can be

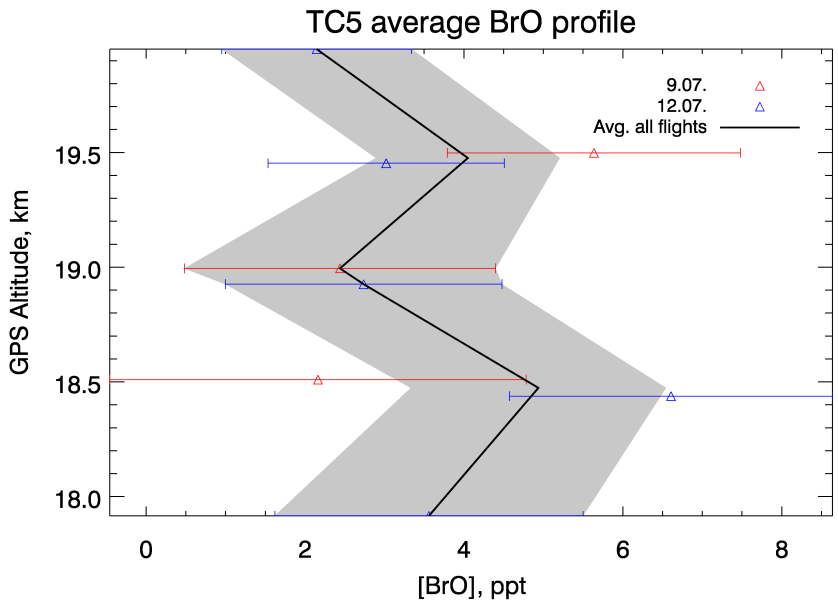

Figure 6.7: The same as in Fig.6.6, but for the mid-latitude test campaign (TC5) in July 2005

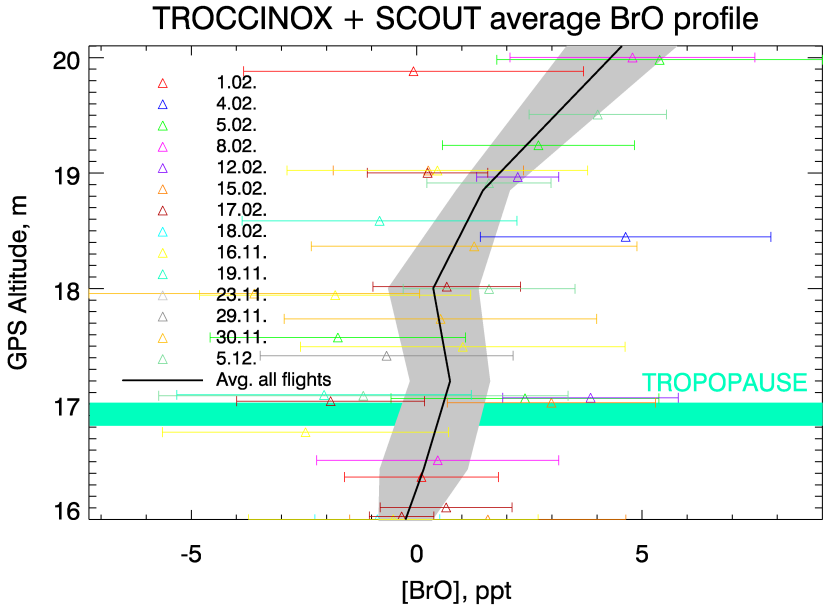

Figure 6.8: The same as in Fig.6.6, but for the two tropical campaigns TROCCINOX and SCOUT-O3 in January-February and November-December 2005, respectively.

considered as repeated measurements of the same quantity. In this case the precision of the mean profile is better than that for every single measurement and the following formula can be applied for the uncertainty of the mean profile

$$\sigma = \frac{\sigma_\mu}{\sqrt{N}} \tag{6.3}$$

where N is the number of averaged data points (*Bevington and Robinson*, 1992).

In the EUPLEX plot also one BrO data point obtained in the balloon flight on March 6, 2003 is shown along with a line connecting to the lower down and higher up balloon measurements. The balloon BrO data point is, however, connected with the neighbor points to get impression about the BrO VMR profile behavior. Excellent agreement between the aircraft and balloon BrO data points is found.

In general, there is not any noticeable difference in VMRs and shape of the Arctic and mid-latitudinal BrO profiles observed by TRIPLE and HALOX, while the tropical one exhibits quite different values: according to the HALOX measurements the amount of BrO around the tropopause and up to 1 km above it is close to zero, starting to increase afterwards, reaching about 5 ppt at 20 km.

To further check the consistency of the BrO profiles, a comparison with tropical profiles measured by other instruments is performed (Fig.6.9). It can be seen that HALOX measurements are persistently lower than the balloon-borne DOAS BrO measurements of Heidelberg University as well as other available BrO DOAS measurements. However, quite good agreement between HALOX BrO and that retrieved from tropical SCIAMACHY observations by the Bremen group (*Sinnhuber et al.*, 2005). Agreement between HALOX BrO and that detected by SAOZ (*Pundt et al.*, 2002) and DOAS (*Dorf et al.*, 2006) balloon instruments is slightly worse but still within the error bars. And with the BrO retrieved from the SCIAMACHY measurements by Harvard there is no agreement at all. Currently there is no indication for a low bias in the TRIPLE CCRF measurements and the above-mentioned systematic difference stays an open question.

Bromine compounds play an important role in ozone chemistry. The contribution of short-lived organic bromine substances (i.e. bromoform, $CHBr_3$) to the entire bromine budget is therefore essential to know. The easiest way to investigate this question is to measure BrO profiles in the tropics, since there air masses rise relatively quickly to the upper tropospheric and stratospheric layers. But because the BrO profiles measured in the tropics are quite different, there is no unanimous answer to this question currently. However, in Chapter 7 a study is presented to test the consistency of the HALOX

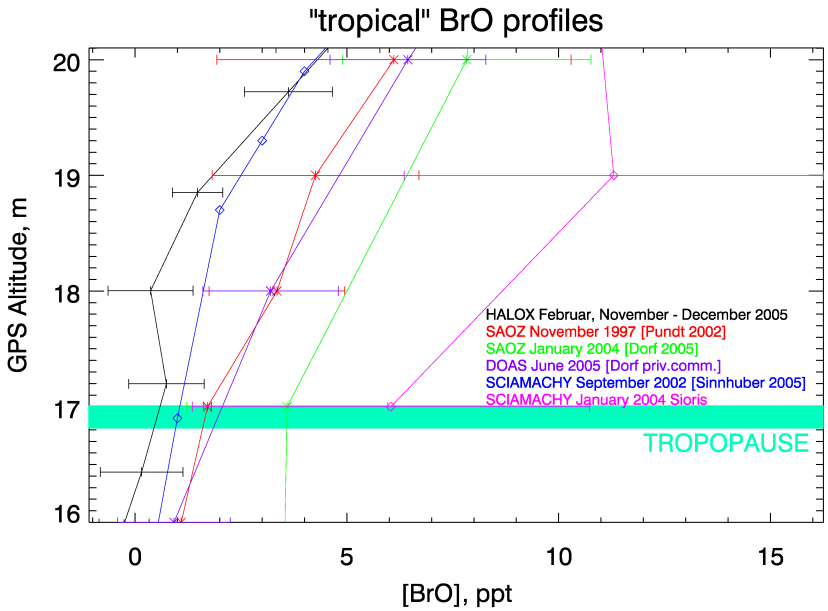

Figure 6.9: Comparison of different tropical *BrO* measurements in the altitude range 16-20 km. The black curve shows the averaged HALOX *BrO* profile from the TROCCINOX and SCOUT campaigns (Fig.6.8).

profiles with our understanding of the photochemistry of the UTLS (Upper Troposphere - Lower Stratosphere).

A joint or very little spaced flight of the Heidelberg DOAS payload and the TRIPLE would be very helpful to clear the above-mentioned discrepancy between the different instruments. Such a flight in the tropics (Teresina, Brazil) is envisaged for the year 2007.

6.5 Latitudinal distribution of *BrO*

More than 50 measurement flights were performed by TRIPLE and HALOX instruments under very different geophysical conditions. Their summary is presented in Fig.6.10, where altitudes and latitudes of the measurements are marked. *BrO* is shown by means of the color code. Balloon flights in Esrange (68°N) and Aire-sur-l'Adour (44°N) are clearly noticeable. Besides that there are also three regions of high flight density: austral tropics, where two aircraft campaigns were conducted in Brazil and Australia; boreal mid-latitudes (45°N-55°N), where different instrument test flights were performed, starting from Southern Germany, and boreal high latitudes, where the EUPLEX and ENVISAT validation campaigns occurred.

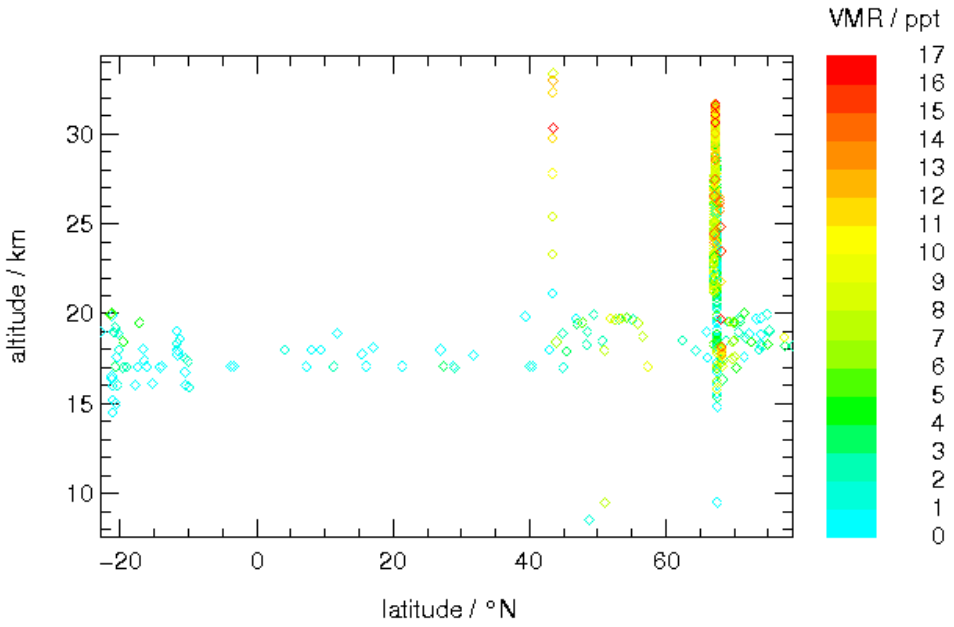

Figure 6.10: Meridional and vertical coverage of BrO measurements performed by TRIPLE and HALOX. BrO VMRs are shown by means of the color code.

To summarize measurement results in a more quantitative manner they were grouped in latitudinal bins and weighted averages (data points with bigger errors had smaller statistical weight in the averaging procedure, see Section 6.4) within each bin have been calculated. Since BrO has a pronounced vertical gradient, this meridional distribution was calculated for two altitude ranges: 14-17.5 km, and 17.5-21 km. This meridional distribution is presented in Fig.6.11. BrO has zero or very low mixing ratios throughout the tropical and subtropical regions. At mid-latitudes BrO slightly increases, but still is very low. Significantly higher mixing ratios were observed in the polar regions. This is in agreement with results of SCIAMACHY measurements published by *Sinnhuber et al.* (2005). This increase in BrO mixing ratios towards the poles can be explained by the general circulation and the age of the air (the "older" the air, the more Br_y has been freed up from the organic bromine compounds). To a smaller extent fast photochemistry may be responsible for enhanced polar BrO as well. TRIPLE and HALOX BrO measurements in polar regions were performed mainly in winter time, when there is low sun and, consequently, low NO_2. In this case BrO is to a lesser extent converted into $BrONO_2$.

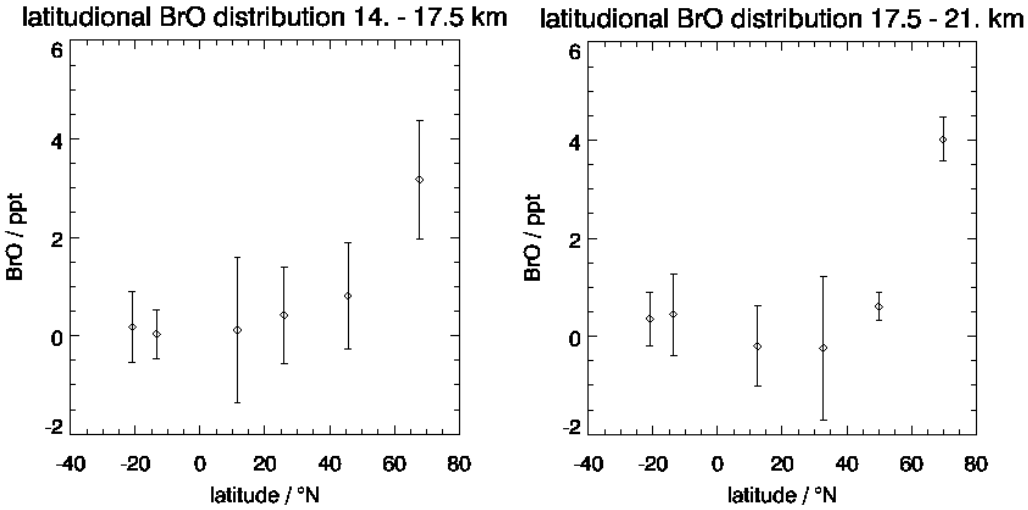

Figure 6.11: Meridional *BrO* distribution based on measurements performed by TRIPLE and HALOX. Weighted averages for latitudinal bins are shown. Bars denote errors as calculated by means of the expression (6.3).

CHAPTER 7

Model simulation of the evolution of inorganic bromine in tropical convection

As mentioned in the previous Chapter (see Fig.6.9), the tropical BrO profiles obtained by different instruments demonstrate significant differences in the tropopause region. In order to investigate this issue, a simulation of the tropospheric bromine chemistry was performed by means of the CLaMS model. Preliminary results of this study are presented in this chapter.

7.1 Problem overview

Recently it was suggested that inorganic bromine at and above the tropopause has to be at least 4 pptv higher than generally assumed (*Salawitch et al.*, 2005). This suggestion was supported by some measurements in the tropical tropopause region. A BrO profile obtained by the SAOZ instrument in Bauru, Brazil (22.4°S) on 31 January 2004 indicates ∼4-5 ppt BrO at the tropopause (*Dorf et al.*, 2006). The corresponding SCIAMACHY BrO retrieved at the University of Harvard demonstrates even higher BrO mixing ratios at the tropopause (∼6-7 ppt). On the other hand the BrO profile measured by SAOZ in Bauru on 29 November 1997 shows only 2 ppt at the tropopause (*Pundt et al.*, 2002). This is in agreement with LPMA-DOAS observations in June 2005 in Teresina, Brazil (5°S), where the same amount of BrO at the tropopause was observed (*Dorf*, 2005). Finally BrO mixing ratios retrieved by the Bremen group (*Sinnhuber et al.*, 2005) as well as obtained by the HALOX instrument (see Fig.6.9) indicate very low BrO at the tropopause not exceeding 1 ppt.

Therefore a simulation of the tropospheric bromine chemistry was performed by means of the CLaMS model in order to establish an upper level of BrO that can be generated from average tropical bromine source gas concentrations within an air parcel rising from the lower troposphere to the tropical tropopause layer (TTL) according to our current understanding of chemistry and dynamics.

7.2 Representation of tropospheric bromine chemistry within CLaMS

The standard CLaMS package concerns only inorganic bromine species neglecting organic bromine, because originally CLaMS was used for simulations of the stratospheric chemistry, where bromine is mostly in inorganic form and available organic Br species are only decomposed very slowly. For the purpose of the current study, however, the following organic bromine source gases were added to CLaMS:

- methyl bromide (CH_3Br);
- bromoform ($CHBr_3$);
- dibromomethane (CH_2Br_2);
- Halon-1011 (CH_2BrCl);
- Halon-1012 ($CHBr_2Cl$);
- Halon-1021 ($CHBrCl_2$);
- Halon-1202 (CBr_2F_2);
- Halon-1211 ($CBrClF_2$);
- Halon-1301 ($CBrF_3$);
- Halon-2402 ($C_2Br_2F_4$).

These are all presently known organic bromine source gases with significant tropospheric background concentrations.

In the troposphere they can react with $O(^1D)$, OH radicals, and Cl atoms or can be photolyzed. Therefore the following chemical and photochemical reactions were included into the CLaMS chemistry scheme:

$$O(^1D) + CH_3Br \rightarrow products \tag{7.1}$$

$$O(^1D) + CH_2Br_2 \rightarrow products \quad (7.2)$$

$$O(^1D) + CHBr_3 \rightarrow products \quad (7.3)$$

$$O(^1D) + CClBrF_2 \rightarrow products \quad (7.4)$$

$$O(^1D) + CBr_2F_2 \rightarrow products \quad (7.5)$$

$$O(^1D) + CBrF_3 \rightarrow products \quad (7.6)$$

$$O(^1D) + C_2Br_2F_4 \rightarrow products \quad (7.7)$$

$$OH + CH_3Br \rightarrow products \quad (7.8)$$

$$OH + CH_2Br_2 \rightarrow products \quad (7.9)$$

$$OH + CHBr_3 \rightarrow products \quad (7.10)$$

$$OH + CH_2ClBr \rightarrow products \quad (7.11)$$

$$OH + CF_2ClBr \rightarrow products \quad (7.12)$$

$$OH + CF_2Br_2 \rightarrow products \quad (7.13)$$

$$OH + CF_3Br \rightarrow products \quad (7.14)$$

$$OH + C_2Br_2F_4 \rightarrow products \quad (7.15)$$

$$Cl + CH_2ClBr \rightarrow products \quad (7.16)$$

$$Cl + CH_3Br \rightarrow products \quad (7.17)$$

$$Cl + CH_2Br_2 \rightarrow products \quad (7.18)$$

$$Cl + CHBr_3 \rightarrow products \quad (7.19)$$

$$CH_3Br + h\nu \rightarrow products \quad (7.20)$$

$$CH_2Br_2 + h\nu \rightarrow products \quad (7.21)$$

$$CHBr_3 + h\nu \rightarrow products \quad (7.22)$$

$$CH_2ClBr + h\nu \rightarrow products \quad (7.23)$$

$$CHClBr_2 + h\nu \rightarrow products \quad (7.24)$$

$$CHCl_2Br + h\nu \rightarrow products \quad (7.25)$$

$$CF_2Br_2 + h\nu \rightarrow products \quad (7.26)$$

$$CF_2ClBr + h\nu \rightarrow products \quad (7.27)$$

$$CF_3Br + h\nu \rightarrow products \quad (7.28)$$

$$C_2Br_2F_4 + h\nu \rightarrow products \quad (7.29)$$

The chemical reaction rate constants as well as the absorption cross sections for the photochemical reactions were taken from *Sander et al.* (2006). Since the main aim of this simulation was to estimate the resulting inorganic bromine amount only bromine atoms were considered as reaction products (e.g. $C_2Br_2F_4 + h\nu \rightarrow Br + Br$). The resulting Br atoms will react with available hydrocarbons and ozone immediately to form HBr and BrO, respectively. This was done in order to keep the chemical system small and computing time within reasonable limits. Including all intermediate reactions would in the sum lead to the same result but with noticeably higher computational costs.

The reactions of the inorganic bromine species, which were included in CLaMS originally are:

$$O(^3P) + BrO \rightarrow Br + O_2 \tag{7.30}$$

$$OH + HBr \rightarrow H_2O + Br \tag{7.31}$$

$$HO_2 + Br \rightarrow HBr + O_2 \tag{7.32}$$

$$HO_2 + BrO \rightarrow HOBr + O_2 \tag{7.33}$$

$$Br + O_3 \rightarrow BrO + O_2 \tag{7.34}$$

$$Br + HCHO \rightarrow HBr + CO + HO_2 \tag{7.35}$$

$$BrO + NO \rightarrow NO_2 + Br \tag{7.36}$$

$$BrO + ClO \rightarrow Br + OClO \tag{7.37}$$

$$BrO + ClO \rightarrow Br + Cl + O_2 \tag{7.38}$$

$$BrO + ClO \rightarrow BrCl + O_2 \tag{7.39}$$

$$BrO + BrO \rightarrow Br + Br + O_2 \tag{7.40}$$

$$BrO + BrO \rightarrow Br_2 + O_2 \tag{7.41}$$

$$O(^3P) + HOBr \rightarrow OH + BrO \tag{7.42}$$

$$OH + Br_2 \rightarrow HOBr + Br \tag{7.43}$$

$$ClONO_2 + HBr \rightarrow BrCl + HONO_2 \tag{7.44}$$

$$BrONO_2 + HCl \rightarrow BrCl + HONO_2 \tag{7.45}$$

$$HOCl + HBr \rightarrow BrCl + H_2O \tag{7.46}$$

$$HOBr + HCl \rightarrow BrCl + H_2O \tag{7.47}$$

$$HOBr + HBr \rightarrow Br_2 + H_2O \tag{7.48}$$

$$BrONO_2 + H_2O \rightarrow HOBr + HONO_2 \tag{7.49}$$

$$BrO + NO_2 \rightarrow BrONO_2 + M \tag{7.50}$$

$$BrONO_2 + hv \rightarrow BrO + NO_2 \tag{7.51}$$

$$BrONO_2 + hv \rightarrow Br + NO_3 \tag{7.52}$$

$$BrCl + hv \rightarrow Br + Cl \tag{7.53}$$

$$HOBr + hv \rightarrow OH + Br \tag{7.54}$$

$$Br_2 + hv \rightarrow Br + Br \tag{7.55}$$

7.3 Tropical atmospheric dynamics and trajectories selection

Atmospheric dynamics in the tropical regions is characterized by convection, which transports air rapidly from the boundary layer to the upper troposphere (Fig.7.1). The time scale of such convective events varies from less

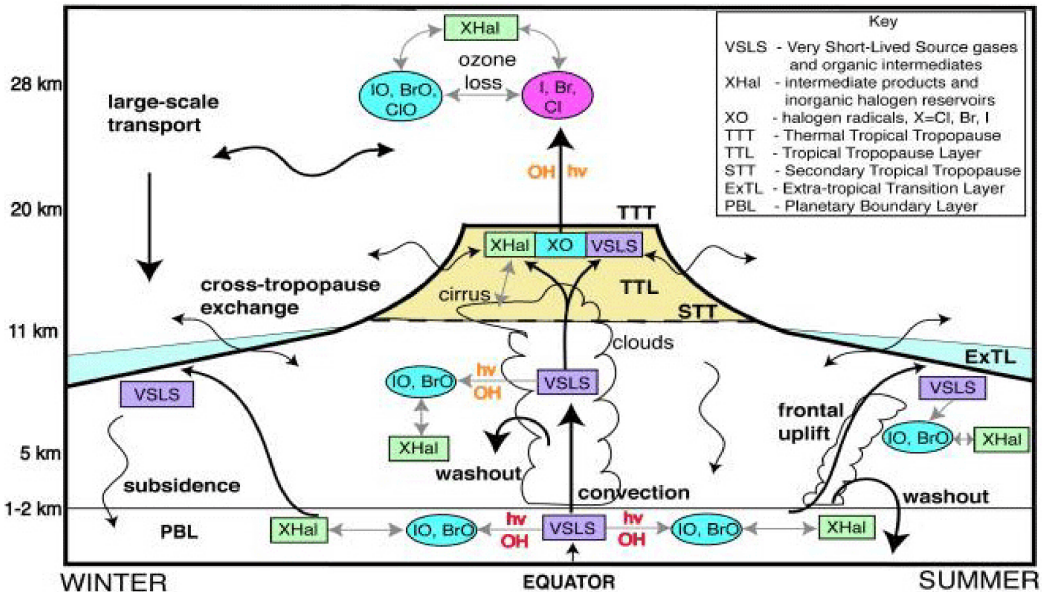

Figure 7.1: Chemical and dynamical processes affecting very short lived substances in the troposphere and stratosphere. Figure adopted from (*WMO*, 2003).

than an hour (deep convection) to 30-50 days (*WMO*, 2003). Air contains the organic bromine source gases of anthropogenic and natural origin, which are transported by convection to the TTL. On the way to the TTL the organic

Table 7.1: Trajectories distribution according to their vertical velocity

Time to reach the tropopause	**Number of trajectories**
6-9 days	9
10-20 days	13
20-30 days	7
30-40 days	6
>40 days	4

bromine source gases are photolyzed and react with $O(^1D)$, OH radicals, and Cl atoms, converting them into inorganic Br species. Some of them - HBr and $HOBr$ - are highly soluble and can, therefore, be dissolved and washed out. All these processes determine an amount of the inorganic bromine in the tropopause region.

In order to reproduce the vertical transport in the troposphere a hybrid vertical coordinate, ζ, was introduced into CLaMS by P. Konopka of the Jülich modelling group (*Dowling and Morales-Juberías*, 2003). It is strongly coupled to the potential temperature in the stratosphere smoothly transiting into a pressure-based coordinate lower in the troposphere turning into the geopotential at the very bottom of the model near the Earth's surface.

39 forward trajectories with a length of 4 months were calculated using the ECMWF winds for air parcels located at pressure levels around 600-800 hPa (∼2-4km altitude) over the Western Pacific and the South China Sea (the area of the TRACE-P mission, which data was used to initialize bromoform, dibromomethane, Halon-1012, and Halon-1021). Some of them reached the tropopause after 6 days, other needed more than 40 days (the fastest convection scenario with the vertical transport within an hour can not be captured using ECMWF wind data due to its coarse temporal and spatial resolution). The trajectories distribution according to their average vertical velocity is presented in Table 7.1. To test different convection scenarios, example trajectories with different vertical velocity (7, 17, and 39 days) were chosen for the (photo-)chemical simulation.

7.4 Chemical initialization

The initialization of the organic bromine species was done as described below:

- methyl bromide CH_3Br (8.1 ppt) and Halon-1211 $CBrClF_2$ (4.1 ppt) were initialized using the global means obtained by the AGAGE (Ad-

vanced Global Atmospheric Gases Experiment) sampling network established by NASA (*Prinn et al.*, 2000);

- initial mixing ratios for bromoform $CHBr_3$ (1.1 ppt), dibromomethane CH_2Br_2 (1.15 ppt), Halon-1012 $CHBr_2Cl$ (0.07 ppt), and Halon-1021 $CHBrCl_2$ (0.19 ppt) are median tropical surface mixing ratios from the TRACE-P (Transport and Chemical Evolution over the Pacific) mission measurements over the Western Pacific and the South China Sea (*Jacob et al.*, 2003), the start region of the air parcels used for the simulation;

- Halon-1011 CH_2BrCl was initialized at 0.14 ppt as was measured at the Earth's surface by *Sturges* (1993). Although this measurement seems to be quite old, there is no reason to believe that VMR of Halon-1011 has increased significantly, since this substance is of entirely natural origin;

- the initial value for Halon-1301 $CBrF_3$ (2.6 ppt) was taken from observations of CMDL (Climate Monitoring and Diagnostics Laboratory; http://www.cmdl.noaa.gov);

- other relevant Halons: Halon-1202 CBr_2F_2 (0.044 ppt), and Halon-2402 $C_2Br_2F_4$ (0.43 ppt) were initialzed using UEA (University of East Anglia) measurements performed at Cape Grim, Australia (41°S) (*Oram*, 1999).

The fact that not all measurements used for the initialization were performed at the start locations of the simulation is not critical, as all above-mentioned species (apart from bromoform, Halon-1012, and Halon-1021) are long-lived substances with tropospheric lifetimes of several years and, hence, have relatively homogeneous mixing ratios in the free troposphere across the globe due to mixing processes. Short-lived compounds (bromoform, Halon-1012, and Halon-1021) were initialized using the measurements close to the simulation start points. Some constraints with this initialization will be discussed in the conclusions of this chapter.

All other species including the inorganic bromine compounds were initialized by means of the Mainz-2D model. However, it is essential to emphasize that the Mainz-2D model suggests VMRs of the inorganic bromine compounds as well as $O(^1D)$ and Cl to be very close to zero at the Earth's surface. The tropospheric values of OH radicals as suggested by Mainz-2D are 0.4-0.6 ppt.

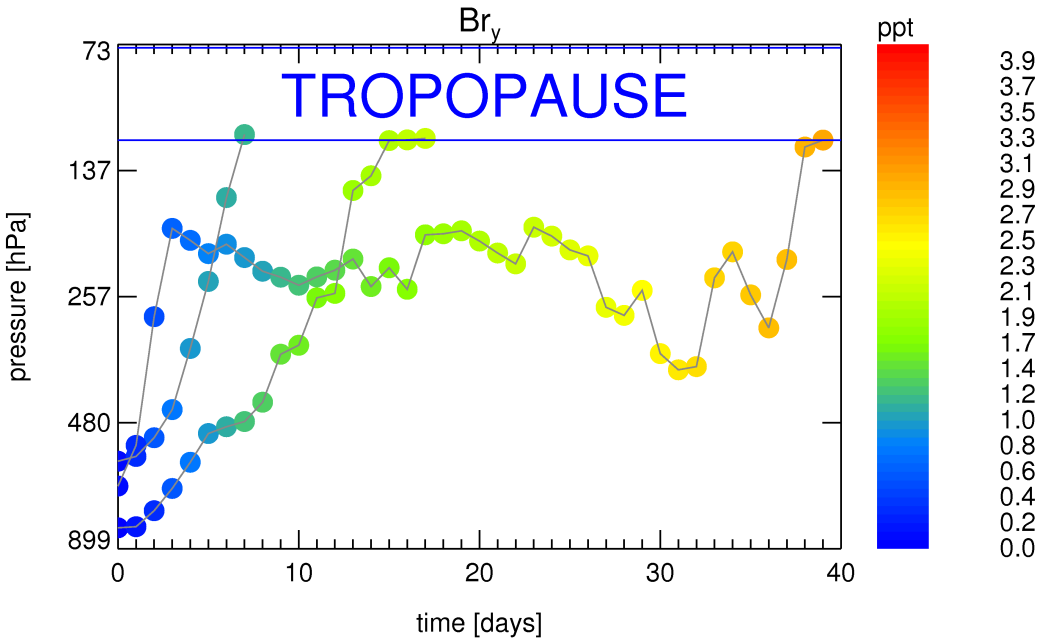

Figure 7.2: Tropospheric inorganic bromine as modeled by CLaMS. Air parcels having different vertical velocity were chosen. Points relating to the same parcel are connected by grey lines.

7.5 Modelling results and their discussion

The results of the simulation are presented in Figures 7.2 and 7.3. From 39 trajectories three were chosen with very different vertical velocities to indicate the dependence of Br_y at the tropopause on the vertical velocity of the tropical convection. The tropical tropopause position is indicated by two blue lines showing the lowest and highest value of the pressure range measured at the tropopause during the TROCCINOX and SCOUT-O3 tropical aircraft campaigns (the lower pressure level around 72 hPa corresponds to maximum of plotted pressure range). The simulation end values for Br_y and BrO (at the tropopause) along with vertical transport duration are presented in Table 7.2. It is important to emphasize that the presented results constitute the upper limit of the Br_y amount at the tropopause, since not all physical phenomena were taken into consideration by CLaMS: first of all, washout of soluble inorganic bromine species. Among them the most soluble are HBr and $HOBr$. The maximal simulated mixing ratios of these species along each trajectory are indicated in Table 7.2 as well. In case they are completely dissolved and subsequently washed out, the total inorganic bromine after washout Br_y^{wo} and, hence, BrO at the tropopause would be correspondingly

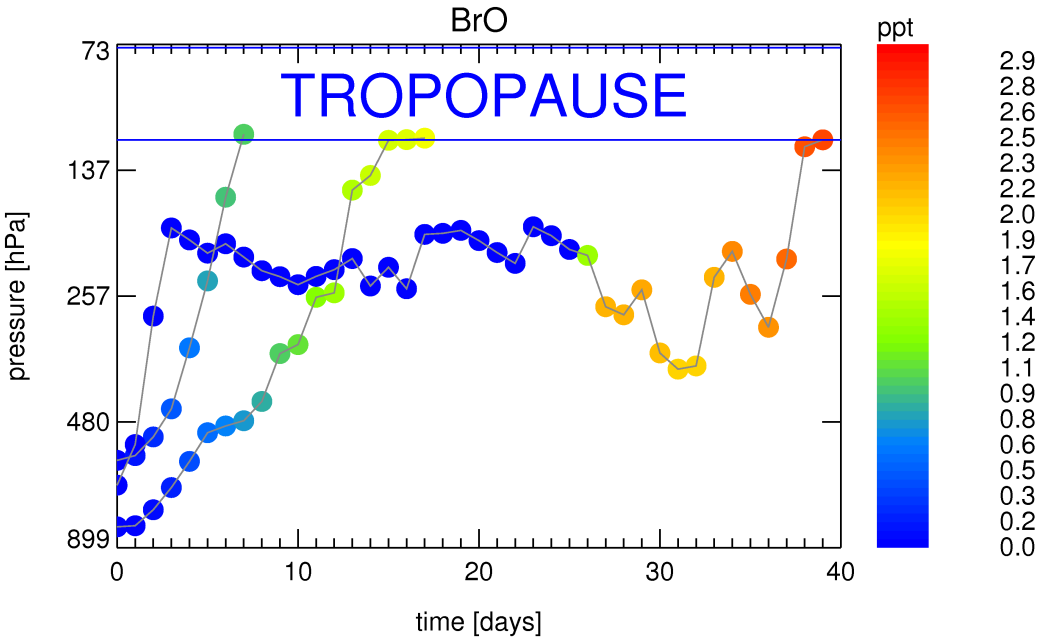

Figure 7.3: The same as in Fig.7.2 but for BrO. Note the different color code scale.

Table 7.2: Br_y, BrO, HBr, and $HOBr$ mixing ratios at the tropical tropopause as simulated by CLaMS. The fraction of BrO within the bromine family is indicated as well. Br_y and BrO mixing ratio approximations taking washout into consideration are also shown.

Vertical transport duration [days]	Br_y **[ppt]**	BrO **[ppt]**	$\frac{BrO}{Br_y}$	HBr **[ppt]**	$HOBr$ **[ppt]**	Br_y^{wo} **[ppt]**	BrO^{wo} **[ppt]**
7	1.24	1.03	0.83	0.12	0.34	0.78	0.65
17	2.07	1.77	0.86	0.18	0.42	1.47	1.26
39	2.97	2.72	0.92	0.09	0.51	2.37	2.18

lower (BrO^{wo}, two last columns in Table 7.2).

These values were calculated as follows:

$$Br_y^{wo} = Br_y - (HBr + HOBr) \tag{7.56}$$

$$BrO^{wo} = Br_y^{wo} \cdot \left(\frac{BrO}{Br_y}\right) \tag{7.57}$$

The more correct way to simulate the physical processes in the troposphere is to include solvation of HBr and $HOBr$ on tropospheric aerosols with their subsequent scavenging due to falling rain or ice using appropriate sedimentation rates. This was, however, not done because it was beyond the scope of this work. Instead, the simplified scheme with subtraction of soluble HBr and $HOBr$ was used as described above.

It is of interest to calculate the tropospheric lifetime (the average time needed for the compound to be reduced by a factor of e) of the organic bromine species. The calculation is based on the CLaMS simulation. The slowest trajectory needed 96 days to reach the tropopause. The lifetimes were calculated based on the chemistry along this trajectory. Only bromoform $CHBr_3$, Halon-1012, and Halon-1021 were reduced by a factor of e within this period. So their lifetimes could be calculated directly. The lifetimes of all other species were calculated by means of extrapolation and they are, in this way, rather rough quantities. The calculated lifetimes are listed in Table 7.3.

Table 7.3: Tropospheric lifetimes of the organic bromine species as calculated from simulation along a 96 day long tropical trajectory.

Compound	**Lifetime**
CH_3Br	4.9 years
CH_2Br_2	1.3 year
$CHBr_3$	33 days
Halon-1011	5.7 years
Halon-1012	56 days
Halon-1021	47 days
Halon-1202	2.3 years
Halon-1211	4.3 years
Halon-1301	46 years
Halon-2402	4.9 years

As it can be seen from Table 7.3 the main organic contributor to the Br_y is bromoform $CHBr_3$, which is destroyed very rapidly in the troposphere and which molecule carries 3 bromine atoms. This fact is in agreement with the recent estimation performed by *Sinnhuber and Folkins* (2006). With the assumption for the mean bromoform mixing ratio in the tropical boundary layer of about 1 ppt and for the lifetime of Br_y due to washout of 10 to 30 days in the tropical tropopause layer, their calculations have shown that bromoform contributes about 1 ppt to the stratospheric bromine loading. However, the variability of bromoform is relatively large ranging from 0.2 to >100 ppt. Highest surface mixing ratios have been reported from regions in the vicinity of extensive beds of macroalgae, where they range from 6 ppt in the Antarctic, 30 ppt in the Arctic to >100 ppt over subtropical coastal areas (*Quack and Wallace*, 2003).

The other two organic bromine compounds with very short lifetimes, Halon-1012, and Halon-1021, have very low mixing ratios of ∼0.07 and 0.19 ppt, respectively, and, hence, do not play any noticeable role in the TTL.

In general the CLaMS simulation of the tropospheric bromine chemistry suggests that if an air parcel is transported from the Earth's surface up to the tropopause within 10-20 days the amount of inorganic bromine released from the organic bromine source gases would not exceed 2 ppt (1.5 ppt BrO). In case of a longer transport time, it would be slightly higher, but still less than 2.4 ppt (2.2 ppt BrO). This simulation is in agreement with the BrO at the tropical tropopause retrieved by the Bremen group and with HALOX tropical BrO. Higher BrO mixing ratios at the tropical tropopause need additional injections of bromine into an air parcel on its way upward to the TTL, e.g. release of bromine due to aerosols evaporation. However, enhanced Br in aerosols in the free troposphere has not been observed up to now. Enhanced BrO amount at the troposphere can also be attributed to source regions with locally higher surface bromoform VMR (extensive beds of macroalgae). This last effect, however, should lead to enhanced variability in BrO mixing ratios. Time and spatial resolution of current measurements unfortunately makes the detection of such enhanced variability very hard.

Bromoform was found to be the main contributor to inorganic bromine at the tropopause. Its lifetime in the tropical troposphere is ∼33 days as calculated by CLaMS.

CHAPTER 8

Conclusions and Outlook

This work presents results of BrO measurements by the TRIPLE balloon and HALOX airborne instruments. These measurements along with appropriate calibrations have been performed in the frame of the ENVISAT validation (mid-latitudes, Arctic), EUPLEX (Arctic), TROCCINOX (tropics), TC5 (mid-latitudes), and SCOUT-O3 (tropics) campaigns (I took part in 3 balloon and 1 aircraft campaigns). These campaigns took place in the years 2002-2005.

Data have been analyzed and quality checked. Final data have been utilized for the purpose of satellite validation and to improve our understanding of the distribution and photochemistry of BrO in the troposphere and lower stratosphere.

The balloon-borne measurements (10 to 34 km) and the aircraft measurements (10 to 20 km) are highly complementary in terms of spatial resolution and coverage. As result of the very good horizontal coverage, aircraft observations provide excellent information on the horizontal distribution of BrO at the aircraft flight altitude. Balloon data provide limited horizontal information but much better vertical coverage. Therefore, they are well suited for the validation of satellite observations (SCIAMACHY on-board ENVISAT). However, these measurements unfortunately have quite poor temporal and spatial resolution and, consequently, do not provide any information on small time and spatial scales.

To ensure the reliability of the measurements every detection module of the instruments was independently calibrated before and after every field campaign. The calibration and data analysis procedure is discussed in Chapter 3. In order to check on the internal consistency of the TRIPLE and

HALOX measurements comparisons of independent measurement modules within TRIPLE as well as comparisons between balloon and aircraft measurements have been carried out with good results giving confidence in the stability of the calibrations and the data analysis procedure.

The TRIPLE and HALOX BrO profiles were also compared with profiles obtained by other balloon-borne (LPMA-DOAS, SAOZ) instruments. In general, the profiles based on CCRF measurements show lower BrO values than that detected by DOAS instruments. This disagreement is at the limit of the measurement accuracy but systematic. The origin of this discrepancy could not be identified yet.

All quality checked data obtained during the balloon and aircraft flights are stored in the NILU (Norsk Institutt for LUftforskning / Norwegian Institute for Air Research) database and are available for all groups involved in the SCIAMACHY validation activities.

All measured balloon profiles were photochemically corrected in order to compare them to the appropriate SCIAMACHY measurements (see Sec.6.2 for details). Validated SCIAMACHY data represent a scientifically valuable database for atmospheric transport, chemistry, and variability studies. However, validation is still on-going, since large part of the SCIAMACHY data retrieval (in particular the operational products) is still not completed. Available SCIAMACHY measurements and comparisons carried out in this work allow for first conclusions on the data quality of Bremen, Heidelberg, and Harvard retrievals. On average Bremen and Heidelberg SCIAMACHY retrievals reveal 43% higher BrO mixing ratios than the corresponding balloon-borne BrO measurements (TRIPLE gondola). As for the HALOX tropical campaigns (TROCCINOX and SCOUT-O3), the agreement between the Bremen and HALOX tropical BrO profiles in the TTL is very good, while BrO retrieved from the SCIAMACHY data by the Harvard group is much higher than that of HALOX (Harvard BrO has 6 ppt in the tropopause increasing up to 11 ppt at 20 km, whereas HALOX reveals BrO very close to zero in the tropopause and 1 km above it, increasing up to 4-5 ppt at 20 km). The described results were presented at ESA validation meetings and at GSVT (German SCIAMACHY Validation Team) meetings and published in *Rozanov et al.* (2005) and *Dorf et al.* (2006).

Currently the different BrO retrieval processors are compared in the frame of the BOOST project (Bromine Oxide in the lOwer STratosphere) in order to locate the source of the internal differences. After that the examined retrievals will be compared to the validation data of the TRIPLE instrument. In view of the complexity of the retrieval procedures this may take months to years. Different validation data sets from averaged profiles to latitudinal distributions based on CCRF measurements are available from

this work.

Bromine compounds play an important role in ozone chemistry. The work presented in this thesis also contributes to the understanding of the stratospheric bromine chemistry under different geophysical conditions. Photochemical simulations employing the Jülich CLaMS package have been performed in order to check on the consistency of the CCRF measurements with our current understanding of Br_y chemistry. Assuming a total Br_y of ∼18.4 ppt, the balloon profile measured on 9 June 2003 could be reproduced very well.

The contribution of short-lived organic bromine substances (i.e. bromoform, $CHBr_3$) to the entire bromine budget is of crucial importance but only poorly understood. The easiest way to assess the influence of short-lived organic bromine species is to measure BrO profiles in the tropics, since here air masses quickly ascend from the lower atmosphere to the upper tropospheric and stratospheric layers. Therefore only short-lived organic species can be converted into inorganic Br species. Compared to previous DOAS observations, very low BrO values were obtained by HALOX measurements at (and just above) the tropopause during two tropical campaigns in Brazil and Australia.

A model study of tropospheric bromine chemistry was conducted within this work to simulate the Br_y amount at the tropopause according to the known (photo-)chemistry of organic bromine source gases. Its results are presented and discussed in Chapter 7. This study suggests that if an air parcel transported from the Earth's surface up to the tropopause within 10-20 days an amount of the inorganic bromine released from the organic bromine source gases would not exceed 2 ppt. In case of a longer transport time, it would be slightly higher. This is in agreement with the recent estimation from (*Sinnhuber and Folkins*, 2006) and consistent with the tropical BrO profiles measured by HALOX.

Refinement of tropical model study to reflect washout and to examine the atmospheric variability of BrO in the model will be performed. This can help to judge which kind of measurements can be carried out to prove or disprove this hypothesis. Besides, a model sensitivity study will be conducted to assess an error of tropical model study.

To further check the injection of Br species into the tropical stratosphere and to investigate the discrepancy in measured BrO between CCRF and DOAS, a joint or nearly coincident flight of the TRIPLE gondola and the Heidelberg DOAS payload is planned for the year 2007 from Teresina (Brazil).

APPENDIX A

Short review of atmospheric structure and dynamics

The distribution of chemical species in the atmosphere results from chemical as well as from dynamical processes. When the rates of formation and destruction of a chemical substance are comparable to the rate at which it is transported by dynamical processes, then transport plays a significant role in the species distribution. This transport is realized by winds and by convection resulting from the solar heating of the Earth's surface. Another reason for transport is the so-called buoyancy. When water condenses, latent heat is released, air parcel warms up and gets additional momentum in upward direction.

The particular type of the air transport strongly depends on the layer of the atmosphere, where it takes place.

Studies of the atmospheric structure began in the late 1800s and started from curiosity about temperature gradients in the air. In 1902, a Frenchman named Leon Philippe Teisserenc de Bort reported that the air temperature decreases with altitude up to a height of about 10 kilometres, after which the temperature starts to increase with height.

The five layers could be identified in the atmosphere (Fig.A.1) taking into consideration the following factors:

- thermal characteristics (character of the temperature changes);
- chemical composition;
- type of the prevailing transport;
- air density.

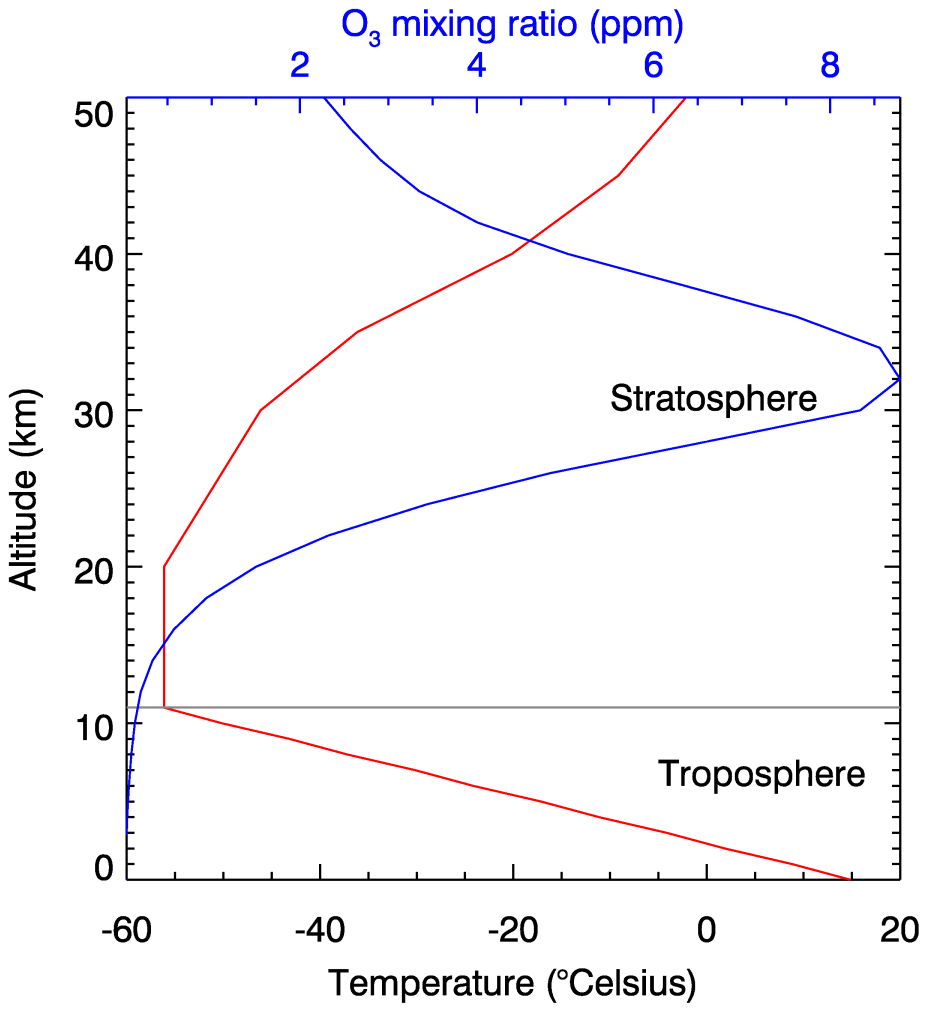

Figure A.1: General vertical structure of the atmosphere together with atmospheric ozone profile

Each of the layers is separated from its neighbors by "pauses" where significant changes in thermal characteristics, chemical composition, and type of transport occur. This thesis deals, however, with two lowermost ones: the troposphere and the stratosphere.

The troposphere begins at the Earth's surface and extends up to 10-18 km altitude depending on latitude. The temperature in the troposphere decreases with altitude due to quasiadiabatic expansion of air parcels. The temperature interval in the troposphere is on average from 290 K (+17°C) on the surface to 213-223 K (-50°..-60°C) at the tropopause. Almost all weather occurs in this region. The troposphere contains almost all of the

atmosphere's water vapor and about 75-80% of the atmosphere's total mass. The height of the tropopause depends on latitude and time of year. At the equator it is around 18-20 km high, at 50°N and 50°S approximately 12 km and at the poles just about 8 km high.

The region between 10 and 50 kilometres of height became known as the stratosphere (it was named so by de Bort from the Latin word *stratum* meaning *layer*). The troposphere and the stratosphere hold together about 99% of the total mass of the atmosphere. The very cold tropopause serves as a trap for the water vapor, that is why there is very little water vapor in the stratosphere. Temperature in the stratosphere increases with height as solar radiation is absorbed by ozone molecules. The temperature rises from on average 213-223 K (-50..-60°C) at the tropopause to a maximum of about 258-263 K (-10..-15°C) at the stratopause due to this absorption of ultraviolet radiation and subsequent release as heat. The increasing temperature also makes it a stable layer with very slow vertical movements of the air. The termal structure of the atmosphere determines its vertical air transport characteristics.

Circulation cells are an important feature of atmospheric dynamics. The Earth is encircled by several broad wind belts, which are separated by regions of air sinking or raising. The direction and location of these wind belts are determined by solar radiation and the rotation of the Earth. The three primary circulation cells are known as the: Hadley cell, Ferrel cell, and polar cell (Fig.A.2).

At or near the equator, where solar radiation is greatest, air is warmed at the surface and rises. This creates a band of low air pressure, centered at the equator, known as the intertropical convergence zone (ITCZ). The ITCZ draws surface air from the subtropics. When this subtropical air reaches the equator, it rises into the upper atmosphere because of convergence and convection. When it reaches a maximum vertical altitude about top of the troposphere, it begins flowing horizontally to the North and South Poles, but predominantly to the winter pole.

Another very important feature of the atmospheric dynamics is the Polar Vortex. During polar night air masses above the corresponding pole become very cold because of the lack of solar heating. The Earth's rotation causes counter-clockwise rotation of these sinking air masses. This rotation produces a transport barrier between polar and mid-latitudinal (warm and rich in ozone) air masses. Vortex air does not mix with warmer air masses and remains very cold (down to -80..-90°C). This separation along with the absence of sun light are the reasons why the stratospheric temperatures in this area can drop so much. Because of specific features of the atmosphere (tropospheric dynamical activity and activity of planetary waves) the vortex

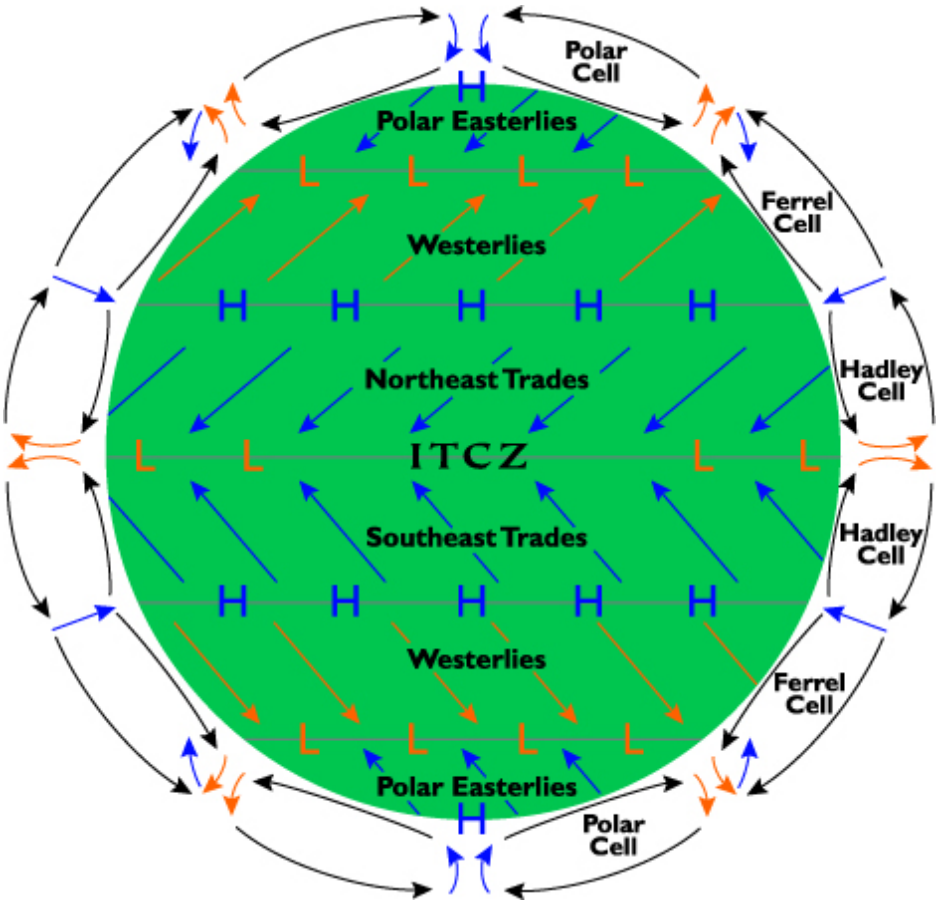

Figure A.2: Primary circulation cells and wind belts of Earth

is located between the tropopause and the upper atmosphere.

Atmospheric investigations need to have a vertical coordinate system. One uses geometric altitude or pressure for this purpose. However, along with them it is often more convenient to use so called "potential temperature". Dynamically it is more important quantity than the actual temperature, because under almost all circumstances potential temperature of an air parcel is conserved over days or weeks and horizontal transport proceeds along isentropes. The potential temperature of a parcel of air at pressure p is the temperature that the parcel would have if adiabatically and without condensation or evaporation brought to a standard reference pressure p_0, 1013.25 hPa. The potential temperature is denoted Θ and is given by

$$\Theta = T \left(\frac{p_0}{p} \right)^{\frac{R}{c_p}}, \tag{A.1}$$

where T is the current temperature of the parcel, R is the gas constant of air, and c_p is the specific heat capacity at a constant pressure.

APPENDIX B

Extended flights' information

Table B.1: Summary of TRIPLE and HALOX flights. During some flights only one point could be extracted due to long integration time needed. That is why for these flights there is only one value for the time and SZA

Date	**Location**	**Geo-physical Condition**	**Time [UTC]**	**SZA range**	**Campaign**
24 Sep 2002	Aire-sur-l'Adour 43.7°N 0.3°W	mid-lat. autumn	08:12 - 10:07	65.63° - 49.28°	ENVISAT validation
15 Jan 2003	Kiruna 67.9°N 20.2°E	high lat. winter	09:13	88.46°	ENVISAT validation
19 Jan 2003	Kiruna 67.9°N 20.2°E	high lat. winter	14:52 - 16:45	110.06° - 102.85°	ENVISAT validation
23 Jan 2003	Kiruna 67.9°N 20.2°E	high lat. winter	14:53 - 16:08	105.38° 102.83°	EUPLEX
26 Jan 2003	Kiruna 67.9°N 20.2°E	high lat. winter	09:32 - 11:47	96.14° - 90.94°	EUPLEX
30 Jan 2003	Kiruna 67.9°N 20.2°E	high lat. winter	13:14	88.38°	EUPLEX
2 Feb 2003	Kiruna 67.9°N 20.2°E	high lat. winter	09:38 - 12:06	89.56° - 88.82°	EUPLEX
6 Feb 2003	Kiruna 67.9°N 20.2°E	high lat. winter	14:51 - 16:12	98.07° - 92.01°	EUPLEX

Date	**Location**	**Geo-physical Condition**	**Time [UTC]**	**SZA range**	**Campaign**
9 Feb 2003	Kiruna 67.9°N 20.2°E	high lat. winter	10:48 - 12:37	90.76° - 84.71°	EUPLEX
11 Feb 2003	Kiruna 67.9°N 20.2°E	high lat. winter	11:34	84°	EUPLEX
28 Feb 2003	Kiruna 67.9°N 20.2°E	high lat. winter	08:03 - 09:16	84° - 82.81°	ENVISAT validation
2 Mar 2003	Kiruna 67.9°N 20.2°E	high lat. winter	19:25 - 21:59	120.16° - 113.08°	ENVISAT validation
6 Mar 2003	Esrange 67.9°N 21.1°N	high lat. winter	06:32 - 09:44	85.48° - 73.12°	ENVISAT validation
8 Mar 2003	Kiruna 67.9°N 20.2°E	high lat. winter	07:17 - 09:42	83.16° - 75.77°	ENVISAT validation
12 Mar 2003	Kiruna 67.9°N 20.2°E	high lat. winter	08:04 - 10:39	82.14° - 74.38°	ENVISAT validation
16 Mar 2003	Kiruna 67.9°N 20.2°E	high lat. winter	07:22 - 09:04	76.94° - 75.21°	ENVISAT validation
9 Jun 2003	Esrange 67.9°N 21.1°N	high lat. spring	07:56 - 09:08	48.99° - 45.36°	ENVISAT validation
18 Jan 2005	Oberpfaffenhofen 48.1°N 11.3°E	mid-lat. winter	13:06	71.97°	TROCCINOX
20 Jan 2005	Oberpfaffenhofen 48.1°N 11.3°E - Seville 37.4°N 6°W	mid-lat. winter	11:14 - 12:25	65.53° - 59.19°	TROCCINOX
23 Jan 2005	Seville 37.4°N 6°W - Sal Island 16.7°N 22.9°W	tropics	11:12	55.54°	TROCCINOX
23 Jan 2005	Sal Island 16.7°N 22.9°W - Recife 8.1°S 34.9°W	tropics	20:40	98.95°	TROCCINOX
27 Jan 2005	Recife 8.1°S 34.9°W - Aracatuba 21.2°S 50.4°W	tropics	09:23	77.95°	TROCCINOX
1 Feb 2005	Aracatuba 21.2°S 50.4°W	tropics	16:37 - 18:34	45.92° - 13.2°	TROCCINOX

Date	**Location**	**Geo-physical Condition**	**Time [UTC]**	**SZA range**	**Campaign**
4 Feb 2005	Aracatuba 21.2°S 50.4°W	tropics	17:50	32.3°	TROCCINOX
5 Feb 2005	Aracatuba 21.2°S 50.4°W	tropics	18:16 - 20:41	72.17° - 39.49°	TROCCINOX
8 Feb 2005	Aracatuba 21.2°S 50.4°W	tropics	14:37 - 16:29	17.61° - 10.92°	TROCCINOX
12 Feb 2005	Aracatuba 21.2°S 50.4°W	tropics	10:12 - 12:16	71.05° - 42.14°	TROCCINOX
15 Feb 2005	Aracatuba 21.2°S 50.4°W	tropics	11:07 - 12:58	60.81° - 29.55°	TROCCINOX
17 Feb 2005	Aracatuba 21.2°S 50.4°W	tropics	10:27 - 13:05	73.77° - 34.68°	TROCCINOX
18 Feb 2005	Aracatuba 21.2°S 50.4°W	tropics	19:22 - 20:22	71.42° - 57.7°	TROCCINOX
24 Feb 2005	Aracatuba 21.2°S 50.4°W - Recife 8.1°S 34.9°W	tropics	12:43	37.79°	TROCCINOX
27 Feb 2005	Sal Island 16.7°N 22.9°W - Seville 37.4°N 6°W	tropics	17:08	66.74°	TROCCINOX
2 Mar 2005	Seville 37.4°N 6°W - Oberpfaffenhofen 48.1°N 11.3°E	mid-lat. winter	11:32 - 12:26	54.57° - 50.56°	TROCCINOX
7 Mar 2005	Oberpfaffenhofen 48.1°N 11.3°E	mid-lat. winter	09:13	65.17°	TROCCINOX
9 Jul 2005	Oberpfaffenhofen 48.1°N 11.3°E	mid-lat. summer	10:31 - 13:18	32.28° - 27.59°	CRISTA-NF test campaign
12 Jul 2005	Oberpfaffenhofen 48.1°N 11.3°E	mid-lat. summer	12:00 - 14:06	40.76° - 23.79°	CRISTA-NF test campaign
4 Nov 2005	Oberpfaffenhofen 48.1°N 11.3°E - Larnaca 34.9°N 33.6°E	mid-lat. autumn	07:57	65.58°	SCOUT-O3
4 Nov 2005	Larnaca 34.9°N 33.6°E - Dubai 25.3°N 55.3°E	mid-lat. autumn	15:46	110.81°	SCOUT-O3

Date	**Location**	**Geo-physical Condition**	**Time [UTC]**	**SZA range**	**Campaign**
8 Nov 2005	Dubai 25.3°N 55.3°E - Hyderabad 17.4°N 78.5°E	tropics	00:29	106.13°	SCOUT-O3
9 Nov 2005	Hyderabad 17.4°N 78.5°E - U Taphao 12.7°N 101°E	tropics	04:13 - 05:28	43.58° - 32.26°	SCOUT-O3
12 Nov 2005	U Taphao 12.7°N 101°E - Brunei 4.9°N 114.9°E	tropics	00:42 - 01:44	65.8° - 46.61°	SCOUT-O3
12 Nov 2005	Brunei 4.9°N 114.9°E - Darwin 12.5°S 130.8°E	tropics	12:22	128.3°	SCOUT-O3
16 Nov 2005	Darwin 12.5°S 130.8°E	tropics	06:34 - 08:00	70.9° - 51.84°	SCOUT-O3
19 Nov 2005	Darwin 12.5°S 130.8°E	tropics	04:36 - 05:13	32.93° - 23.86°	SCOUT-O3
23 Nov 2005	Darwin 12.5°S 130.8°E	tropics	07:05	60.97°	SCOUT-O3
29 Nov 2005	Darwin 12.5°S 130.8°E	tropics	06:35	50.36°	SCOUT-O3
30 Nov 2005	Darwin 12.5°S 130.8°E	tropics	05:41 - 06:46	53.44°	SCOUT-O3
5 Dec 2005	Darwin 12.5°S 130.8°E	tropics	20:05 - 22:22	96.70° - 66.51°	SCOUT-O3
9 Dec 2005	Darwin 12.5°S 130.8°E - Brunei 4.9°N 114.9°E	tropics	22:47	73.86°	SCOUT-O3
10 Dec 2005	Brunei 4.9°N 114.9°E - U Taphao 12.7°N 101°E	tropics	05:51 - 07:13	48.11° - 36.54°	SCOUT-O3
13 Dec 2005	U Taphao 12.7°N 101°E - Hyderabad 17.4°N 78.5°E	tropics	02:23	64.8°	SCOUT-O3

Date	**Location**	**Geo-physical Condition**	**Time [UTC]**	**SZA range**	**Campaign**
14 Dec 2005	Hyderabad 17.4°N 78.5°E - Dubai 25.3°N 55.3°E	tropics	04:15	64.24°	SCOUT-O3
16 Dec 2005	Dubai 25.3°N 55.3°E - Larnaca 34.9°N 33.6°E	mid-lat. autumn	04:15 - 05:59	81.44° - 72.18°	SCOUT-O3
17 Dec 2005	Larnaca 34.9°N 33.6°E - Oberpfaffenhofen 48.1°N 11.3°E	mid-lat. autumn	10:24	63.23°	SCOUT-O3

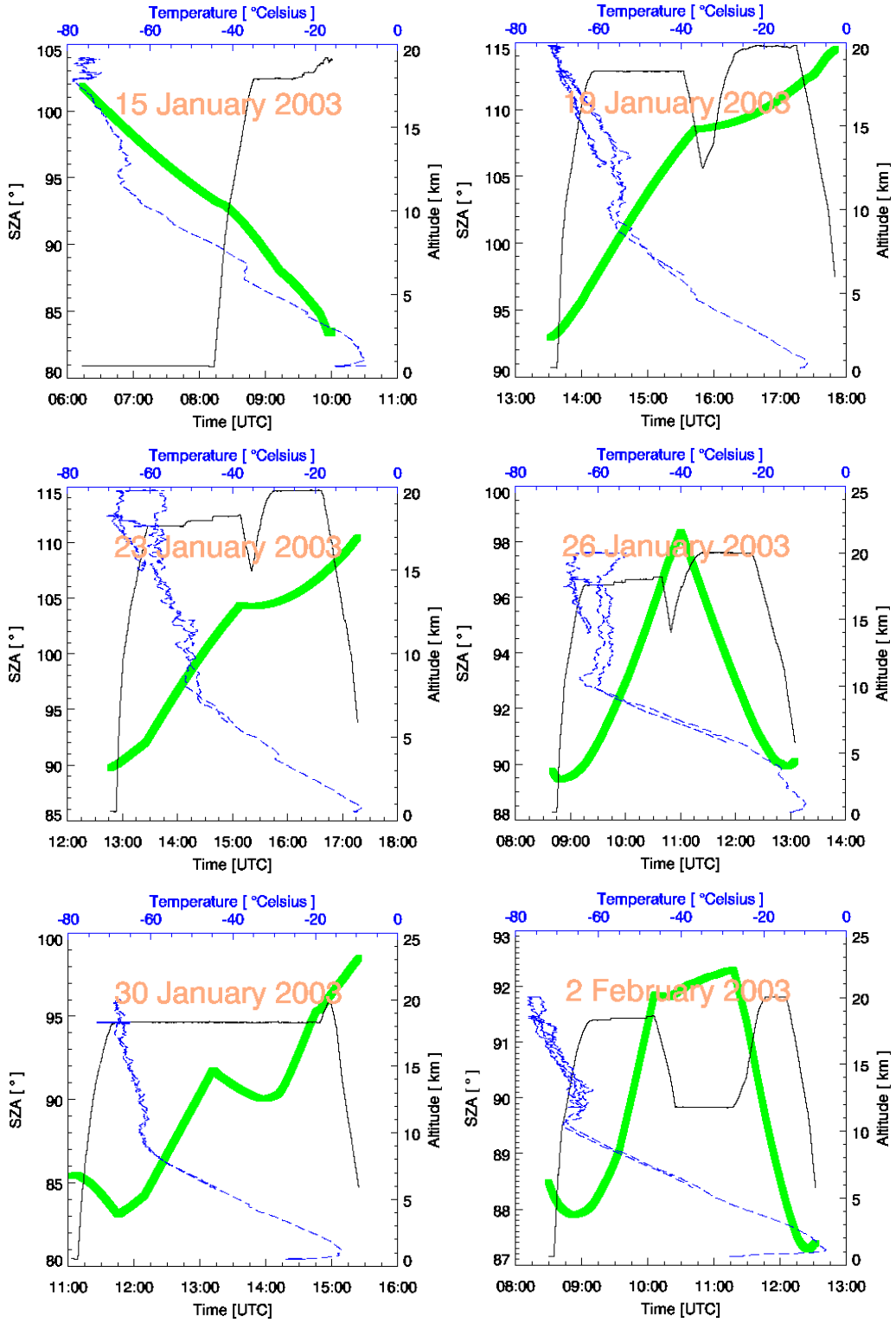

Figure B.1: Flight profiles, temperatures and the SZAs for the EUPLEX campaign (part I)

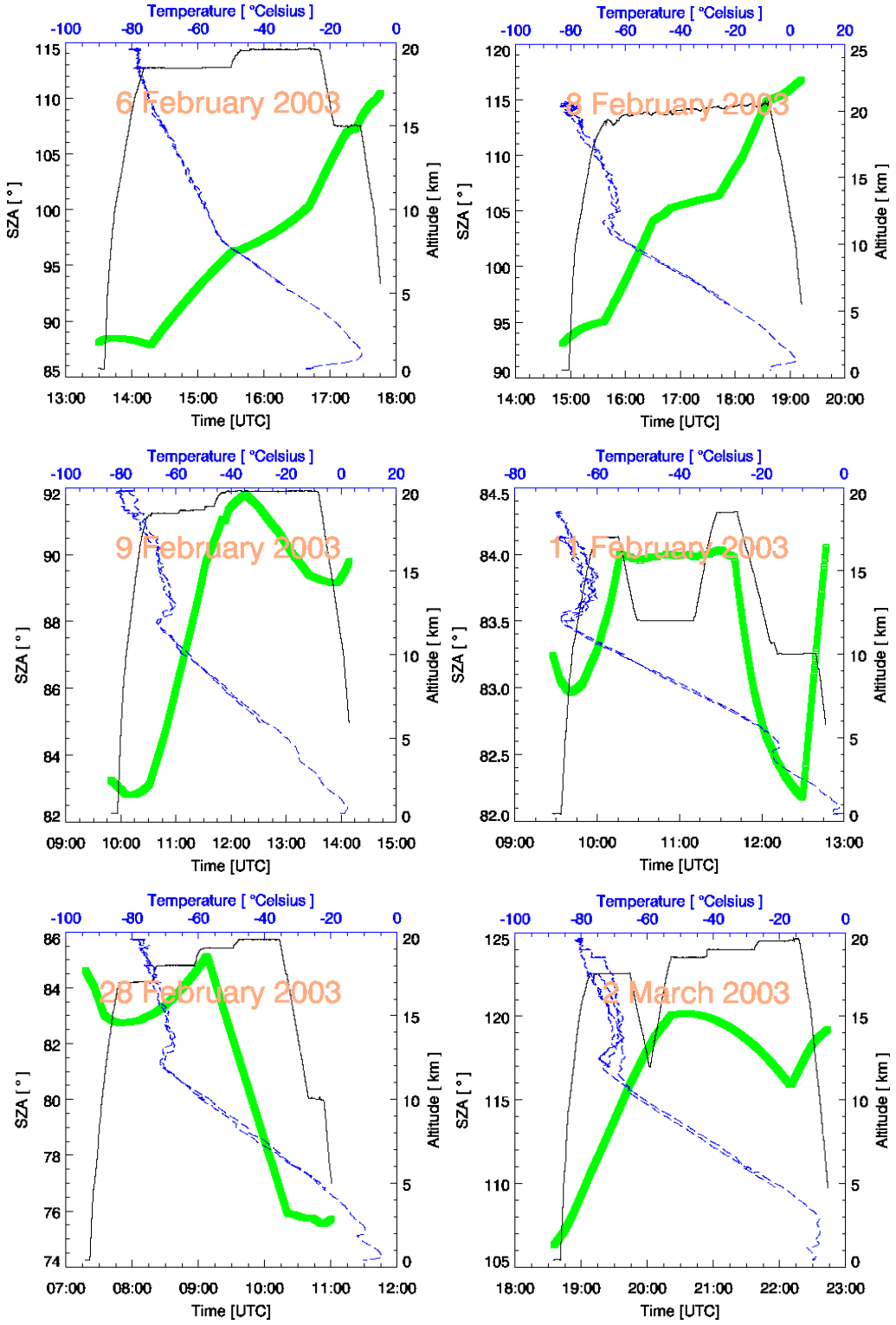

Figure B.2: Flight profiles, temperatures and the SZAs for the EUPLEX campaign (part II)

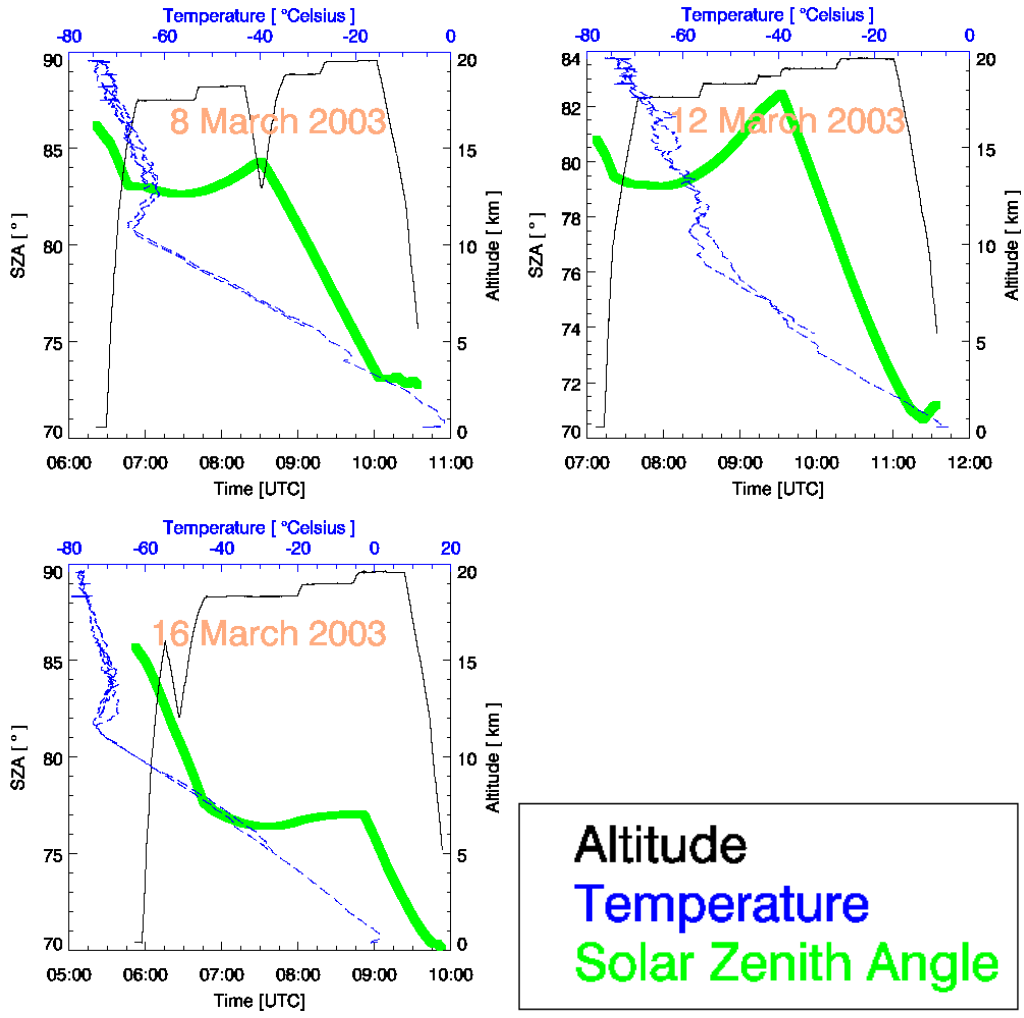

Figure B.3: Flight profiles, temperatures and the SZAs for the EUPLEX campaign (part III)

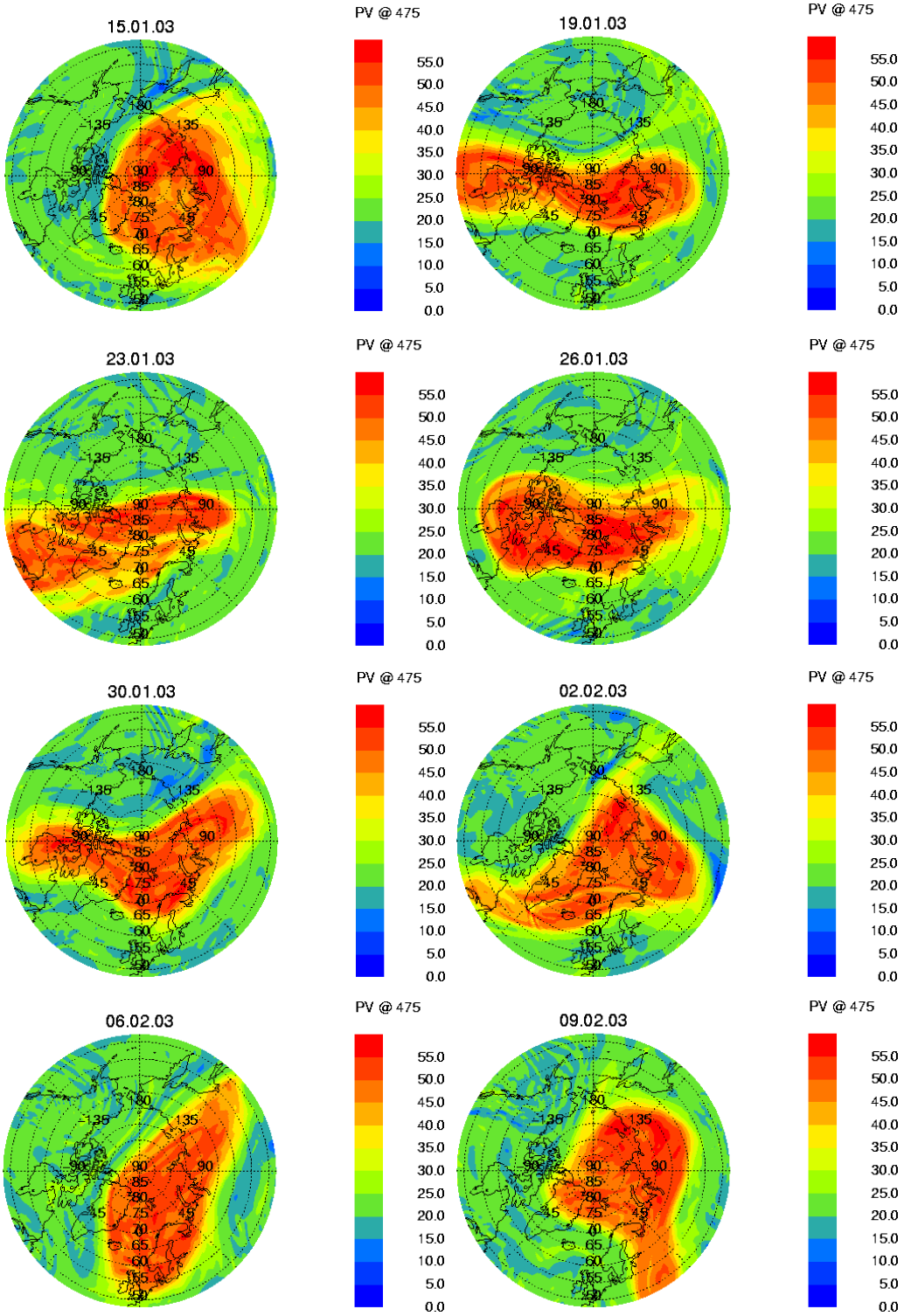

Figure B.4: The northern hemispheric polar vortex characterized by PV during the EUPLEX campaign for the potential temperature level of 475 K $\approx$ 20 km (part I)

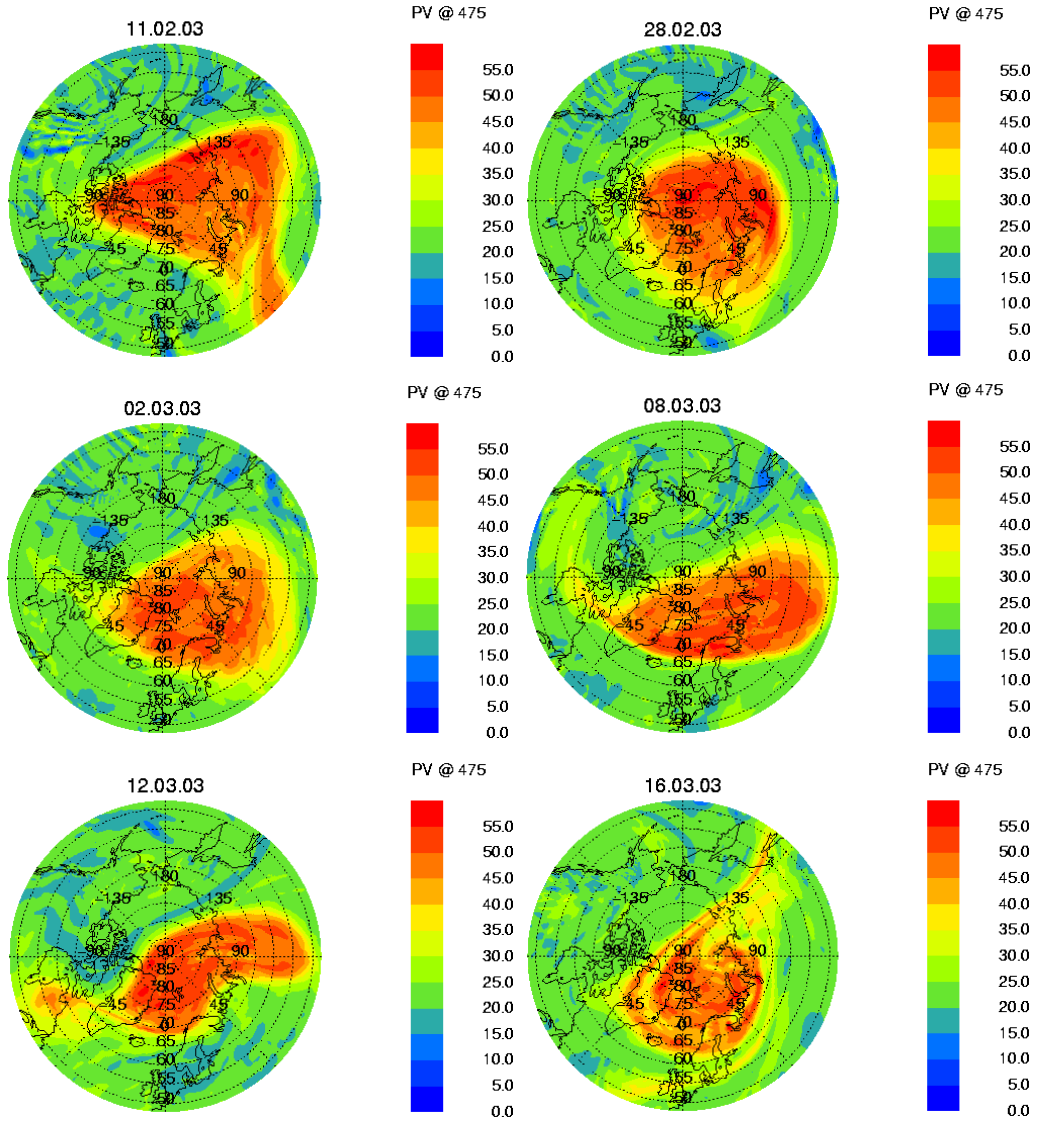

Figure B.5: The northern hemispheric polar vortex characterized by PV during the EUPLEX campaign for the potential temperature level of 475 K $\approx$ 20 km (part II)

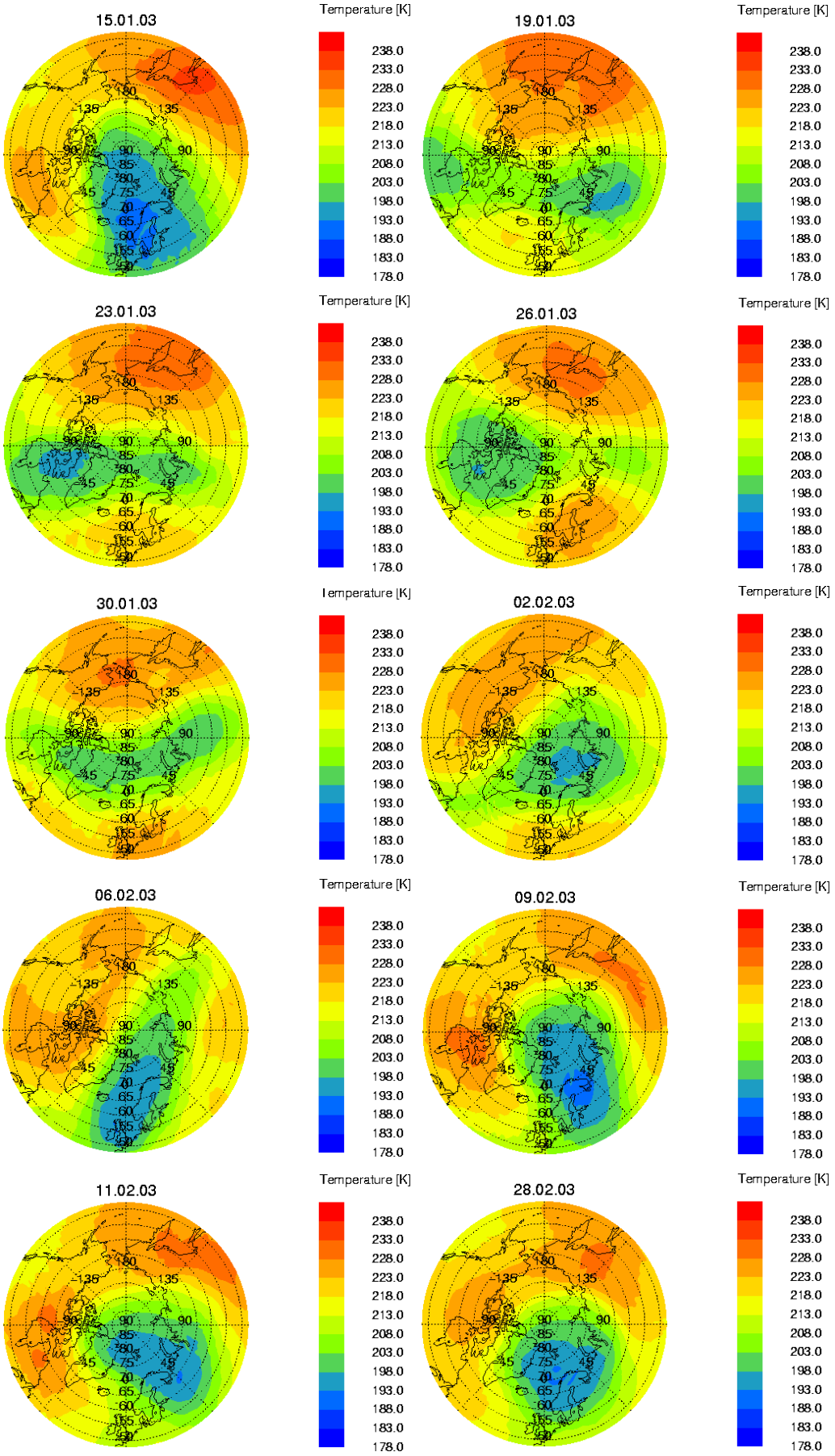

Figure B.6: Temperatures of the Arctic polar vortex for the EUPLEX flight days for the potential temperature level of 475 K ≈ 20 km (part I)

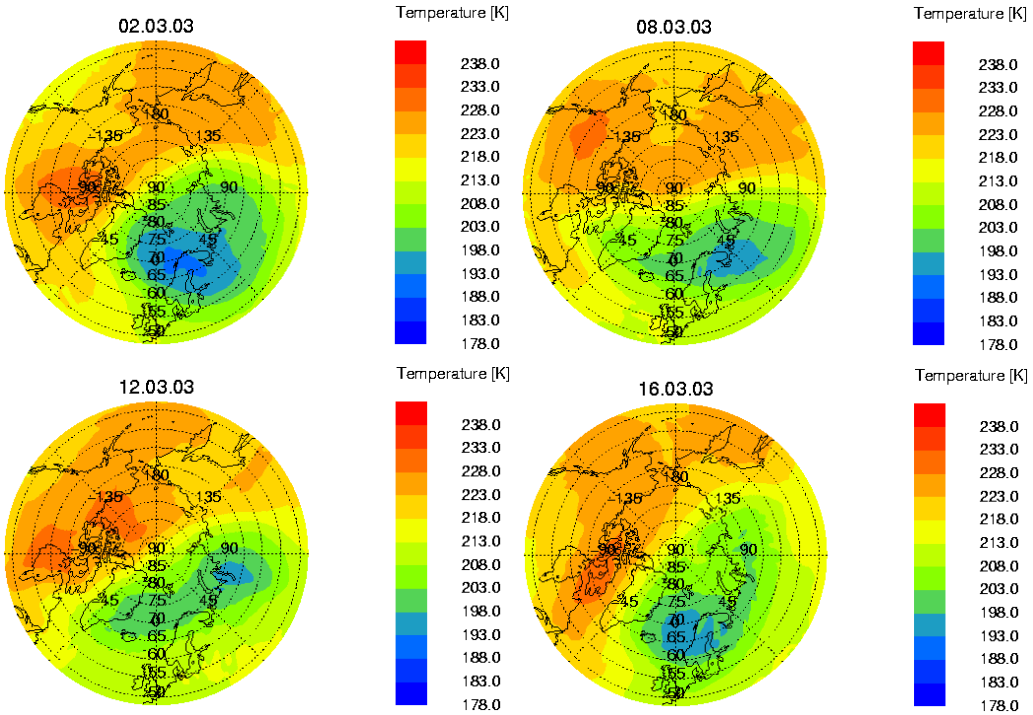

Figure B.7: Temperatures of the Arctic polar vortex for the EUPLEX flight days for the potential temperature level of 475 K $\approx$ 20 km (part II)

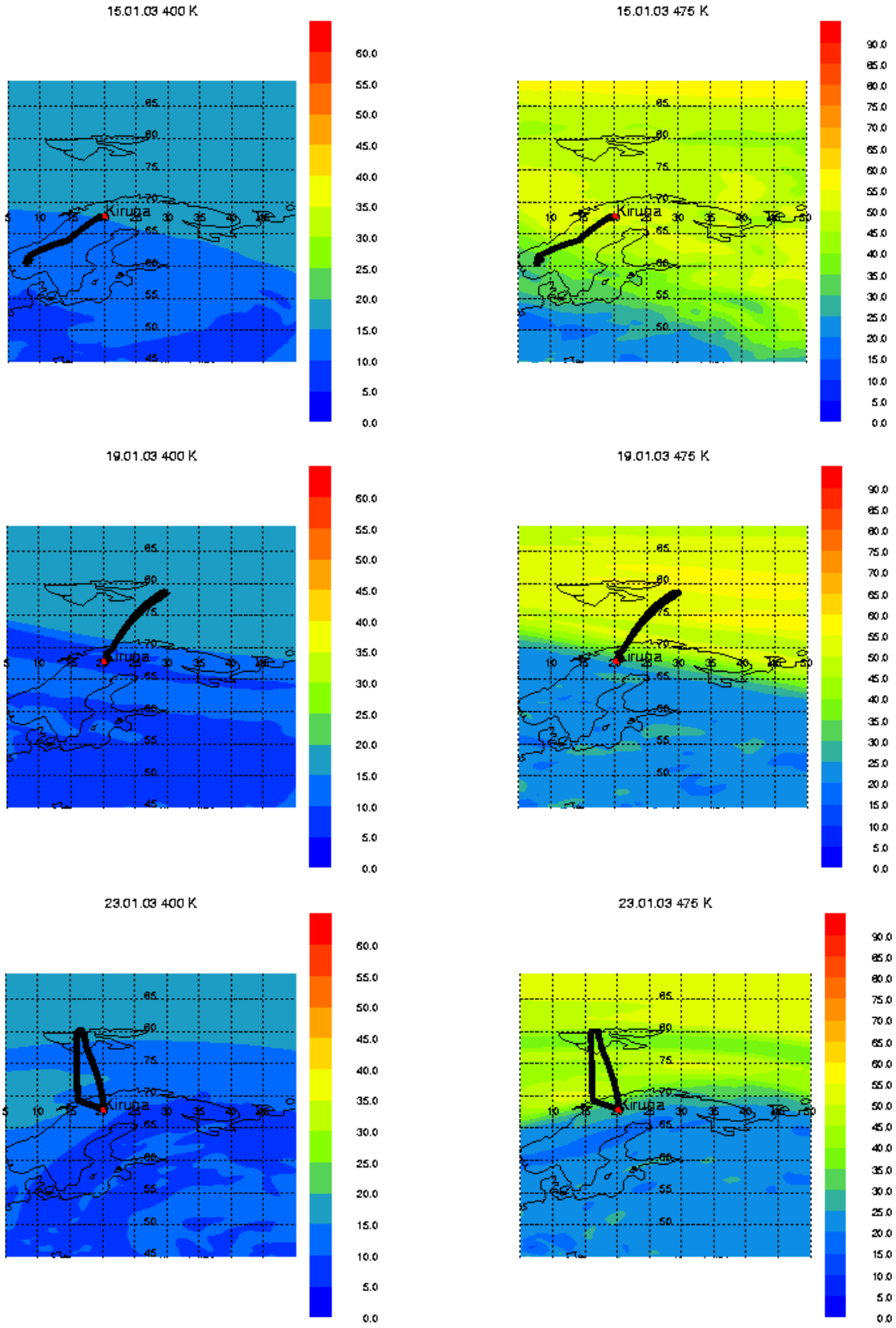

Figure B.8: Flights' trajectories and potential vorticity of the EUPLEX flights. The trajectories are shown by thick black lines. The potential vorticity is shown by means of colour code in PV units for two potential temperature levels of 400 and 475 K. Note, that the scale for PV is changed from the left to the right panels (part I)

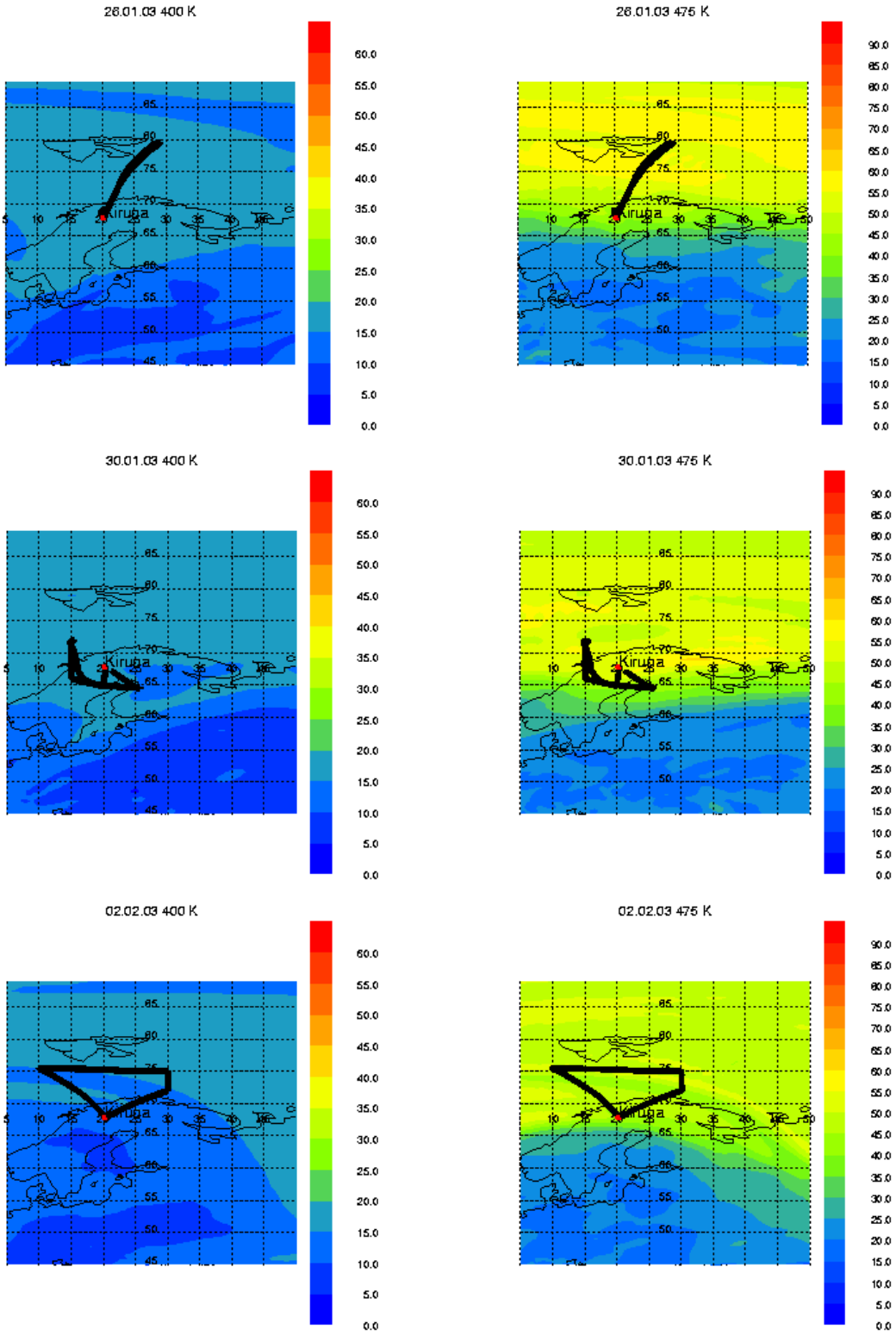

Figure B.9: Flights' trajectories and potential vorticity of the EUPLEX flights. The trajectories are shown by thick black lines. The potential vorticity is shown by means of colour code in PV units for two potential temperature levels of 400 and 475 K. Note, that the scale for PV is changed from the left to the right panels (part II)

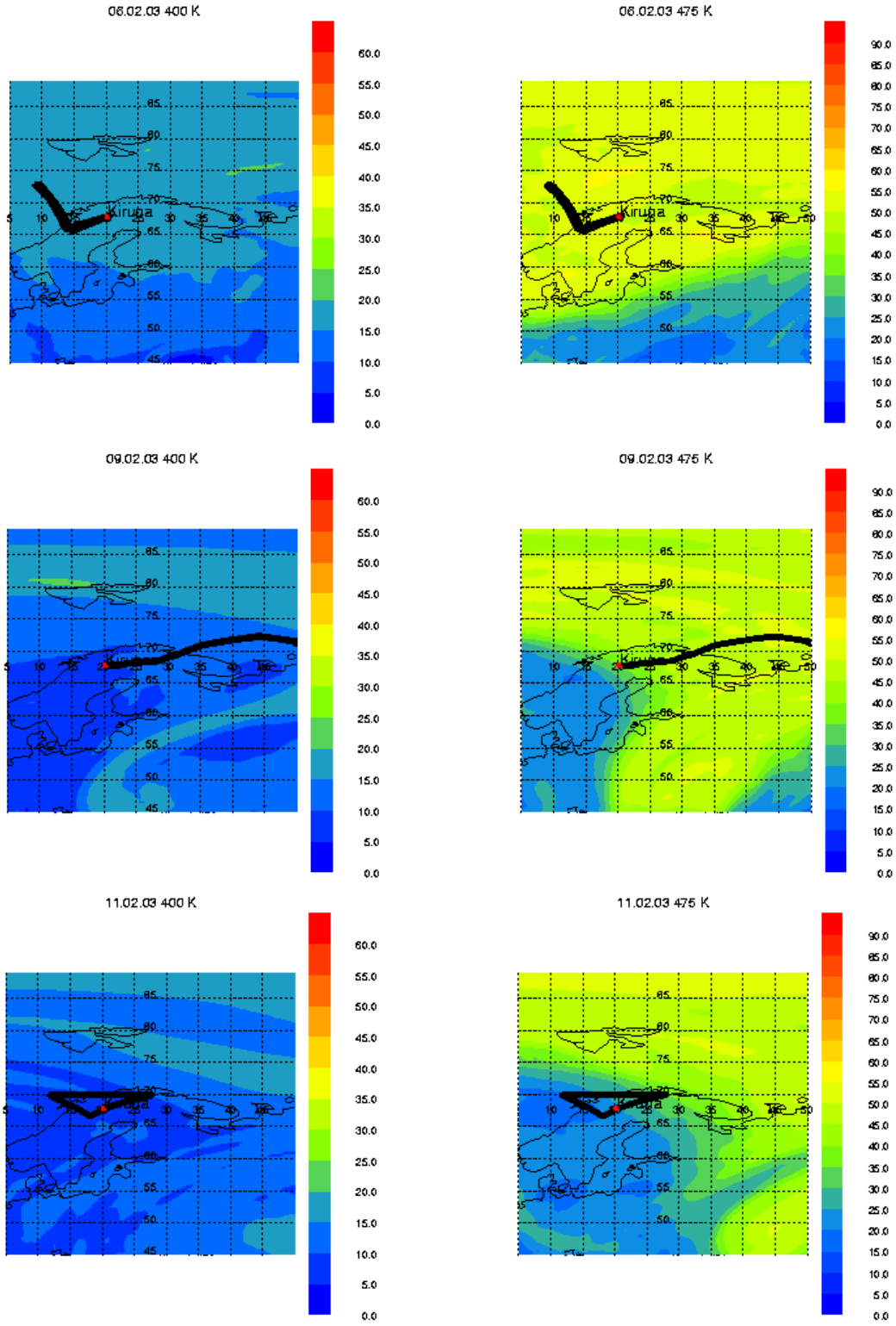

Figure B.10: Flights' trajectories and potential vorticity of the EUPLEX flights. The trajectories are shown by thick black lines. The potential vorticity is shown by means of colour code in PV units for two potential temperature levels of 400 and 475 K. Note, that the scale for PV is changed from the left to the right panels (part III)

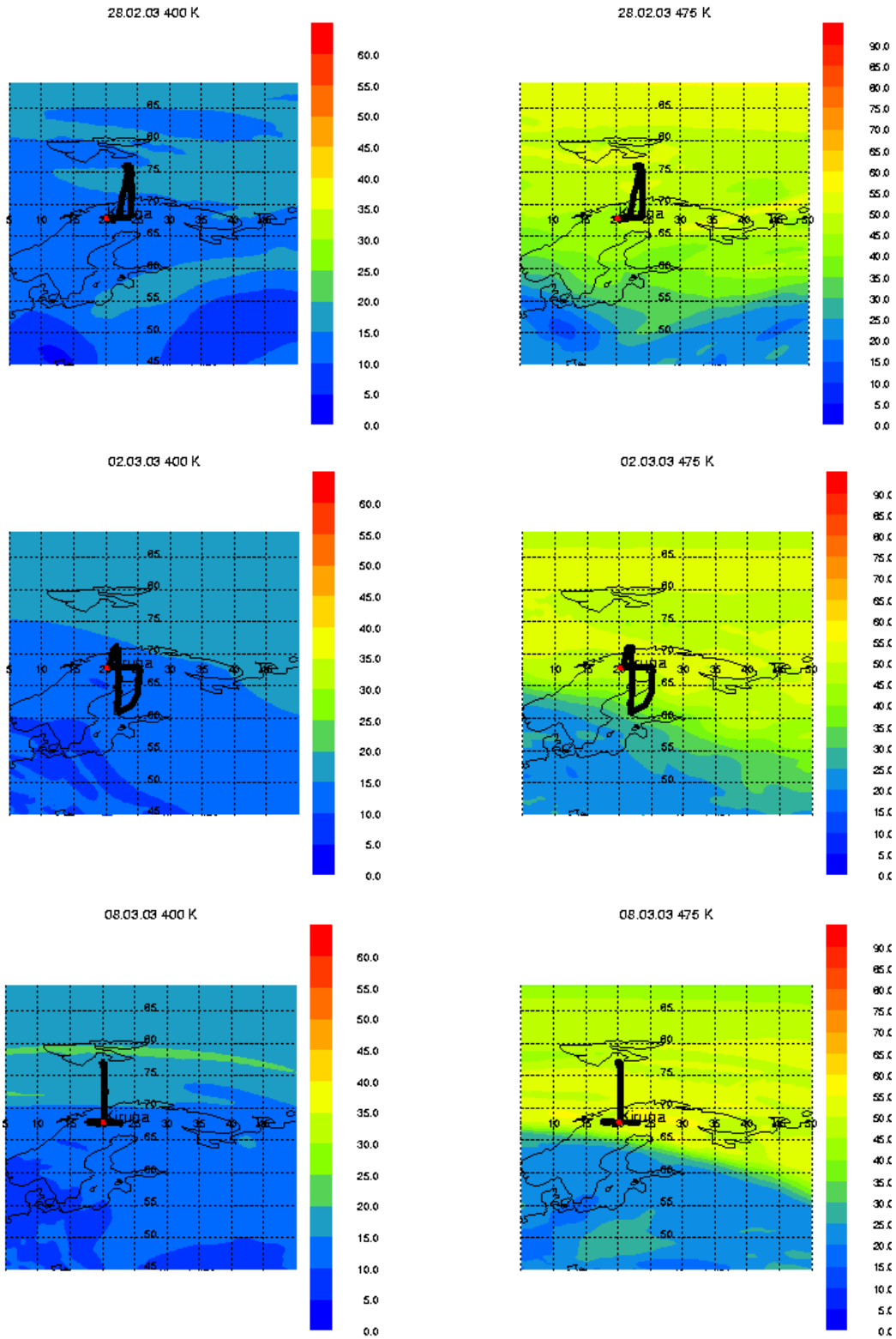

Figure B.11: Flights' trajectories and potential vorticity of the EUPLEX flights. The trajectories are shown by thick black lines. The potential vorticity is shown by means of colour code in PV units for two potential temperature levels of 400 and 475 K. Note, that the scale for PV is changed from the left to the right panels (part IV)

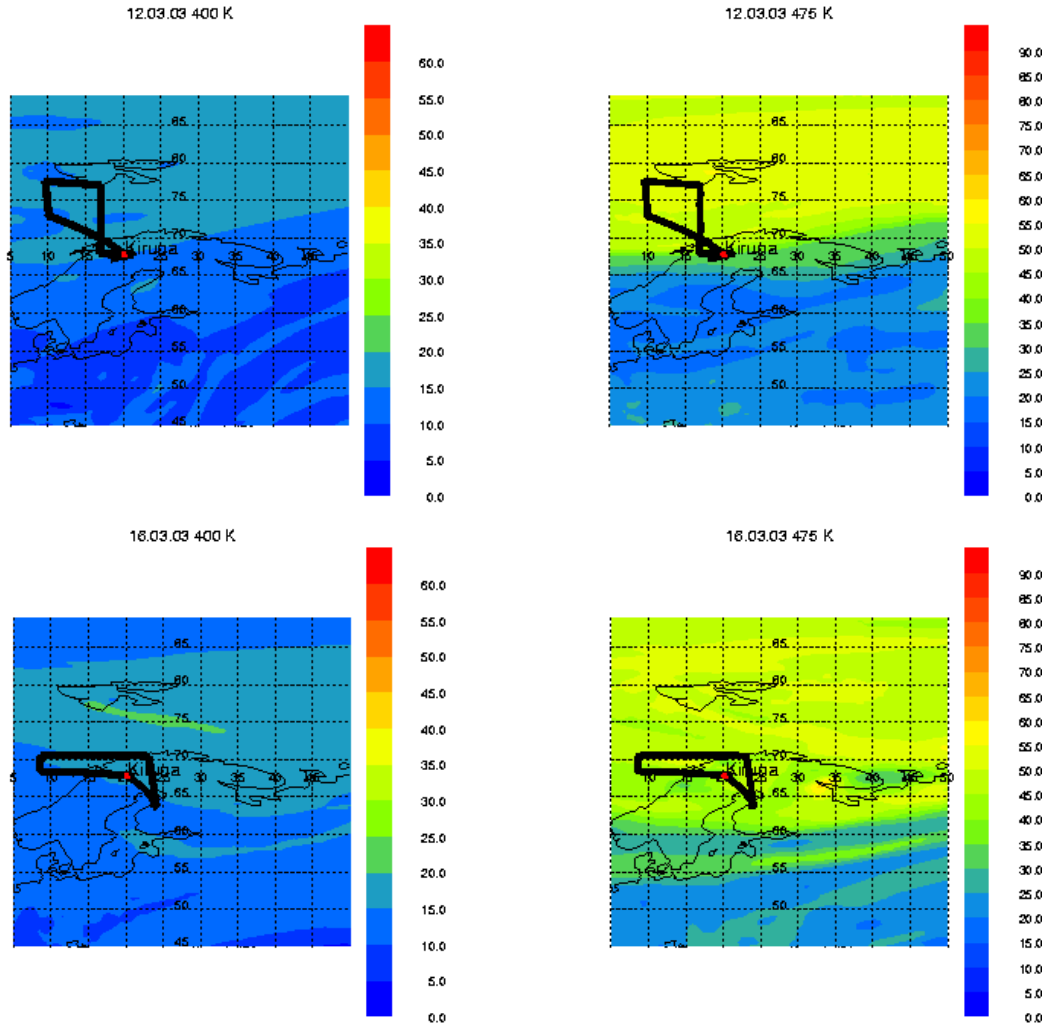

Figure B.12: Flights' trajectories and potential vorticity of the EUPLEX flights. The trajectories are shown by thick black lines. The potential vorticity is shown by means of colour code in PV units for two potential temperature levels of 400 and 475 K. Note, that the scale for PV is changed from the left to the right panels (part V)

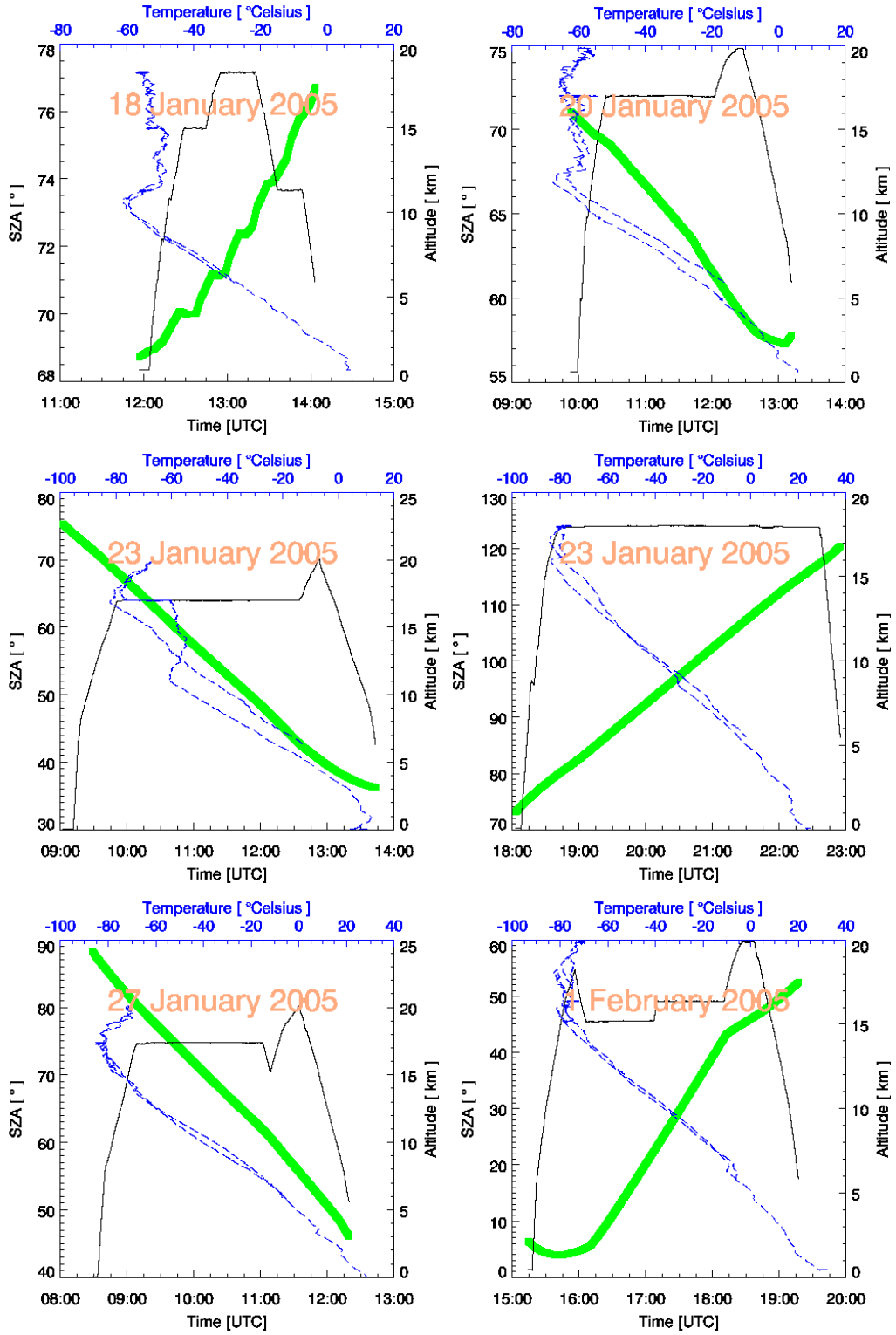

Figure B.13: Flight profiles, temperatures and the SZAs for the TROCCINOX campaign (part I)

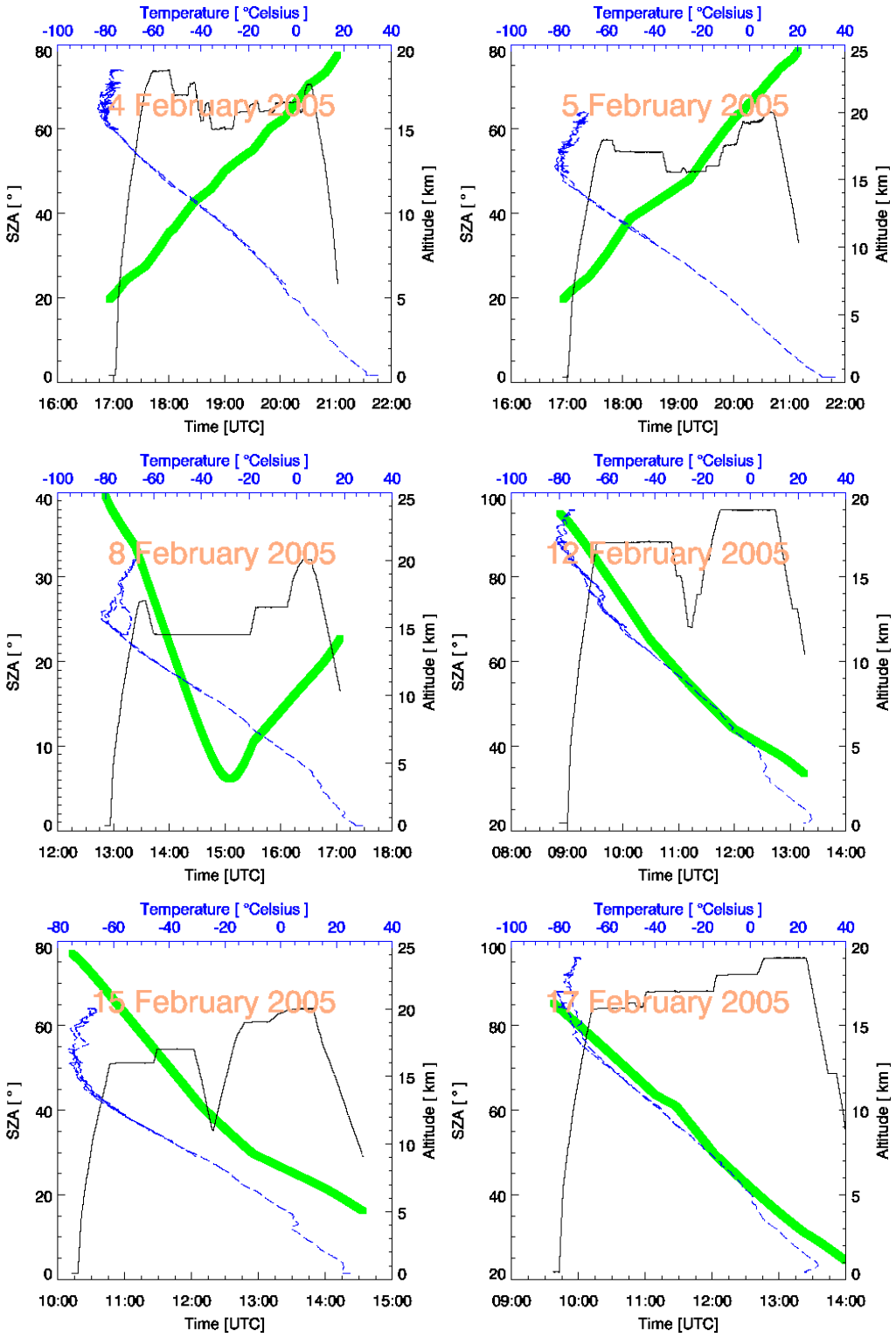

Figure B.14: Flight profiles, temperatures and the SZAs for the TROCCINOX campaign (part II)

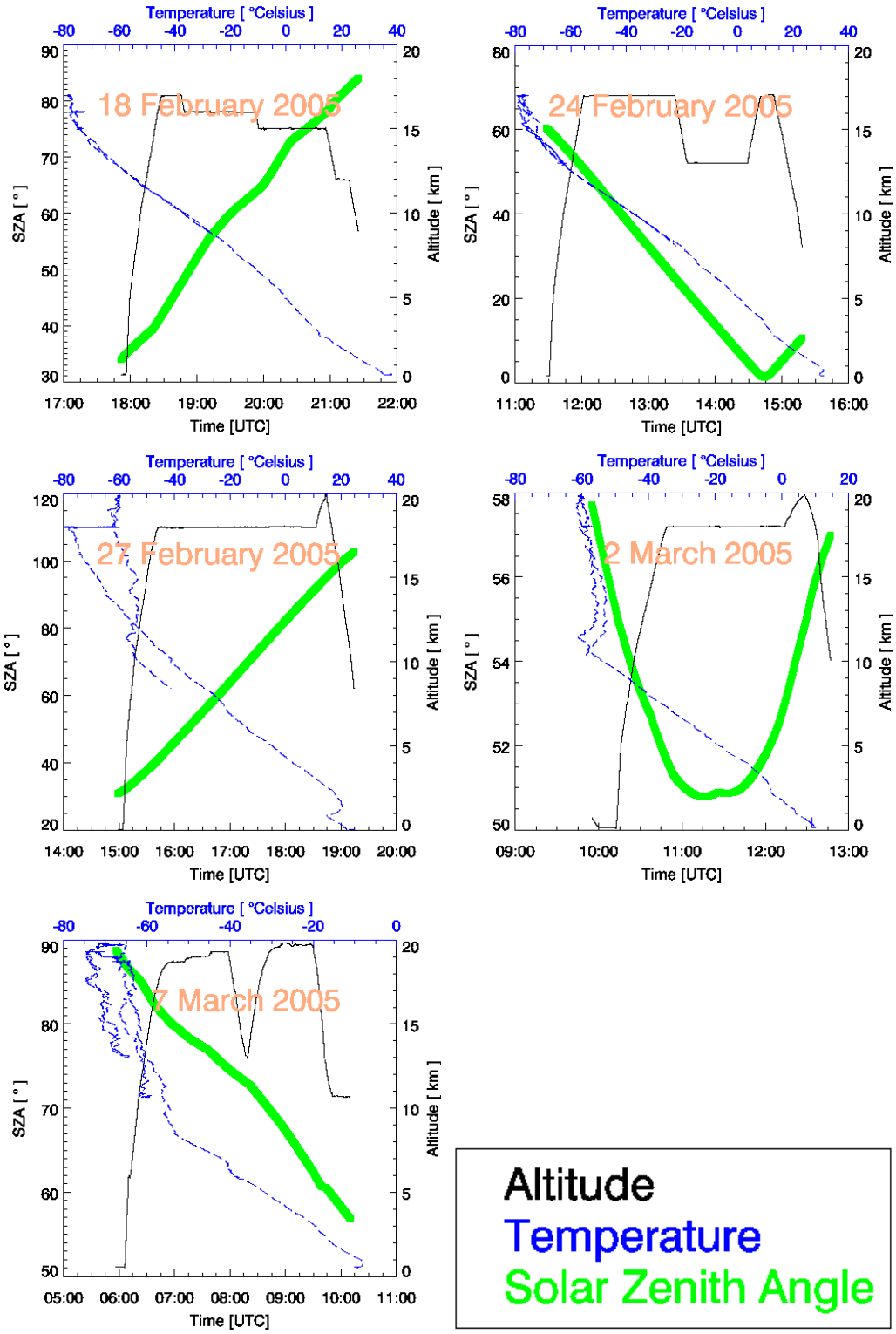

Figure B.15: Flight profiles, temperatures and the SZAs for the TROCCINOX campaign (part III)

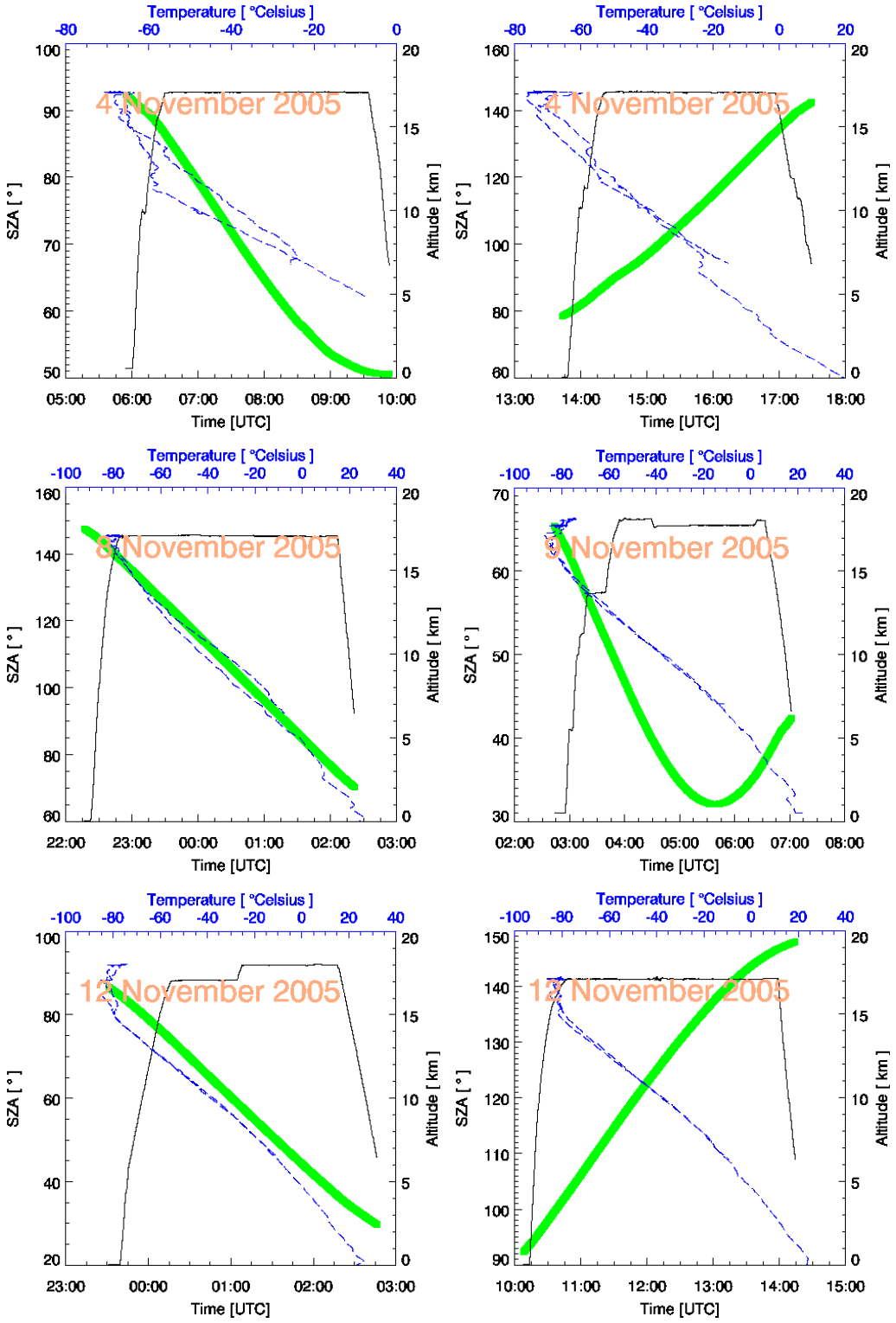

Figure B.16: Flight profiles, temperatures and the SZAs for the SCOUT-O3 campaign (part I)

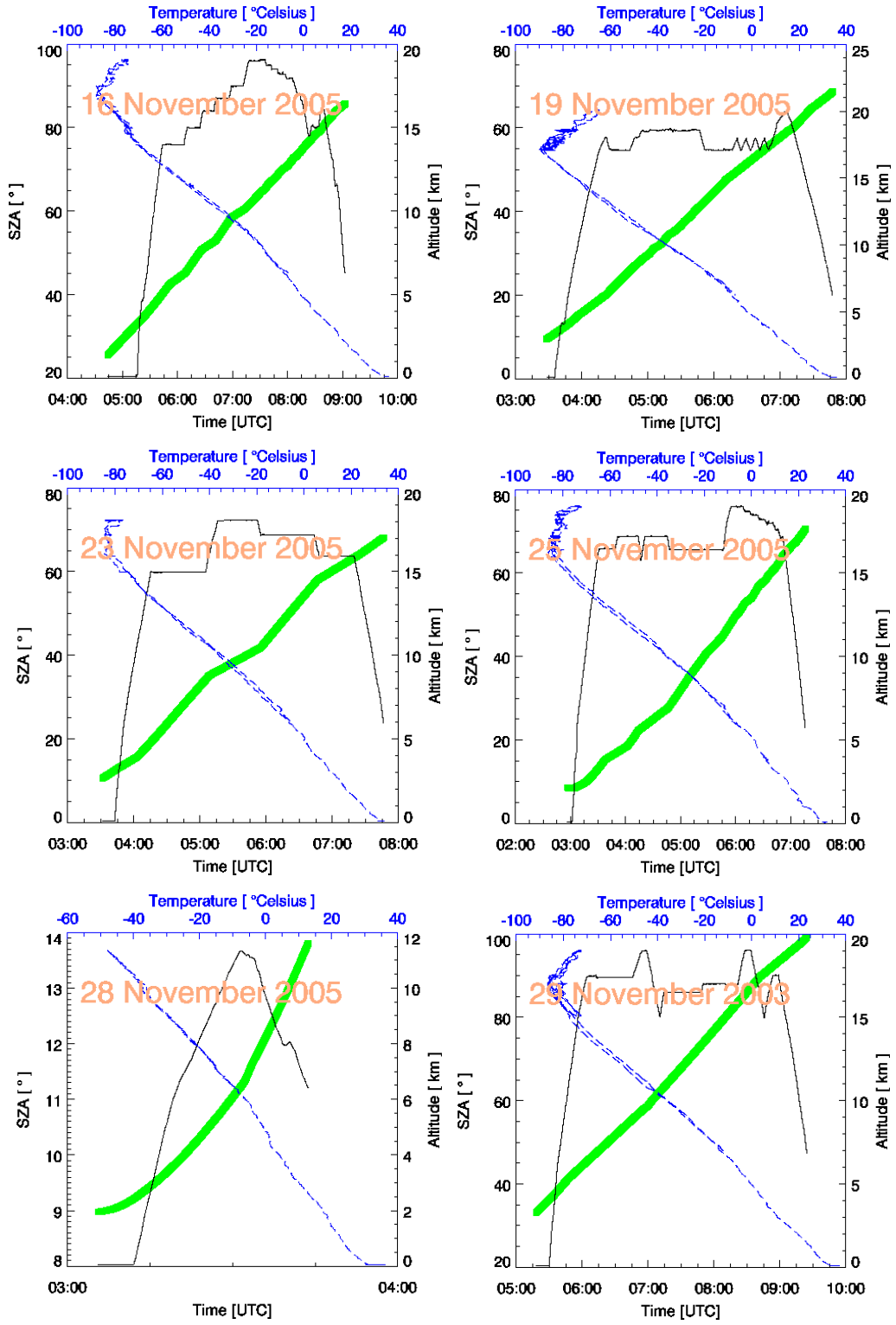

Figure B.17: Flight profiles, temperatures and the SZAs for the SCOUT-O3 campaign (part II)

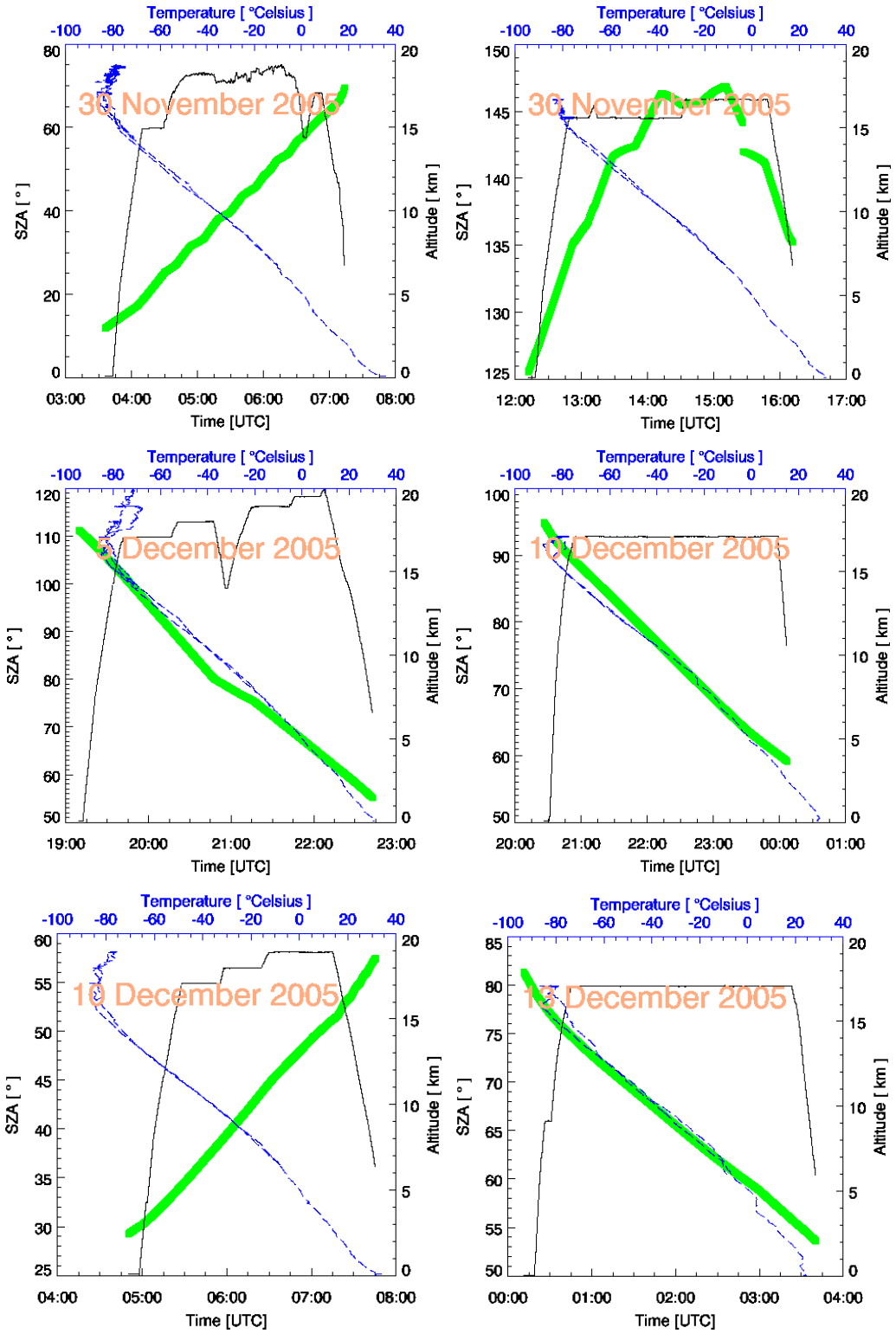

Figure B.18: Flight profiles, temperatures and the SZAs for the SCOUT-O3 campaign (part III)

BIBLIOGRAPHY

Aliwell, S., et al. (2002), Analysis for BrO in zenith-sky spectra: An intercomparison exercise for analysis improvement, *J. Geophys. Res.*, *107*.

Aliwell, S. R., R. L. Jones, and D. J. Fish (1997), Mid-latitude observations of the seasonal variation of BrO, 1, Zenith-sky measurements, *J. Geophys. Res.*, *24*, 1195 – 1198.

Anderson, J. G., J. J. Margitan, and D. H. Stedman (1977), Atomic chlorine and the chlorine monoxide radical in the stratosphere: Three in situ observations, *Science*, *198*, 501–503.

Arpag, K. H., P. V. Johnston, H. L. Miller, R. W. Sanders, and S. Solomon (1994), Observations of the stratospheric BrO column over Colorado, 40°N, *J. Geophys. Res.*, *99*, 8175–8181.

Atkinson, R., D. L. Baulch, R. A. Cox, J. N. Crowley, R. F. Hampson, J. A. Kerr, M. J. Rossi, and J. Troe (2001), Summary of Evaluated Kinetic and Photochemical Data for Atmospheric Chemistry: IUPAC Subcommittee on Gas Kinetic Data Evaluation for Atmospheric Chemistry, Web Version.

Avallone, L. M., D. W. Toohey, S. M. Schauffler, W. H. Pollock, L. E. Heidt, E. L. Atlas, and K. R. Chan (1995), In situ measurements of BrO during AASE II, *Geophys. Res. Lett.*, *22*, 831–834.

Berg, W. W., L. E. Heidt, W. Pollock, P. D. Sperry, R. J. Cicerone, and S. Gladney (1984), Brominated organic species in the Arctic atmosphere, *Geophys. Res. Lett.*, *11*, 429 – 432.

Bevington, P. R., and D. K. Robinson (1992), *Data reduction and error analysis for the physical science*, McGraw-Hill, Inc., the USA, edited by S. J. Tubb and J. M. Morriss.

Bobrowski, N., G. Hönninger, B. Galle, and U. Platt (2003), Detection of bromine monoxide in a volcanic plume, *Nature*, *423*, 273–276.

Brasseur, G. P., J. J. Orlando, and G. S. Tyndall (Eds.) (1999), *Atmospheric Chemistry and Global Change*, A textbook prepared by scientists at the National Center for Atmospheric Research, Boulder, Colorado, USA.

Brauers, T., M. Hausmann, U. Brandenburger, and H.-P. Dorn (1995), Improvment of differential optical absorption spectroscopy with a multichannel scanning technique, *Appl. Opt.*, *34*(21), 4472–4479.

Brewer, A. W., C. T. McElroy, and J. Kerr (1973), Nitrogen dioxide concentrations in the atmosphere, *Nature*, *246*, 129–133.

Brune, W. H., and J. G. Anderson (1986), In situ observations of midlatitude stratospheric ClO and BrO, *Geophys. Res. Lett.*, *13*, 1391–1394.

Brune, W. H., J. G. Anderson, and K. R. Chan (1989a), In-situ observations of ClO in the Antarctic: ER-2 aircraft results from 54°S to 72°S latitude, *J. Geophys. Res.*, *94*, 16,649–16,663.

Brune, W. H., J. G. Anderson, and K. R. Chan (1989b), In-situ observations of BrO over Antarctica: ER-2 aircraft results from 54°S to 72°S latitude, *J. Geophys. Res.*, *94*, 16,639–16,647.

Bureau of Meteorology, Ozone Science Unit (1991), *Depletion of the ozone layer*.

Burkholder, J. B., A. R. Ravishankara, and S. Solomon (1995), UV/visible and IR absorption cross sections of $BrONO_2$, *J. Geophys. Res.*, *100*, 16,793–16,800.

Burrows, J. P., et al. (1999), The Global Ozone Monitoring Experiment GOME: Mission concept and first scientific results, *J. Atmos. Sci.*, *56*, 151–175.

Carroll, M. A., R. W. Sanders, S. Solomon, and A. L. Schmeltekopf (1989), Visible and near-ultraviolet spectroscopy at McMurdo station, Antarctica, 6, Observations of BrO, *J. Geophys. Res.*, *94*, 16,633–16,638.

Carslaw, K. S., S. L. Clegg, and P. Brimblecombe (1995), A thermodynamic model of the system HCl-HNO_3-H_2SO_4-H_2O, including solubilities of HBr, from 328 K to $<$ 200 K, *J. Phys. Chem.*, *99*, 11,557–11,574.

Chance, K. (1998), Analysis of BrO measurements from the Global Ozone Monitoring Experiment, *Geophys. Res. Lett.*, *25*, 3335–3338.

Christensen, T., et al. (2005), Vortex-averaged Arctic ozone depletion in the winter 2002/2003, *Atmos. Chem. Phys.*, *5*, 131–138.

Cicerone, R. J., L. E. Heidt, and W. H. Pollock (1988), Measurements of atmospheric methyl bromide and bromoform, *J. Geophys. Res.*, *93*, 3745–3749.

Curtis, A. R., and W. P. Sweetenham (1987), *Facsimile/Chekmat User's Manual*, Computer Science and Systems Division, Harwell Laboratory, Oxford, 135 pp.

Danilin, M. Y., et al. (2002), Trajectory hunting as an effective technique to validate multiplatform measurements: Analysis of the MLS, HALOE, SAGE-II, ILAS, and POAM-II data in October–November 1996, *J. Geophys. Res.*, *107*(D20), 4420, doi:10.1029/2001JD002012.

DeMore, W. B., S. P. Sander, D. M. Golden, R. F. Hampson, M. J. Kurylo, C. J. Howard, A. R. Ravishankara, C. E. Kolb, and M. J. Molina (1997), Chemical kinetics and photochemical data for use in stratospheric modeling, JPL Publication 97-4.

Dorf, M. (2005), Investigation of Inorganic Stratospheric Bromine using Balloon-Borne DOAS Measurements and Model Simulations, PhD thesis, University of Heidelberg.

Dorf, M., et al. (2006), Balloon-borne stratospheric BrO measurements: comparison with Envisat/SCIAMACHY BrO limb profiles, *Atmos. Chem. Phys.*, *6*, 2483–2501.

Dowling, T., and R. Morales-Juberías (2003), DPS 35th Meeting poster.

Dvortsov, V. L., M. A. Geller, S. Solomon, S. M. Schauffler, E. L. Atlas, and D. R. Blake (1999), Rethinking reactive halogen budget in the midlatitude stratosphere, *Geophys. Res. Lett.*, *26*, 1699–1702.

Estupinan, E. G., J. M. Nicovich, and P. H. Wine (2001), A Temperature-Dependent Kinetics Study of the Important Stratospheric Reaction $O(^3P) + NO_2 = O_2 + NO$, *J. Phys. Chem. A*, *105*, 9697–9703.

Fabian, P., R. Borchers, and K. Kouritidis (1994), Bromine-containing source gases during EASOE, *Geophys. Res. Lett.*, *21*, 1219–1222.

Fahey, D. W. (2003), *Twenty Questions and Answers About the Ozone Layer: Scientific Assessment of Ozone Depletion: 2002*, WMO.

Ferlemann, F., et al. (1998), Stratospheric BrO profiles measured at different latitudes and seasons: Instrument description, spectral analysis and profile retrieval, *Geophys. Res. Lett.*, *25*, 3847–3850.

Fish, D. J., S. R. Aliwell, and R. L. Jones (1997), Mid-latitude observations of the seasonal variation of BrO, 2, Interpretation and modelling study, *Geophys. Res. Lett.*, *24*, 1199–1202.

Fitzensberger, R., H. Bösch, C. Camy-Peyret, M. P. Chipperfield, H. Harder, U. Platt, B.-M. Sinnhuber, T. Wagner, and K. Pfeilsticker (2000), First profile measurements of tropospheric BrO, *Geophys. Res. Lett.*, *27*, 2921 – 2924.

Fleischmann, O. C., M. Hartmann, J. P. Burrows, and J. Orphal (2004), New ultraviolet absorption cross-sections of BrO at atmospheric temperatures measured by time-windowing Fourier transform spectroscopy, *J. Photochem. Photobiol. A*, *168*, 117–132.

Friess, U., M. P. Chipperfield, H. Harder, C. Otten, U. Platt, J. Pyle, T. Wagner, and K. Pfeilstiker (1999), Intercomparison of measured and modelled BrO slant column amounts for the Arctic winter and spring 1994/95, *Geophys. Res. Lett.*, *26*, 1861–1864.

Gidel, L. T., P. J. Crutzen, and J. Fishman (1983), A two-dimensional photochemical model of the atmosphere; 1: Chlorocarbon emissions and their effect on stratospheric ozone, *J. Geophys. Res.*, *88*, 6622–6640.

Goldfarb, L., J. B. Burkholder, and A. R. Ravishankara (2001), Kinetics of the $O + ClO$ Reaction, *J. Phys. Chem. A*, *105*, 5402–5409.

Grendel, A., A. Grundt, and D. Perner (1996), Transall DOAS-measurements of stratospheric OClO, BrO, NO_2 and O_3 in winter 1994/95, in *Proc. 3rd Eur. Polar Ozone Symp., EC Air Pollut. Res., vol. 56, Eur. Comm., Brussels, Belgium*, edited by J. A. Pyle et al., pp. 319–322.

Grooß, J.-U. (1996), Modelling of stratospheric chemistry based on HALOE/UARS satellite data, PhD thesis, University of Mainz.

Grooß, J.-U., R. Müller, P. Konopka, H.-M. Steinhorst, A. Engel, T. Möbius, and C. Volk (2006), The impact of mixing across the polar vortex edge on ozone loss estimates, *Geophys. Res. Lett.*, in preparation.

Grooß, J.-U., et al. (2002), Simulation of ozone depletion in spring 2000 with the Chemical Lagrangian Model of the Stratosphere (CLaMS), *J. Geophys. Res.*, *107*, doi:10.1029/2001JD000456.

Hegels, E., P. J. Crutzen, T. Cluepfel, and D. Perner (1998), Global distribution of atmospheric bromine monoxide from GOME on earth observing satellite ERS-2, *Geophys. Res. Lett.*, *25*, 3127–3130.

Jacob, D. J., et al. (2003), The Transport and Chemical Evolution over the Pacific (TRACE-P) aircraft mission: design, execution, and first results, *J. Geophys. Res.*, *108*, doi:10.1029/2002JD003276.

Johnson, D. G., W. A. Traub, K. V. Chance, and K. W. Jucks (1995), Detection of HBr and upper limit for HOBr: Bromine partitioning in the stratosphere, *Geophys. Res. Lett.*, *22*, 1373–1376.

Kaleschke, L., et al. (2004), Frost flowers on sea ice as a source of sea salt and their influence on tropospheric halogen chemistry, *Geophys. Res. Lett.*, *31*(L16114), L16,114, doi:10.1029/2004GL020655.

Kaye, J. A., S. A. Penkett, and F. M. Ormond (Eds.) (1994), *Report on concentrations, lifetimes, and trends of CFCs, halons, and related species*, vol. NASA Ref. Pub. 1339, NASA, Washington, D. C.

Ko, M. K. W., N. D. Sze, C. Scott, and D. K. Weisenstein (1997), On the relation between chlorine/bromine loading and short-lived troposheric source gases, *J. Geophys. Res.*, *102*, 25,507 – 25,517.

Konopka, P., J. U. Grooß, G. Günther, D. S. McKenna, R. Müller, J. W. Elkins, D. Fahey, and P. Popp (2003), Weak impact of mixing on chlorine deactivation during SOLVE/THESEO2000: Lagrangian modeling (CLaMS) versus ER-2 in situ observations., *J. Geophys. Res.*, *108*, 8324, doi:10.1029/2001JD000876.

Kreher, K., P. V. Johnston, S. Wood, B. Nardi, and U. Platt (1997), Ground-based measurements of tropospheric and stratospheric BrO at Arrival Heights, Antarctica, *Geophys. Res. Lett.*, *24*, 3021–3024.

Lary, D. J. (1996), Gas phase atmospheric bromine photochemistry, *J. Geophys. Res.*, *101*, 1505–1516.

McElroy, C. T., C. A. McLinden, and J. C. McConnel (1999), Evidence for bromine monoxide in the free troposhere during the arctic polar sunrise, *Nature*, *1997*, 338–341.

McElroy, M. B., R. J. Salawitch, S. C. Wofsy, and J. A. Logan (1986), Antarctic ozone: Reductions due to synergistic interactions of chlorine and bromine, *Nature*, *321*, 759–762.

McKenna, D. S., J.-U. Grooß, G. Günther, P. Konopka, R. Müller, G. Carver, and Y. Sasano (2002a), A new Chemical Lagrangian Model of the Stratosphere (CLaMS): Part II Formulation of chemistry-scheme and initialisation, *J. Geophys. Res.*, *107*(D15), 4256, doi:10.1029/2000JD000113.

McKenna, D. S., P. Konopka, J.-U. Grooß, G. Günther, R. Müller, R. Spang, D. Offermann, and Y. Orsolini (2002b), A new Chemical Lagrangian Model of the Stratosphere (CLaMS): Part I Formulation of advection and mixing, *J. Geophys. Res.*, *107*(D16), 4309, doi:10.1029/2000JD000114.

McKinney, K. A. (1998), In situ measurements of BrO and the photochemistry of the inorganic bromine in the Arctic stratosphere, Ph.d. thesis, Univ. of California at Irvine, Calif., USA.

McKinney, K. A., J. M. Pierson, and D. W. Toohey (1997), Altitude distribution of stratospheric constituents from ground-based measurements at twilight, *Geophys. Res. Lett.*, *24*, 853–856.

Molina, M. J., and F. S. Rowland (1974), Stratospheric sink for chlorofluoromethanes: Chlorine atom catalysed destruction of ozone, *Nature*, *249*, 810–812.

Morcrette, J.-J. (1991), Radiation and cloud radiative properties in the European Centre for Medium-Range Weather Forecasts forecasting system, *J. Geophys. Res.*, *96*(D5), 9121–9132.

Nolt, I. G., et al. (1997), Stratospheric HBr concentration profile obtained from far-infrared emission spectroscopy, *Geophys. Res. Lett.*, *24*, 281–284.

Oram, D. E. (1999), Trends of long-lived anthropogenic halocarbons in the Southern Hemisphere and model calculations of global emissions, Dissertation, University of East Anglia, Norwich, England.

Otten, C., F. Ferlemann, U. Platt, T. Wagner, and P. Pfeilsticker (1998), groundbased DOAS UV/visible measurements at Kiruna (Sweden) during the SESAME winters 1993/94 and 1994/95, *J Atmos Chem*, *30*, 141–162.

Penkett, S. A., B. M. R. Jones, M. J. Rycroft, and D. A. Simmons (1985), An interhemispheric comparison of the concentration of bromine compounds in the atmosphere, *Nature*, *318*, 550–553.

Pfeilsticker, K., et al. (1994), Correlation between stratospheric temperature, total ozone and tropospheric weather systems, *Geophys. Res. Lett.*, *21*, 1203–1206, doi:10.1029/93GL03020.

Platt, U., and G. Hönninger (2003), The role of halogen species in the troposphere, *Chemosphere*, *52*, 325–328.

Platt, U., D. Perner, and H. Pätz (1979), Simultaneous measurement of atmospheric CH_2O, O_3 and NO_2 by differential optical absorption, *J. Geophys. Res.*, *84*, 6329–6335.

Pommereau, J.-P., and F. Goutail (1988), O_3 and NO_2 ground-based measurements by visible spectrometry during Arctic winter and spring 1988, *Geophys. Res. Lett.*, *15*, 891–894.

Prinn, R. G., et al. (2000), A history of chemically and radiatively important gases in air deduced from ALE/GAGE/AGAGE, *J. Geophys. Res.*, *105*(D14), 17,751–17,792, doi:10.1029/2000JD900141.

Pundt, I., J.-P. Pommereau, M. P. Chipperfield, M. Van Roozendael, and F. Goutail (2002), Climatology of the stratospheric BrO vertical distribution by balloon-borne UV-visible spectrometry, *J. Geophys. Res.*, *107*, 4806, doi:10.1029/2002JD002230.

Quack, B., and D. W. R. Wallace (2003), Air-sea flux of bromoform: Controls, rates, and implications, *Global Biogeochem. Cycles*, *17*, 1023, doi: 10.1029/2002GB001890.

Rasmussen, R. A., and A. K. Khalil (1984), Gaseous bromine in the Arctic and Arctic haze, *Geophys. Res. Lett.*, *11*, 433–436.

Richter, A., F. Wittrock, M. Eisinger, and J. P. Burrows (1998), GOME observations of tropospheric BrO in Northern Hemispheric spring and summer 1997, *Geophys. Res. Lett.*, *25*, 2683–2686.

Richter, A., M. Eisinger, A. Ladstätter-Weißenmayer, and J. P. Burrows (1999), DOAS zenith sky observations, 2, seasonal variation of BrO over Bremen (53°N) in 1994 -1995, *J. Atmos. Chem.*, *32*, 83–99.

Richter, A., F. Wittrock, A. Ladstätter-Weißenmayer, and J. P. Burrows (2002), GOME measerements of stratospheric and tropospheric BrO, *Adv. Space Res.*, *29*, 1667–1672.

Rodgers, C. (2000), *Inverse methods for atmospheric sounding*, World Scientific, Singapore, New Jersey, London, Hongkong.

Rowland, F., and M. Molina (1975), Chlorofluoromethanes in the environment, *Rev. Geophys.*, *13*, 1–35.

Rozanov, A., H. Bovensmann, A. Bracher, S. Hrechanyy, V. Rozanov, M. Sinnhuber, F. Stroh, and J. P. Burrows (2005), NO_2 and BrO vertical profile retrieval from SCIAMACHY limb measurements: Sensitivity studies, *Adv. Space Res.*

Russell, J. M., L. L. Gordley, J. H. Park, S. R. Drayson, A. F. Tuck, J. E. Harries, R. J. Cicerone, P. J. Crutzen, and J. E. Frederick (1993), The Halogen Occultation Experiment, *J. Geophys. Res.*, *98*, 10,777–10,797.

Salawitch, R. J., D. K. Weisenstein, L. J. Kovalenko, C. E. Sioris, P. O. Wennberg, K. Chance, M. K. W. Ko, and C. A. McLinden (2005), Sensitivity of ozone to bromine in the lower stratosphere, *Geophys. Res. Lett.*, *32*, L05811, doi:10.1029/2004GL021504.

Sander, S. P., et al. (2003), *Evaluation number 14*, Chemical kinetics and photochemical data for use in atmospheric studies, NASA Panel for Data Evaluation, JPL Publication 02-25, Jet Propulsion Laboratory, California Insitute of Technology, Pasadena, California.

Sander, S. P., et al. (2006), Chemical kinetics and photochemical data for use in stratospheric studies, JPL Publication 06-2.

Schauffler, S. M., E. L. Atlas, D. R. Blake, F. Flocke, R. A. Lueb, J. M. Lee-Taylor, V. Stroud, and W. Travnicek (1999), Distributions of brominated organic compounds in the troposphere and lower stratosphere, *J. Geophys. Res.*, *104*, 21,513–21,536.

Schmidt, U., G. Kulessa, E. Klein, E.-P. Röth, P. Fabian, and R. Borchers (1987), Intercomparison of balloon-borne cryogenic whole air samplers during the MAP/GLOBUS 1983 campaign, *Planet Space Sci*, *35*, 647–656.

Schofield, R., K. Kreher, B. J. Connor, P. V. Johnston, A. Thomas, D. Shooter, M. P. Chipperfield, C. D. Rodgers, and G. H. Mount (2004), Retrieved tropospheric and stratospheric BrO columns over lauder, new zealand, *J. Geophys. Res.*, *109*, D14,304, doi:10.1029/2003JD004463.

Schwab, J. J., and J. G. Anderson (1982), Oscillator Strength of Cl(I) in the Vacuum Ultraviolet: The $^2D - ^2P$ Transitions, *J. Quant. Spectr. Radiat. Transfer*, *27*, 445–457.

Simmons, A. J., D. M. Burridge, M. Jarraud, C. Girard, and W. Wergen (1989), The ECMWF medium-range prediction models development of the numerical formulations and the impact of increased resolution, *Meteorol. Atmos. Phys.*, *40*, 28–60.

Sinnhuber, B.-M., and I. Folkins (2006), Estimating the contribution of bromoform to stratospheric bromine and its relation to dehydration in the tropical tropopause layer, *Atmos. Chem. Phys.*, *6*, 4755–4761.

Sinnhuber, B.-M., et al. (2002), Comparison of measurements and model calculations of stratospheric bromine monoxide, *J. Geophys. Res.*, *107*, 4398, doi:10.1029/2001JD000940.

Sinnhuber, B.-M., et al. (2005), Global observations of stratospheric bromine monoxide from SCIAMACHY, *Geophys. Res. Lett.*, *32*, L20,810, doi: 10.1029/2005GL023839.

Sioris, C. E., et al. (2006), Latitudinal and vertical distribution of bromine monoxide in the lower stratosphere from SCIAMACHY limb scattering measurements, *J. Geophys. Res.*, *111*, D14,301, doi: 10.1029/2005JD006479.

Solomon, S. (1989), The earth's fragile ozone shield, in *Global Change and Our Common Future*, edited by R. S. DeFries and T. Malone, Papers from a Forum, Washington, D.C., p. 73, National Academy Press.

Solomon, S., R. W. Sanders, M. A. Carroll, and A. L. Schmeltekopf (1989), Visible and near-ultraviolet spectroscopy at McMurdo station, 5, Observations of the diurnal variations of BrO and OClO, *J. Geophys. Res.*, *94*, 11,393–11,403.

Stimpfle, R. M., et al. (1999), The coupling of $ClONO_2$, ClO and NO_2 in the lower stratosphere from in situ observations using the NASA ER-2 aircraft, *J. Geophys. Res.*, *104*, 26,705–26,714.

Stolarski, R. S., and R. J. Cicerone (1974), Stratospheric chlorine: A possible sink of ozone, *Canad. J. Chem.*, *52*, 1610–1615.

Sturges, W. T. (1993), *Halocarbons in the Arctic and Antarctic atmosphere*, 117-130 pp., Springer-Verlag, New York, NY, USA, edited by H. Niki and K. H. Becker.

Sturges, W. T., D. E. Oram, L. J. Carpenter, S. A. Penkett, and A. Engel (2000), Bromoform as a source of stratospheric bromine, *Geophys. Res. Lett.*, *27*, 2081–2084.

Stutz, J., and U. Platt (1996), Numaerical analysis and estimation of the statistical error of differential optical absorption spectroscopy measurement with least-squares method, *Appl. Opt.*, *35*, 6041–6053.

Tilmes, S., R. Müller, J.-U. Grooß, M. Höpfner, G. C. Toon, and J. M. Russell (2003), Very early chlorine activation and ozone loss in the Arctic winter 2002–2003, *Geophys. Res. Lett.*, *30*(23), 2201, doi:10.1029/2003GL018079.

TOMS team (2006), *Data Product: OZONE*, Responsible NASA official: Dr. Richard McPeters, Principal Investigator for Earth Probe TOMS.

Toohey, D. W., J. G. Anderson, W. H. Brune, and K. R. Chan (1990), In situ observations of BrO in the Arctic stratosphere, *J. Geophys. Res.*, *17*, 513–516.

Toumi, R., R. L. Jones, and J. A. Pyle (1993), Stratospheric ozone depletion by $ClONO_2$ photolysis, *Nature*, *365*, 37–39.

Vaida, V., and J. D. Simon (1995), The Photoreactivity of Chlorine Dioxide, *Science*, *268*, 1443–1448.

van Geffen, J., and M. V. Roozendael (2006), Slant Column and Vertical Column Densities, in *Volcanic and Air Quality SO_2 Service*, BIRA-IASB / PROMOTE / TEMIS, http://www.oma.be/BIRA-IASB/Molecules/SO2archive/info/?kind=scdvcd.

Van Roozendal M. et. al (2002), Intercomparison of BrO measurements from ERS-2 GOME, ground-based and balloon platforms, *Adv. Space Res.*, *29*, 1661–1666.

Vogel, B. (1998), Herstellung und Kalibration von VUV-Strahlungsquellen zum Einsatz in einem ballongetragenen In-situ Halogenoxid-Meßgerät, Diplomarbeit, Universität Köln.

von der Gathen, P., et al. (1995), Observational evidence for chemical ozone depletion over the Arctic in winter 1991-92, *Nature*, *375*, 131–134, doi: 10.1023/A:1010607521870.

Wagner, T. (1999), *Satellite observation of atmospheric halogen oxides*, Univ. of Heidelberg, Ph.D. thesis.

Wagner, T., and U. Platt (1998), Satellite mapping of enhanced BrO concentrations in the troposphere, *Nature*, *395*, 486–490.

Watson, R. T. (1975), *Chlorine, the chlorine oxides, and other halogen species*, DOT-TST-75-S1, Dept. of Transp.

Weidner, F., et al. (2005), Balloonborne limb profiling of UV/vis skylight radiances, O_3, NO_2, and BrO: technical set-up and validation of the method, *Atmos. Chem. Phys.*, *5*, 1409–1422.

WMO (1990), *Scientific assessment of ozone depletion: 1989*, Report No. 20, Geneva, Switzerland.

WMO (1992), *Scientific assessment of ozone depletion: 1991*, Report No. 25, Geneva, Switzerland.

WMO (2003), *Scientific assessment of ozone depletion: 2002*, Report No. 47, Geneva, Switzerland.

Wofsy, S. C., M. B. McElroy, and Y. C. Young (1975), The chemistry of atmospheric bromine, *Geophys. Res. Lett.*, *2*, 215–218.

Woyke, T. (1998), In-Situ Messung von Halogenoxiden in der polaren Stratosphäre: Untersuchungen zur Ozonchemie im Winter 1994/95, Dissertation, Universität Bonn.

Yung, Y. L., J. P. Pinto, R. T. Watson, and S. P. Sander (1980), Atmospheric bromine and ozone perturbations in the lower stratosphere, *J. Atmos. Sci.*, *37*, 339–353.

Zandbergen, R., M. Otten, P. L. Righetti, D. Kuijper, and J. M. Dow (2003), Routine operational and high-precision orbit determination of Envisat, *Adv. Space Res.*, *31*, 1953 – 1958.

Zhong, W., and J. D. Haigh (1995), Improved broadband emissivity parameterization for water vapor cooling rate calculations, *J. Atmos. Sci.*, *52*(1), 124–138.

Acknowledgement

This work was performed in Institute of Stratospheric Chemistry of Research Center Jülich. Fruitful friendly climate in the institute and permanent willingness of all colleagues to help are essential contributions to this work.

First of all, my sincere gratitude belongs to Dr. Fred Stroh, who was for me a very valuable guardian in the new country and new field of science, who showed much patience, understanding, and tolerance in different scientific, road and everyday situations, and who sacrificed his days off time during the last phase of this thesis preparation in order to form out of wordy paste the proper scientific work.

I kindly thank the head of our institute Prof. Dr. Martin Riese for his inexhaustible optimism and powerful support in all, often not expected, difficulties.

Dr. Cornelius Schiller - who was fulfilling the duties of the head of our institutes as I was employed - is kindly acknowledged for the given opportunity to perform this work.

I thank all my examiners, foremost Prof. Dr. Martin Riese and Prof. Dr. Ralf Koppmann, who were the reviewers of this thesis.

I appreciate deeply comments of Dr. Marc von Hobe to this work as well as an introduction of a magnificent world of running to me.

My special thanks to Dr. Martin Kaufmann and Dr. Lars Hoffmann, who satisfied my burning interest to theoretical physics.

I thank Jochen Barthel, who contributed significantly during preparations of the balloon and aircraft instruments to the field campaigns and during campaigns itself.

Electronic wizards - Vicheith Tan, Axel Schönfeld, and Markus Boremski - helped to overcome intolerable temper of our photomultipliers.

In frame of this work the chemical model CLaMS was used. Its Lords

- Dr. Gebhard Günther, Dr. Paul Konopka, Dr. Rolf Müller - are greatly acknowledged for their help in use of CLaMS. The help of Dr. Jens-Uwe Grooß with CLaMS enhancement for the purposes of this work and with interpreting of its results is kindly appreciated.

Frau Brigitte Berger, Frau Roswitha Bley as well as her predecessor Frau Heidrun Acker-Mantel, Frau Sandra Stein, and Frau Bettina Scheid are thanked heartedly for their help in "paper" and visa formalities.

Dr. Marc Krebsbach and his wife Maria provided excellent base for my disposition and relaxation during a scientific activities in Jülich.

An advice about above-mentioned flat with "evergreen view" was given by Dr. Susanne Rohs, who, besides that, demonstrated superhuman fortitude during sometimes +6℃ conditions in our office and was the closest German "native speaker" enabled daily conversational exercises.

Sincere thanks belongs to Verena Cals and Reimar Bauer, who were and are all the time ready to reanimate and encourage my computer.

This work was written using the publishing make-up system LaTeX. My very first steps into it were performed under solicitous care of Dr. Rolf Müller and our Brazilian gaucho Fábio Henrique Silva dos Santos.

Dr. Alexei Rozanov was always ready to share SCIAMACHY *BrO* profiles retrieved by him, which has given integrity this thesis. Thanks a lot!

My thanks belong certainly to all other, not mentioned here because of chaotic end phase of this work, colleagues from our institute as well as from partner institutes (Frankfurt, Bremen, Heidelberg, Karlsruhe).

The role of my parents in my coming into the world and their maintenance of me during the early stage of my life formed favorable basis for the accomplishment of this thesis.

A very special gratitude I express to my wife, friend and legal consultant Maria, for whom this all was initiated.....

I assure that I accomplished this work on my own and did not use any sources and textbooks other than those noted here. I assure also that I indicated all quotation.